ABSTRACT

Title of dissertation: MYOSINS IIIA AND IIIB REGULATE STEREOCILIA LENGTH BY TRANSPORTING ESPIN 1 TO THE POLYMERIZING END OF ACTIN FILAMENTS

Raymond Clyde Merritt, Jr., Doctor of Philosophy, 2009

Dissertation directed by: Professor Arthur N. Popper
Department of Biology

Mutations in the myosin IIIa gene are linked to *DFNB30* late onset deafness, in which those affected individuals can hear for the first twenty years of life. Mutations in the espin gene are linked to *DFNB36* congenital deafness. Both myosin IIIa and espin 1 are expressed in the inner ear hair cells and colocalize at stereocilia tips, the site of actin polymerization. Overexpression of these proteins in hair cells produce an increase in stereocilia length, and when both are co-expressed together they produce a length increase greater than when each one are overexpressed individually. These results suggest that these proteins interact and influence stereocilia length regulation. We confirmed the interaction of these two proteins in heterologous COS-7 cells. We observed that when co-expressed, these proteins promote elongation of filopodial actin protrusions in a synergistic manner. Mutational analyses show that myosin IIIa^{3THDI} binds to the ankyrin repeats of espin 1. Live and fixed cell imaging shows that myosin IIIa transports espin 1 to the filopodia tips where espin 1 promotes actin polymerizations through its WH2 domain. Because of the late onset of deafness associated with myosin IIIa, it has been

speculated that the lack of myosin IIIa function is partially compensated by the paralogous protein, myosin IIIb. Myosin IIIb, encoded by a distinct gene, lacks a C-terminal actin-binding domain shown to be essential for myosin IIIa filopodia tip localization. We observed that myosin IIIb localizes at stereocilia tips and is expressed at an earlier stage than myosin IIIa. We confirmed that myosin IIIb transports espin 1 to stereocilia tips and promotes actin polymerization, consistent with the hypothesis that it partially compensates for myosin IIIa. We found that binding to espin 1 is required for myosin IIIb movement and localization. We observed that myosin IIIb can downregulate the myosin IIIa localization in vestibular, but not in cochlear, hair cells. The interplay of myosins IIIa, IIIb, and espin 1 and their influence on stereocilia length unravels a novel molecular complex at the polymerizing end of F-actin and a framework to understand the cause of *DFNB30* and *DFNB36* deafnesses.

MYOSINS IIIA AND IIIB REGULATE STEREOCILIA LENGTH BY TRANSPORTING ESPIN 1 TO THE POLYMERIZING END OF ACTIN FILAMENTS

By

Raymond C. Merritt, Jr.

Dissertation submitted to the Faculty of the Graduate School of the
University of Maryland, College Park in partial fulfillment
of the requirements for the degree of
Doctor of Philosophy
2009

Advisory Committee:

Dr. Bechara Kachar, Co-Chair
Professor Arthur N. Popper, Co-Chair
Professor Elizabeth M. Quinlan
Professor David D. Yager
Professor Thomas W. Castonguay

DEDICATION

I dedicate this dissertation to my incredible family. Particularly to my understanding wife, Jamie, who has put up with these years of research, and to our precious daughter Hazel, who is the joy of our lives. I must also thank my wonderful family and in-laws who have given me their unwavering support. Finally, I dedicate this work to my employer, Gallaudet University, and Dr. Ann Powell, whom believed in me and the pursuit of academic excellence.

ACKNOWLEDGEMENTS

I am grateful to Dr. Bechara Kachar for mentorship on my dissertation research at the National Institutes of Health and Professor Arthur Popper for his guidance through my Ph.D. years at the University of Maryland. I thank Drs. Felipe Salles, M'Hamed Grati, Leonardo Andrade, and Mr. Uri Manor for assistance with experiments and for productive discussions related to this dissertation, Drs. Aurea de Sousa, Mark Schneider, and Gerry Dougherty for initial assistance with experiments and research ideas, Dr. Andrea Dosé for collaboration, and Mr. Matthew Schwerin for editorial comments on the manuscript. I am indebted to my dissertation committee members, Professor Elizabeth Quinlan, Professor David Yager, and Dr. Matthew Kelley for their time and positive criticism, Dr. Ann Powell for her professional support, and Ms. Jamie Merritt for proofreading this manuscript. I am thankful for the opportunity to be part of the NACS program at University of Maryland with guidance from Ms. Pamela Komarek and others in the program and to be part of the Graduate Partnerships Program (GPP) at National Institutes of Health. I am also appreciative to the Ford Foundation Predoctoral Fellowship for granting me the opportunity to benefit from an enriching experience. This dissertation work was supported by NIDCD, DIR, NIH and in part by NIH grants to Andrea C. Dosé (no. EY003575) and to Chris M. Yengo (no. EY016419).

TABLE OF CONTENTS

LIST OF TABLES, FIGURES, AND MOVIES

TABLES

FIGURES

MOVIES

Chapter 1: Introduction

1.1 Scope of Research

The purpose of this dissertation is to present experimental research that offers a deeper understanding of the structure of the stereocilia tips of mammalian inner ear sensory hair cells and the roles of the underlying deafness-associated proteins in actin elongation and stereocilia lengthening. These proteins, class III myosin isoforms and espin 1, constitute a novel dynamic molecular complex encircling the distal tip of the actin core of the stereocilia. This molecular complex is close to the site of actin polymerization, the sound transduction apparatus and other stereocilia-tip specializations. Deciphering the exquisite mechanosensory organelles, stereocilia, is instrumental in understanding how hearing and balance work. Stereocilia also serve as an excellent model system for comparing their actin machinery with those in other actin-based membrane protrusions such as filopodia of fibroblasts, microvilli of intestinal epithelial cells, growth cones of axons, dendritic spines, inner and outer segments interface of photoreceptors, and bristles of *Drosophila melanogaster*. Several key proteins in the stereocilia tips are actin regulators found to be responsible for stereocilia degeneration and deafness. To elucidate the functions of espin 1 as well as myosins IIIa and IIIb, cell biology and molecular techniques were used to investigate colocalization of these proteins in the stereocilia and filopodia and their ability to interact, elongate actin filaments, and regulate stereocilia length.

1.2 Background

1.2.1 Molecular composition and morphology of stereocilia bundle

Microscopic anatomy and physiology of the hair cell stereocilia in the inner ear end organs are important for high-speed, sensitive mechanoelectrical transduction—the transformation from the mechanical energy of sound pressure or motion into electrical signals through the hair cells (reviewed by Grillet *et al.*, 2009; reviewed by Gillespie and Müller, 2009). The stereocilia bundle, a microvillar staircase-shaped structure clustered together in different rows by tethering extracellular links at the apex of hair cells, is rich in filamentous actin decorated with unconventional myosins and actin-associated regulatory proteins. The paracrystalline actin core of each stereocilium contains uniformly polarized parallel actin filaments, tightly bundled by regularly spaced cross-linking proteins (Tilney *et al.*, 1983). These actin bundles have polymerizing ends at the tip and depolymerizing ends at the base that give rise to a retrograde "conveyor belt" of the actin molecular treadmill (Rzadzinska *et al*., 2004). The entire staircase stereocilia bundle turns over continuously and synchronously such that the tonotopic organization is preserved by the proportionality of the actin flux rate to the length of stereocilia from the base to the apex of the cochlea (Rzadzinska *et al*., 2004). That is, the longer stereocilia of the apical region of the cochlea have faster actin flux rates than those shorter stereocilia in the basal region. This highly regulated actin treadmilling mechanism is controlled by those myosins and actin associated proteins.

The site of intracellular actin polymerization is close to other stereocilia-tip specializations such as the transmembrane mechanoelectrical transduction (MET) complex and extracellular matrix protein ensembles. The MET complex consists of: a

molecularly unidentified mechanically gated channel, also known as the MET channel (Ricci *et al.*, 2006), that is permeable to Ca^{2+} and K^{+}; tip link, an extracellular filamentous structure connecting the tip and side of neighboring stereocilia (Kachar *et al.*, 2000; Kazmierczak *et al.*, 2007; reviewed by Manor and Kachar, 2008); gating spring, an unidentified hypothetical elastic element (Ricci *et al.*, 2006; reviewed by Fettiplace and Hackney, 2006); and an adaptation motor, myosin 1c, that modulates the tension of MET channel (Gillespie and Cyr., 2004). The extracellular matrix surrounding stereocilia tips and beneath tectorial membrane presents an array of extramembranous structures in addition to the tip link including: attachment crowns; horizontal top connectors; cell surface coat; and contact regions (Furness *et al.,* 1997*;* Goodyear *et al.*, 2005; Legan *et al*., 2005). The understanding of how these molecular subdivisions interact physiologically to carry out the exquisite operation of sound transduction has been fragmentary.

The stereocilia plasma membrane tightly envelops the actin core leaving a narrow cytosol space between the actin core and the membrane. The diffusion of ions, intracellular proteins (such as actin monomers and actin regulatory proteins), and other molecules is constrained into a one-dimensional flow between the stereocilia tip and base. Generally, the tips of tallest stereocilia at the upper row of the bundle have a rounded edge contour while the tethering tips of the shorter stereocilia have a bevelled conical shape pointed obliquely to the side of the taller stereocilia in the adjacent taller row. Sometimes, the tip membrane of these shorter stereocilia is pulled by the tip link which causes what is called ‘membrane tenting’ (Kachar *et al.*, 2000). The base, also

known as the ankle region, of stereocilia has a tapered appearance that reflects a pivotal hinge of the whole stereociliary body to coordinate stereocilia bundle deflections. PTPRQ and myosin VI are among molecular players believed to be responsible for maintaining the tapered shape of this ankle region (Sakaguchi *et al.*, 2008). The core of the ankle region, which a relatively few actin filaments transverse, presents a heavily stained osmiophilic structure called a rootlet that stretches into the cuticular plate and lower part of the stereocilia shaft. The rootlet is believed to act as an anchor that reinforce the pivotal tapered base (Furness *et al.*, 2008). Immunogold labeling data by Furness *et al.* (2008) localized tropomyosin, spectrin, β-, and γ-actin to these osmiophilic rootlets. There is speculation that the rootlet may also present myosin isoforms since tropomyosin has been implicated as a binding competitor of myosin to actin (Karkanevatos, 2001; Furness and Hackney, 2006).

To date, very few transmembrane proteins, including the tip-link proteins, have been localized to the plasma membrane of stereocilia. Two of them are the plasma membrane Ca^{2+}-ATPase isoform 2 (PMCA2) pump and P2X receptor. PMCA2 is a calcium pump that use ATP to extrude Ca^{2+} from stereocilia, thereby maintaining a low cytosolic Ca^{2+} to counteract Ca^{2+} influxes during mechanotransduction. These pumps promote a high extracellular Ca^{2+} around the stereocilia bundle and the endolymph (Wood *et al.*, 2004; Grati *et al*., 2006a). Mouse *PMCA2* gene has been linked to several allelic mutations causing deafness and vestibular dysfunction in deafwaddler (*dfw*) mice (Street *et al*., 1998; McCullough and Tempel, 2004). The *dfw* mutant mouse emerged spontaneously in a C3H/HeJ colony strain which waddles when walking, bobs its head,

and is deaf (Lane, 1987). Mapping the mouse chromosome 6 homologous to human chromosome 3p25-26, three mutant alleles, *dfw*, *dfw*^{2J}, and *dfw*^{3J}, have been identified to date. Each mutation leads to a similar phenotype yet a different inheritance pattern–i.e. partial loss-of function, functional null, or haplo-insufficiency of protein products (McCullough and Tempel, 2004). PMCA2 was used as a marker to track membrane trafficking using a combination of fluorescence recovery after photobleaching (FRAP) and computer simulation models to examine stereocilia membrane turnover (Grati *et al*., 2006b). Interestingly, a large amount of PMCA2 embedded in the stereocilia surface exhibited high mobility of 0.1-0.2 $\mu m^2/s$, which is relatively proportional to the speed of actin turnover in the stereocilia core. The remaining pool of PMCA2 was immobilized. Immunofluorescence data show that the mobile PMCA2 molecules are sequestered from stereocilia membrane into the cuticular plate and cytoplasm and are replaced with newly synthesized PMCA2 molecules that are incorporated into the stereocilia (Grati *et al*., 2006b). These results suggest that stereocilia membrane proteins, like the proteins associated with the stereocilia actin core, are turned over rapidly between the apical membrane and cytoplasm. The immobilized pool PMCA2 molecules stay fixed through interaction with other components of the stereocilia while the mobile pool of PMCA2 is constantly exchanged.

Another stereocilia membrane protein identified to date is P2X receptor, which is an ATP-gated, nonspecific, cation channel. P2X receptors have been localized to the stereocilia and cuticular plate and are found in many other cell types (North, 2002). The physiological role of these receptors in stereocilia is not clear (Housley *et al*., 1999; Crumling *et al*., 2009).

Identification and characterization of individual molecules present in the hair cell stereocilia is an indispensable step closer to understanding the mechanosensory function of the hair cell but this dissertation also takes into account the interaction between molecules and their influence on the structure and function of stereocilia. The major facet of this work specifically focuses on the connection between the interacting espin 1, myosins IIIa and IIIb, their spatial and temporal expression patterns around the stereocilia tip actin core, and the lengthening of stereocilia.

1.2.2 Actin treadmilling

Actin treadmilling concept was first proposed by Wegner in 1976 (Wang, 1985) and corroborated numerous times in several types of cellular protrusions (Small, 1995; Tilney and DeRosier, 2005; and Medeiros *et al*., 2006). In stereocilia, Schneider *et al*. (2002) was first to demonstrate that the steady-state stereocilia undergo rapid turnover of actin filaments and the entire actin core of the mature stereocilium is renewed every 48-72 hours (Schneider *et al.*, 2002). Rapid incorporation of β-actin monomers and actin cross-linker espin into actin filaments at the tips of stereocilia was monitored in hair cells of organ of Corti and vestibular explants transfected with a plasmid DNA encoding either β-actin or small espin isoform fused with green fluorescent protein (actin-GFP or espin-GFP; Rzadzinska *et al.*, 2004). This observation, in terms of polymerization at the barbed end and depolymerization at the pointed end of actin filaments, is in good agreement with the general actin treadmilling mechanism observed in other cellular protrusions and somewhat resembles the migration and renewal of the photoreceptor discs in the retina (Nguyen-Legros and Hicks, 2000; Schneider *et al.*, 2002). Additionally, the treadmill

rates were found to be scaled proportionally to the lengths of the stereocilia in the bundle, i.e. there was a faster actin flux rate in long stereocilia than in short stereocilia (Rzadzinska *et al.*, 2004).

Retention and recycling of actin monomers are thought to contribute to actin treadmilling. The tight membrane encapsulation of the actin core and a tapered base with a narrow opening to the cytoplasm below are among the morphological features believed to promote the actin retention and recycling within the stereocilium (reviewed by Manor and Kachar, 2008). Lechene *et al.* (2006) reported experimental results using multi-isotope imaging mass spectrometry in adult mice and frogs that the renewal rate of newly synthesized proteins migrating into the stereocilia is relatively slow—on the order of months. These results put forward for consideration that the availability of actin monomers are maintained largely by the recycling of actin monomers within each stereocilium and, to a lesser extent, by migration of newly synthesized monomers from the cytoplasm (reviewed by Manor and Kachar, 2008). However, to what extent the stereocilia actin monomer pool is compartmentalized from the cytoplasmic pool remains to be determined.

The research on actin treadmilling in stereocilia has intensified where physical modeling continues to be revised as the list of newly identified molecular players in stereocilia gets longer and new parameters unraveled. A new concept of actin treadmilling now includes an active localization of actin regulatory proteins by myosins to the tip (e.g. espin [Rzadzinska *et al.*, 2004], whirlin [Mburu *et al.*, 2003] the formin protein mDia1 [Evangelista *et al.*, 2003]) and to base (e.g. radixin [Pataky *et al.*, 2004],

PTPRQ [Sakaguchi *et al.*, 2008], and tropomyosin [Furness *et al.*, 2008]) of stereocilia (reviewed by Manor and Kachar, 2008; Naoz *et al.*, 2008). These actin and membrane associated cargoes have been implicated in assembly of the actin core and maintenance of the steady-state stereocilia.

1.2.3 Molecular composition and functional properties of stereocilia tips

During the formation and maturation of the stereocilia, the hair cell assembles actin filaments into fibers of various dimensions to bolster the mechanical rigidity necessary for proper sensory function. These actin fibers are polarized such that the 'plus' or 'barbed' ends are at the tips of the protrusions and the 'minus' or 'pointed' ends at the base. The site of actin polymerization is at the plus ends where localized pools of actin monomers are being nucleated (Rzadzinska *et al.*, 2004; Lin *et al.,* 2005; Schneider *et al.*, 2006). Electron-dense structures bridging the plus ends of actin filaments with the overlying plasma membrane have been routinely observed via electron microscopy (EM), a feature also commonly seen in microvilli and filopodia (reviewed by DeRosier and Tilney, 2000; Lin *et al*., 2005). This electron-dense structure, also termed the 'tip density,' presumably contains an ensemble of heterologous proteins that directly or indirectly influence actin polymerization for the maintenance of stereocilia. This tip density may also sustain the shearing and tenting of the membrane pulled by the tip link during stereocilia bundle deflection (Kachar *et al.*, 2000).

Significant data, based on calcium (CG-1) and styryl (FM1-43) dye imaging, extracellular current flow, and susceptibility to antagonists, indicate that the transmembrane MET complexes are present at the tips of the stereocilia (Jaramillo and

Hudspeth, 1991; Denk *et al*., 1995; Lumpkin and Hudspeth, 1995; Géléoc and Holt, 2003; Si *et al*., 2003; Meyers *et al.*, 2003). Recently, structural (Kachar *et al.*, 2000) and biophysical data (Beurg *et al.*, 2009) as well as unpublished data presented during the 2009 Association for Research on Otolaryngology (ARO) Midwinter meeting (Harasztosi and Gummer, 2009) suggest that the MET channel is present specifically at shorter stereocilia tips nearby the insertion of the lower end of the tip link. An unidentified elastic element closely associated with the MET channel was also proposed to be present beneath the insertion (Kachar *et al.*, 2000). If these results hold true, the MET channel is presumably located beneath the lower tip link and above an elastic element, the tip density, and the site of actin polymerization.

MET channels open with a short latency (~10 μs at mammalian temperature; Corey and Hudspeth, 1983) in response to a deflection of the stereocilia bundle, stay open for approximately a hundred milliseconds, and then re-close in series of two different adaptation phases independent of the deflection duration (reviewed by Fettiplace and Hackney, 2006). The fast adaptation phase occurs rapidly on the microsecond scale and the other phase takes tens or hundreds of milliseconds (reviewed by Eatock, 2000). Second messenger cascades for the fast adaptation and activation of MET channel open and re-closure are precluded because the opening and fast re-closure of channel is too rapid (Corey and Hudspeth, 1983; Ricci *et al.*, 1998; Fettiplace *et al.*, 2001). Instead, a direct deactivation of the MET channel is favored. Biophysical experiments suggest that Ca^{2+} enters the channel upon mechanical deflection, immediately binds to the channel at the cytoplasmic side, and closes it (Howard and Hudspeth, 1988; Holt and Corey, 2000;

Kennedy *et al.*, 2003; Cheung and Corey, 2006). The slow adaptation uses a distinct mechanism where the upper insertion point of the tip link slides down the taller stereocilium in response to elevated tension on it during a positive bundle displacement rendering channel(s) to re-close. The sliding of the tip link mechanism is believed to be exerted by myosin 1c (Gillespie and Cyr, 2004). One function of these adaptations is thought to keep the MET channels sensitive within their operating range (reviewed by Fettiplace and Hackney, 2006; also by Hudspeth, 2008).

The molecular identity of the tip-link filament has been resolved by Kazmierczak *et al.* (2007) to be an asymmetric double helical adhesion fiber consisting of cadherin 23 (CDH23) and protocadherin 23 (PCDH15) that interact at their N-termini. Fluorescent and electron microscopic data show that the upper and lower parts of the tip link are comprised of CDH23 and PCDH15, respectively. Furthermore, advanced electron microscopy imaging indicate that the upper tip-link filament bifurcates into two branches inserting at the side of a taller stereocilium and the lower tip-link filament branches into three smaller filaments inserting at the top of the shorter stereocilium (Kachar *et al.*, 2000).

Although the molecular identity of the tip density and other compartments at the stereocilia tip is poorly charted, a number of molecular players have been localized to these compartments. For instance, a molecular complex localized at the stereocilia tip, right above the actin core, was recently identified by Mburu *et al.* (2006) which may mediate membrane-to-cytoskeleton interactions as well as actin polymerization. This complex constitutes a combination of a scaffolding protein, whirlin (Mburu *et al.*, 2003),

membrane associated proteins, protein 4.1R, erythrocyte protein p55 and Ca^{2+}-calmodulin serine kinase (CASK) (Mburu *et al*., 2006), and a motor protein, myosin XVa (Belyantseva *et al.*, ARO 2002; Rzadzinska *et al.*, 2004).

Other proteins such as filamentous actin capping proteins (e.g. gelsolin), 'leaky' caps (e.g. Ena/VASP, formins), signaling proteins (e.g. integrins), and membrane proteins (e.g. protein 4.1R) are present in the tip density of filopodia or microvilli (Lin *et al.,* 2005; reviewed by Manor and Kachar, 2008), however many of these proteins have not been detected in stereocilia at the time of writing. The tip of the shorter stereocilium was often found to be in physical contact with the taller stereocilium where some form of an extracellular membrane specialization in what is called a 'contact region' has been frequently visualized via EM (Furness *et al.*, 1997).

Integrin and integrin-associated proteins (i.e. fibronectin and integrin-regulated focal adhesion kinase [FAK]) are cell-surface receptors known to interact with a variety of extracellular ligands. These proteins colocalize to the apical hair-cell surface when stereocilia are forming during hearing development. One of them, integrin α8β1, has been implicated in stereocilia defects. The integrin-α8β1-deficient knockout mice that withstood lethal kidney defects demonstrate the difficulty in balancing. Integrin α8β1, and possibly other integrins, are likely to regulate stereocilia maturation (Evans and Müller, 2000).

1.2.4 Unconventional myosins in stereocilia

The evolution of stereocilia can be reflected in the diversity of endogenous myosin isoforms known to regulate structural and functional integrity of these cellular

protrusions. A large number of reports have been published suggesting that myosins are expressed in all unicellular and multicellular eukaryotes, from yeasts to mammals and plants (reviewed by Sellers, 2000). Myosins comprise a vast superfamily, containing 24 different classes identified to date (Foth *et al.*, 2006), of actin-activated ATPases that directionally translocate either towards the plus or minus ends of actin filaments (reviewed by Warrick and Spudich, 1987; Sellers, 2000; Berg *et al*., 2001; Thompson and Langford, 2002). Myosins, originally isolated from muscle tissues, are subcategorized into bipolar filament forming conventional myosins and non-filamentous unconventional myosins. Conventional myosins are generally implicated in contractile function and unconventional myosins implicated in structural or transport function (Rędowicz, 2007; Dosé *et al*., 2003). All conventional myosins from either muscle or non-muscle tissue are members of class II myosins that multimerize into bipolar filaments through their long coiled-coil tails as seen in the thick filament of sarcomeres in the striated muscle (reviewed by Stull, 1996; and by Sellers, 2000). The members of the other myosin classes are termed unconventional since they do not form bipolar filaments. These unconventional myosins are involved in a variety of cellular functions, including cell migration, intracellular trafficking, adhesion, cytokinesis (reviewed by Rędowicz, 2002), gene transcription (Vreugde *et al.,* 2006), and actin elongation in stereocilia (Belyantseva *et al.*, 2003).

Unconventional myosins share common features of an N-terminal ATPase, designated as a motor or head domain, a short regulatory neck domain containing a variable number of calmodulin binding, IQ, motifs (reviewed by Cheney and Mooseker,

1992), and a C-terminal tail region often unique to each myosin isoform due to different combinations of conserved functional domains and divergent amino acid sequences (Thompson and Langford, 2002). Myosins are mechanoenzymatic in that their motor domain uses the energy of ATP hydrolysis to translocate along the actin cables.

Calmodulin has been implicated in regulating certain myosin molecules in either Ca^{2+}dependent or independent manner via binding to the IQ motifs (Furness and Hackney, 2006; Dosé *et al.*, 2003). Calmodulin has been found in both inner hair cells (IHCs) and outer hair cells (OHCs) including stereocilia and immunogold labeling which has shown concentrations of calmodulin that overlaps the presence of myosins in the tip link insertions (Furness *et al.*, 2002).

The ability of a myosin to perform specific cellular functions has been extrapolated by several principles including: 1) processivity—the ability to take multiple steps without detaching from the actin cable; 2) duty ratio—the fraction of the total ATPase cycle time spent firmly attached to the actin cable; and 3) directionality—the direction of a motor moving toward barbed end and/or point end of the polarized actin cable (reviewed by Krendel and Mooseker, 2005). Many myosins, designated as processive motors, are dimeric, in which their dual motor heads take alternative steps via transitions between two states of actomyosin-ADP in the ATPase cycle (Mehta, 2001).

Myosin was first reported in the stereocilia by Macartney *et al.* (1980) where immunofluorescent microscopy was used with purified polyclonal antibodies against muscle myosin. Myosins were previously suspected to participate in active nonlinear sound amplification processes in mammalian cochlea because these actin-dependent

enzymes have the capacity to generate force using ATP. Eventually, it was suggested that one of these myosins, unconventional myosin 1c, participate in the slow adaptation in the hair cells. More unconventional myosins in the stereocilia and their functions have been steadily unraveled and the distribution of these myosin isoforms appears to be highly compartmentalized from the base, through the shaft, to the tip. Many of them have been implicated in deafness as well as lengthening, shaping, and/or bundling the stereocilia.

Myosin XVa is found to be expressed in IHCs and OHCs (Anderson *et al.*, 2000). *MYO15A*, mapped to human chromosome 17p11.2, harbors autosomal recessive mutations associated with sensorineural deafness in humans (*DFNB3*). An x-ray radiation induced mutation in the mouse *Myo15* gene homologous to the human counterpart led to profound deafness and vestibular dysfunction in mice. These affected mice, called *shaker-2* mice, demonstrate typical head-tossing and circling behavior (Probst *et al.*, 1998). Inner ear hair cells of *shaker-2* mice have abnormally short stereocilia (Beyer *et al.*, 2000). Fluorescence and electron microscopies have shown that myosin XVa is localized to the electron-dense structure at the very top of stereocilia tips where the actin cores terminate (Rzadzinska *et al.*, 2004) with highest concentration in the tallest stereocilia. Colocalization and live-cell imaging indicate that myosin XVa transports the scaffolding protein, whirlin to the tips of stereocilia (Belyantseva *et al.*, 2005). Mutations in *whirlin* also lead to abnormally short stereocilia in *whirler* mice, which present pathology similar to that of *shaker-2* mice. Whole-cell patch-clamp recordings in *Myo15*$^{sh/sh}$ hair cells indicate that myosin XVa is not required for mechanotransduction but is required for fast adaptation and Ca^{2+} sensitivity in IHCs (Stepanyan *et al.*, 2006;

Stepanyan and Frolenkov, 2009). It is generally postulated that myosin XVa is responsible for stereocilia elongation and transport of functional cargoes including whirlin and other proteins to the stereocilia tip.

Myosin VIIa harbors mutations that underlie hearing, balance, and vision defects in humans with Usher syndrome 1B (Weil *et al*., 1995), hearing and balance defects in *shaker-1* mice (Gibson *et al*., 1995), circling behavior in zebrafish mutants (Ernest *et al*., 2000), and deafness in *Drosophila melanogaster* (Kiehart *et al*., 2004; Todi *et al*., 2005). Myosin VIIa, mapped to human chromosome 11q13.5 (*DFNB2*, Weil *et al*., 1995; *DFNA11*, Tamagawa *et al*., 1996), is expressed in inner ear hair cells and retinal pigmented epithelial (RPE) cells, and localizes to cytoplasm and stereocilia of hair cells (Rzadzinska *et al*., 2004) as well as to the actin-rich apical portion of RPE cells and connecting cilia of photoreceptors (Hasson *et al*., 1995; Liu *et al*., 1999). Colocalization and binding assays have shown that myosin VIIa interacts with other Usher I gene products–i.e. harmonin and CDH23–in stereocilia. Harmonin, implicated in both human and mouse deafness (Verpy *et al*., 2000), is a PDZ (postsynaptic density, disc large, zonula occludens) containing protein that bundles actin filaments and anchors cadherin 23, the lower part of the tip link. These three proteins are believed to participate in maintaining proper cohesiveness of the stereocilia bundle (Boëda *et al*., 2002; Kros *et al*., 2002). More recently, studies using an *in vivo* mouse X-linked transgenic mosaic complementation approach indicate that myosin VIIa acts as a rate-limiting factor of stereocilia lengthening (Prosser *et al*., 2008).

Myosin VI is different from other unconventional myosins in that it moves along actin filaments toward the minus end (Wells *et al*., 1999) and is believed to function as an

actin-based anchor and a minus-end transporter (reviewed by Sweeney and Houdusse, 2007). The *MYO6* gene, mapped to chromosome 6q13, is implicated in both autosomal dominant and recessive non-syndromic sensorineural deafness (*DFNA22*, Melchionda *et al*., 2001; *DFNB37*, Ahmed *et al*., 2003) and has been linked to mouse *Snell's waltzer* deafness gene on mouse chromosome 9. *Snell's waltzer* mice exhibit circling behavior, head-tossing, and deafness seen in other deaf mutant mice (Avraham *et al*., 1995). Myosin VI is localized to the tapered base of the stereocilia and is required for the integrity of this structure (Seiler *et al*., 2004). Recently, a cargo of myosin VI was putatively identified to be protein tyrosine phosphatase receptor Q (PTPRQ), in which PTPRQ and myosin VI knockout mice demonstrated similar pathological phenotype where the tapered base of stereocilia was disrupted and the neighboring stereocilia were partially fused in both knockout mice inner ears (Sakaguchi *et al*., 2008) suggesting that these proteins form a complex that maintains the organization of the stereocilia base as well as the structure of the stereocilia bundle.

Myosin IIa, also known as MYH9 or non-muscle myosin heavy chain-2A (NMHC-IIa), mapped to chromosome 22q11.2, is linked to both syndromic and non-syndromic progressive deafness dominant forms (*DFNA17*), in which the former include platelet abnormalities, nephritis, and/or cataracts (Balduini *et al*., 2002; Mhatre *et al*., 2003). Myosin IIa has been localized via immunogold labeling and immunofluorescence along the peripheral and central parts of the actin core in the stereocilia as well as cuticular plate at the base and in the hair cell cytoplasm (Lalwani *et al*., 2008).

Myosin 1c (formerly known as myosin 1β), probably the most intensively studied myosin isoform in stereocilia to date, is another unconventional myosin that has been

implicated in the slow adaptation of the MET response (reviewed by Gillespie and Cyr, 2004). Members of the class I myosins has been found to express in microvilli of brush border intestinal cells (Tyska *et al.*, 2005). Although the *MYO1C* gene has not been linked directly to a form of deafness, it is mapped to a genetic locus, 17p13, nearby the locus of the deafness-harboring *MYO15A* at 17p11.2.

Holt *et al.* (2002) devised a clever pharmacogenetic strategy using conditional transgenic mice to investigate the role of myosin 1c on the slow adaptation of MET response. In their transgenic model, they mutated tyrosine-61 of myosin 1c to glycine, in order to render it susceptible to inhibition by an ADP analog while the overall health of the mice is virtually intact without the inhibition treatment. Their strategy intended to circumvent potential issues associated with conventional knockout mice and to delineate the functional contribution of myosin 1c upon slow adaptation. In their whole-cell patch clamp recording results, the MET adaptation following hair bundle deflections was rapidly blocked in the transgenic utricular hair cells but not in wild-type utricular hair cells when treated with N^6-modified ADP, confirming that myosin 1c plays an important role in the slow form of adaptation. Myosin 1c was localized to the lower and upper anchors of the tip links and around the actin core of bull frog utricular and saccular vestibular stereocilia (Gillespie *et al.,* 1993; Garcia *et al.*, 1998; Steyger *et al.*, 1998), to the base near the cuticular plate in frog saccular hair cells (Garcia *et al.*, 1998), at the tips of rodent vestibular stereocilia, and the entire shaft of cochlear stereocilia (Dumont *et al.*, 2002). Myosin 1c was found to interact with the tip-link associated CDH23 (Siemens *et al.*, 2004; Phillips *et al.*, 2006), which is known to interact indirectly with myosin VIIA

(Boëda *et al.*, 2002). Collectively, it is conceivable that myosin 1c, considering its anchor and transport functions, actively regulates the tension of the tip link complex during the slow adaptation where it crawls along the actin core.

The panoply of unconventional myosins in stereocilia does not end here. There is also a class of myosins characterized by a unique *cis* kinase domain at the N-terminus designated as the class III myosins. A myosin III *Drosophila* orthologue, *ninaC*, has been localized to rhabdomeral photoreceptors of the fruit fly eye (Edwards and Battelle, 1987; Montell and Rubin, 1988; Battelle *et al*., 1998) and implicated as a requirement for phototransduction (Wes *et al*., 1999; reviewed by Bähler, 2000). The human myosin IIIa has been implicated in deafness (Walsh *et al*., 2002) as well as influencing stereocilia shape (Schneider *et al*., 2006). A large portion of this dissertation focuses on two class III myosin isoforms—myosins IIIa and IIIb—encoded by separate genes on human chromosomes 10 and 2, respectively.

1.2.5 Mutations in *MYO3A* are linked to late onset non-syndromic deafness

Although at least two main class III myosin isoforms, IIIa and IIIb, and their splice variants are known to express in humans, mice, and other vertebrate species, recent studies have focused largely on myosin IIIa (MYO3A; Dosé and Burnside, 2000) because autosomal recessive mutations in the human *MYO3A* gene are implicated in non-syndromic progressive deafness (*DFNB30,* chromosome 10q12.1; Walsh *et al*., 2002). Family members with *DFNB30* mutations (i.e. homozygous and compound heterozygous mutations) in a three-generation extended Israeli family experienced bilateral age-dependent progressive deafness beginning in the second decade. The deafness became more severe at high and middle frequencies and moderate at low frequencies by age 50.

Surprisingly, since myosin IIIa is expressed in the retina, vestibule, and cochlea (Walsh *et al.*, 2002), the hearing affected members had normal vision and balance. Three loss-of-function mutations were detected using a genome-wide linkage analysis technique on 18 affected family members. These three mutant alleles are 3126T→G, 1777G→A, and 732A→G. The 3126T→G substitution is a nonsense point mutation at amino acid position 1043 that causes a premature protein truncation at the junction of the head and neck domains of myosin IIIa. 1777G→A is a base substitution in the splice acceptor of intron 17, which leads a deletion of exon 18 and protein truncation at amino acid 668 in the myosin IIIa head domain. 732A→G is a base substitution in the splice acceptor of intron 8 that seems to destabilize the RNA message resulting in a myosin IIIa null (Walsh *et al.*, 2002). Three different myosin IIIa mutations were observed in the same family. An existence of other unknown mutations in the *MYO3A* gene cannot be ruled out (Walsh *et al.*, 2002).

Myosin IIIb is another class III myosin isoform encoded by a paralogous gene (GeneCards.org, 2008), *MYO3B*, that has been mapped to human chromosome 2q31.1-q31.2. Myosin IIIb has a shorter C-terminal tail than myosin IIIa. Myosin IIIb was originally detected in retina, kidney, and testis (Dosé *et al.*, 2002). No hearing defects have been reported to date in association with the *MYO3B* gene. Nonetheless, the gene is near two other genetic loci implicated in deafness or retinal dystrophy. One of these genetic loci linked to an autosomal recessive non-syndromic deafness, *DFNB59,* is mapped to 2q31.1-2q33.1, which is near the *MYO3B* locus. *DFNB59* has been linked to a protein known as pejvakin. Although pejvakin is implicated in pathologies related to

auditory nerve and outer hair cell deformities (Delmaghani *et al.*, 2003; Schwander *et al*., 2007), the function of this protein is unknown (Collin *et al.*, 2007). The other gene locus, implicated in vision, excretory, and male reproductive dysfunctions known as Bardet-Biedl syndrome, is also mapped to 2q31.1-2q31.2. Since myosin IIIb is found to express in mammalian photoreceptors (Dosé *et al.*, 2003), investigators suspected that myosin IIIb may play a role in vision. Although *MYO3B* may not be linked directly to either *DFNB59* or Bardet-Biedl syndrome (Dosé *et al.*, 2002), the proximity of these genetic loci conjectures that *MYO3B* is recombined into a cluster of a gene repertoire that has been evolutionarily conserved for sensory function (e.g. see Kappen, 2000).

1.2.6 Expression patterns of class III myosins

Presently, class III myosins are found to be expressed, at either the mRNA transcript or the protein level, in the inner ear hair cells of American bullfrog (*Rana catesbeiana*), domestic chicken (*Gallus gallus domesticus*), guinea pig (*Cavia porcellus*), rat (*Rattus norvegicus*), and mouse (*Mus musculus*) (Schneider *et al*., 2006), in the photoreceptors of fruit fly (*Drosophila melanogaster*) (Montell and Rubin, 1988), horseshoe crab (*Limulus polyphemus*; Battelle *et al.*, 1998), several fish species including striped bass (*Morone saxatilis*), zebrafish (*Danio rerio*), green sunfish (*Lepomis cyanellus*), albino trout (*Oncorhynchus mykiss*; Lin-Jones *et al*., 2009), African clawed frog (*Xenopus laevis*; Lin-Jones *et al*., 2004), mouse (Katti *et al*., 2009), as well as the human (*Homo sapiens*) retinal pigment epithelial (RPE) cell line, ARPE-19 (Dosé and Burnside, 2000). Furthermore, myosin III is predicted, via computational analyses, to express in mosquito (*Anopheles gambiae*; NCBI accession number XM_318814), dog

(*Canis lupus familiaris*; XM_544234), cattle (*Bos taurus*; XM_615938 and XM_616244), horse (*Equus caballus*; XM_001495240), rhesus monkey (*Macaca mulatta*; XM_00101244, XM_001082604, XM_001082477, XM_001082224, XM_001082351), and chimpanzee (*Pan troglodytes*; XM_507703 and XM_525960).

The myosin IIIa tissue expression in vertebrates is restricted (Dosé and Burnside, 2000), with the strongest expression in the IHCs and OHCs of organ of Corti (Walsh *et al.*, 2002; Schneider *et al.*, 2006) and retina (Dosé *et al.*, 2003). The *Drosophila* myosin III orthologue, *ninaC* (neither inactivation nor afterpotential C), is expressed specifically in the fruit fly photoreceptor cells (Montell and Rubin, 1988) and is required for the deactivation of phototransduction (Wes *et al*., 1999). Recently, immunocytochemical studies indicated that myosin IIIa is localized around the stereocilia tips forming a thimble-like pattern (Schneider *et al*., 2006). Myosin IIIa expression was detected in the rat IHCs and vestibular hair cells (VHCs) at postnatal day 0 (P0) and, subsequently, in OHCs at P3. The myosin IIIa immunoreactivity levels were at their highest between P6 and P10 before the levels dropped very low in the adults (Schneider *et al.*, 2006). By using a special technique of antigen retrieval step, the immunoreactivity of myosin IIIa in the adults (>P30) was recovered. The brightest fluorescent puncta were often seen among the second row of stereocilia tips in the mature OHC bundles. Moreover, robust hybridization signals, using a 1 kilobase riboprobe corresponding to the N-terminal mouse IIIa, were observed in mouse cochlear and vestibular hair cells from P8 through P50 (Schneider *et al.*, 2006). Myosin IIIa has also been localized to the inner segment of

mouse photoreceptors as well as calycal processes of rod and cone photoreceptors and sacculus in striped bass (Dosé *et al.*, 2003).

The spatiotemporal expression patterns of myosin IIIa and the deaf phenotype of *DFNB30* human subjects suggest that the mutations in the *MYO3A* gene affect the structure and function of the stereocilia. Nonetheless, there is no definitive explanation how these mutations affect hearing later in life but not balance or vision (Schneider *et al.*, 2006). A speculative explanation by a consensus in the literature is that myosin IIIb or another unidentified protein partially compensates for the loss of function of myosin IIIa in hearing but only during the early years of life. The mechanistic reason why the hearing compensation does not endure through *DFNB30* adulthood is unknown.

The vertebrate myosin IIIb tissue expression is found in the sensory epithelia of the retina and the olfactory bulbs, the neural tissue of the brain (Katti *et al*. 2009), and the non-sensory epithelia of the intestine and testis (Dosé *et al.*, 2003). A recent study using a modified mass spectrometry technique, presented by Peter Gillespie during the 2009 Association for Research on Otolarynology MidWinter Meeting, reported that myosin IIIb is present in the hair bundles of chicken VHCs (Gillespie *et al*., 2009). Myosin IIIb is also localized to the inner and outer segments of photoreceptors, cells in the inner nuclear layer and ganglion cells in the mouse retina (Katti *et al.*, 2009), as well as the calycal processes and ellipsoids of green sunfish cone photoreceptors (Lin-Jones *et al.*, 2009). These observed expression patterns indicate that both myosins IIIb and deafness-associated IIIa localize to several similar cellular compartments. These localizations are consistent with the possibility that these proteins compensate for each other. Myosin III

knockout or transgenic mice would be good models to examine the physiologic and phenotypic relationship between deafness and class III myosins.

1.2.7 Functional domains of class III myosins

Class III myosins are among the most divergent members of the myosin superfamily identified to date since they possess a peculiar kinase domain (Fig. 1-1) at their N-terminus. This built-in kinase autophosphorylates serine and threonine residues in the *cis* motor domain (Komaba *et al.*, 2003; Montell and Rubin, 1988; Ng *et al*., 1996; Dosé *et al.*, 2007a) and other *trans* protein substrates (Kempler *et al.*, 2007).

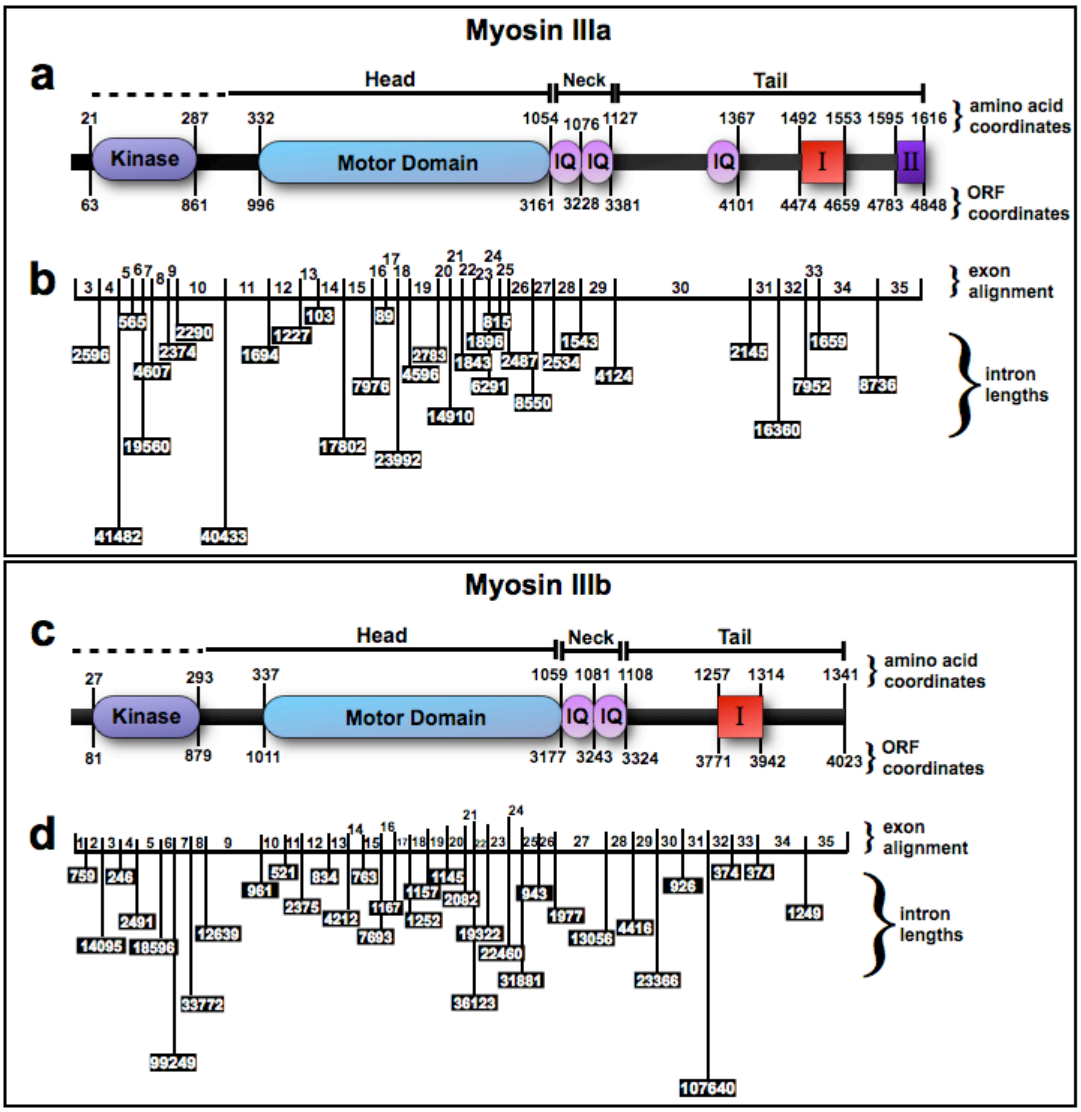

Figure 1-1. Molecular maps of human myosin paralogues, IIIa and IIIb*. (**a, c**) Schematic diagrams of myosins IIIa (**a**; NCBI accession number AY101367) and IIIb (**c**; NM_138995) illustrating the orientation of head, neck, and tail regions as well as the functional domains. Polypeptide amino acid (aa) and open reading frame (ORF) nucleotide (nt) coordinates are displayed at each myosin (top and bottom, respectively). The aa coordinates are predicted by SMART unless otherwise cited. Dotted/solid bar (head) represents the N-terminal kinase and the motor domain (ATPase). The N-terminal kinase domain is a member of the highly conserved Ste20/PAK family kinases (Dosé *et al.*, 2000; Dosé *et al.*, 2003) and is implicated in downregulating the motor activity of myosin III. The motor domain contains two conserved ATP-binding sites, residues for conformation change and movement, and an actin-binding site (Dosé *et al.*, 2000; Rayment *et al.*, 1993). Two IQ motifs are predicted in the neck region. An extra IQ motif is located in the myosin IIIa tail region. Both myosins contain the conserved cargo-binding 3THDI (myosin III Tail Homology Domain I) in the tail but only myosin IIIa has the actin-binding domain, 3THDII (II, aa positions 1595—1616; Les Erickson *et al.*, 2003; Dosé *et al.*, 2003). (**b, d**) Coarse exon alignments** of myosins IIIa (**b**) and IIIb (**d**). Exon coordinates are numbered horizontally and intron coordinates are numbered (black boxes) vertically according to nucleotide length between exons (NCBI Spidey; Wheelan *et al.*, 2001). Exons and introns encompassing the 5′ and 3′-untranslated regions (-UTRs) are excluded. See text for further details. *Not to scale. **Use NCBI Spidey or elsewhere for precise alignment.

This kinase domain is homologous to the Ste20/GCK family of protein kinases (Dosé and Burnside, 2000; Dan *et al.*, 2001; Dosé *et al.,* 2003). Bioinformatics searches via several models and databases (e.g. Simple Modular Architecture Research Tool [SMART, Schultz *et al.*, 1998] database, CLUSTALW [Thompson *et al.*, 2002]; Pfam [Finn *et al.*, 2008]; UniProtKB [Boutet *et al.*, 2007]) indicate a highest amino acid identity of 56% between myosin IIIa kinase and a GCK member namely misshapen-like kinase 1 (MINK1; Swiss-Prot accession no. Q9JM52; Accessed September 2009). MINK1 is found to respond to environmental stresses through the c-Jun N-terminal kinase signaling pathway (Dan *et al*., 2000) and is implicated in cytoskeleton rearrangement and cell motility (Sells *et al.*, 1997). Deletion of this kinase domain affects phototransduction in *Drosophila* (Porter and Montell, 1993a), causes stereocilia elongation and stereocilia tip bulging in rodents, and enhances filopodia localization in transfected COS-7 (Schneider *et al*., 2006) and HeLa cells (Les Erickson *et al*., 2003). Biochemical studies indicate that the autophosphorylation of myosin IIIa decreases the affinity for actin in the presence of ATP (Dosé *et al.*, 2007a; Dosé *et al.*, 2008; Kambara *et al.*, 2006), suggesting that the phosphorylation attenuates the movement of myosin IIIa. Further studies are needed for clarifying the role of autophosphorylation of myosin III by the catalytic kinase domain.

The head region contains the canonical ATPase that catalyzes ATP hydrolysis promoting motor activity and movement of myosin III along the actin filaments (Fig. 1-1 a, c). This motor domain contains several consensus sequences that predict ATP and actin-binding sites and a conserved region known to involve conformational movements

(Dosé and Burnside, 2000). The neck region (Fig. 1-1a, c) contains IQ domains and is believed to act as a 'lever arm' of the power stroke of myosin III (Rayment *et al.*, 1993; Uyeda *et al.*, 1996; Dosé *et al.*, 2003). These IQ domains contain calmodulin-binding sites described earlier.

The diversity of C-terminal tails of unconventional myosins are reflected by divergent amino acid sequences, a variety of tail lengths, and the presence of various functional domains implicated in a number of functions including anchoring the actin filament, dimerization, and binding cargoes (Foth *et al.*, 2006). The tail region of myosins IIIa and IIIb encompasses a conserved domain called tail homology domain I (3THDI; Fig. 1-1a, c; Dosé *et al*., 2002). The function of this ~60 amino-acid long 3THDI (Lin-Jones *et al*., 2004) has been unclear. The tail region of myosin IIIa also has a C-terminal conserved domain, 3THDII that is ~22 amino acids long. At the end of this C-terminal 3THDII presents a consensus actin-binding site, DFRXXL (Smith *et al.*, 1999). 3THDII is required for actin filament binding activity *in vitro* and colocalizes with the actin filaments in HeLa cells (Les Erickson *et al*., 2003). A point mutation in 3THDII disrupted targeting of striped bass myosin IIIa to filopodia tips in the transfected HeLa cells (Les Erickson *et al*., 2003) but not to the photoreceptor calycal processes in frog (Lin-Jones *et al*., 2004), or targeting of a human myosin IIIa to the stereocilia tips in rodents (Schneider *et al*., 2006).

Unlike many other myosins, myosins IIIa and IIIb are probably monomeric in that they are single-headed molecules. No coiled-coil region has been predicted in the tail of these molecules. A gel filtration chromatography analysis, a size exclusion

chromatography technique often used instead of the gel electrophoresis to preserve quaternary protein structures (Eisenstein, 2006), showed no sign of dimerization of the myosin IIIa molecules (Komaba *et al.,* 2003). The walking mechanism of myosin IIIa is unknown (Dosé *et al.*, 2007a), but there is speculation suggesting that the 3THDII domain tethers myosin IIIa to the actin filament (Les Erickson *et al*., 2003) while the single-headed motor domain is taking a step on the actin filament (Kambara *et al*., 2006). The kinetic mechanism of myosin IIIa has been examined by several investigators. Although there is some contradiction in their conclusions, the current consensus is that myosin III has a high affinity for actin (K_{actin} = 7 μM), has a high duty ratio, behaves as a processive motor that stays associated with the actin bundles for a relatively long time in the actomyosin-ADP state (Dosé *et al.*, 2007a; Kambara *et al.*, 2006). These studies used human myosin IIIa. Detailed analyses of myosin IIIb kinetics should be pursued in future research.

1.2.8 Espin isoforms in stereocilia

The actin core is a tight bundle of polarized actin filaments found to be cross-linked by at least two actin cross-linkers: espin and fimbrin (Tilney *et al.*, 1989; reviewed by Manor and Kachar, 2008). Fimbrin, a member of the plastin/α-actinin family, is probably calcium sensitive (Glenney *et al.*, 1981; Daudet and Lebart, 2002) whilst espin is not (Bartles *et al.,* 1998; Chen *et al.*, 1999). Espin was given its name based on its immunolocalization (i.e. *e*ctoplasmic *sp*ecialization + in) by Bartles *et al.* (1996) when it was initially found in the actin-containing ectoplasmic region between Sertoli and maturing sperm cells in rodent testes. Espin mediates actin bundling and microvillar

elongation in several cell types (Bartles *et al.*, 1998; Chen *et al.*, 1999; Loomis *et al.*, 2003; Sekerková *et al.*, 2004; Rzadzinska *et al.*, 2005). A total of six identified espin splice isoforms, 1, 2A, 2B, 3A, 3B, and 4, are encoded by a single *Espn* gene (NCBI accession number NC_000070) in the mouse genome (Chen *et al.,* 1999; Loomis *et al*., 2006). Protein expression of espin isoforms, 1, 2B, 3A, and 4 isoforms in hair cells was reported (Zheng *et al*., 2000; Sekerková *et al*., 2006a). Recent research indicates that these espin isoforms are localized to the stereocilia along the actin core and are key molecular players in hair cell differentation, morphogenesis, maturation, and maintenance (Li *et al*., 2004; Rzadzinska *et al.*, 2005; Sekerková *et al*., 2006b).

1.2.9 Mutations in *ESPN* are linked to deafness and vestibular dysfunction

The human *ESPN* gene is mapped to chromosome 1q36.3-p36.1 (Naz *et al.*, 2004). Several mutations in both *ESPN* and mouse *Espn* genes have been linked to autosomal recessive (Zheng *et al.*, 2000; Naz *et al.*, 2004; Boulouiz *et al.*, 2008) *DFNB30* as well as autosomal dominant (Donaudy *et al.*, 2006) inheritance patterns of deafness and/or vestibular dysfunction. Naz *et al.* (2004) reported two *ESPN* recessive mutations prevailing in two consanguineous Pakistani families, in which affected subjects were inherited with deafness and imbalance. Each of these naturally occurring mutations have a distinct frameshift 4-bp deletion (1988delAGAG or 2469delGTCA) that leads to a protein truncation that affects the actin bundling module (ABM), a key functional domain for actin bundling and elongation activities (Loomis *et al.*, 2003; Loomis *et al.,* 2006). A single point, frameshift deletion mutation in the *Espn* gene of *jerker* mice, that affects the same C-terminal ABM shared by other espin isoforms, leads to stereocilia degeneration,

vestibular dysfunction, and deafness (Donaudy *et al*., 2006; Loomis *et al.*, 2006; Naz *et al.,* 2004; Rzadzinska *et al*., 2005; Zheng *et al*., 2000). The behavioral phenotype of this mutation in *jerker* mice is circling movements, head tossing (Grüneberg *et al*., 1941), and poor swimming performance (Jones *et al.*, 2005) which bears resemblance to the phenotypes of *Snell's waltzer* and *shaker* mice. The deaf *jerker* has shorter, thinner stereocilia at P0 in both vestibular and cochlear tissues (Rzadzinska *et al*. 2005; Sjöström and Anniko, 1992a) associated with motor abnormalities and dysequilibrium (Sjöström and Anniko, 1992b). Furthermore, there are indications that while these *jerker* mice have normal espin mRNA levels, they lack functional espin proteins (Loomis *et al*., 2006; Zheng *et al*., 2000).

Donaudy *et al.* (2006) identified another four *ESPN* mutations, i.e. three missense mutations (2155A→C, 2230G→A, 2321G→A) and one deletion (2541-2543delAAG), that were associated with autosomal dominant deafness. The majority of patients in their study came from Italy, while others were from Spain, Belgium, and Israel. Affected patients with the 2155A→C mutation show progressive sensorineural deafness that starts in the second decade and, by age forty, moderate deafness. Their high frequencies were mainly affected. The 2230G→A mutation causes severe sensorineural deafness including all frequencies. One patient that has the 2321G→A mutation, had a late onset deafness in all frequencies beginning at age 42. The 2541-2543delAAG mutation leads to congenital severe deafness. All these four mutations do not lead to any detectable vestibular problems (Donaudy *et al.*, 2006).

More recently, a novel mutation that leads to an autosomal recessive form of deafness without vestibular involvement has been reported in a Moroccan family. This mutation is caused by a 1-bp insertion, 1757insG, which is predicted to induce a frameshift and a premature truncation of the protein after 71 erroneous amino acids (Boulouiz *et al.*, 2008). This truncation renders the protein, if expressible, without the conserved C-terminal ABM and another functional domain, WH2, implicated in actin polymerization and bundling activity (Loomis *et al.*, 2006).

1.2.10 Expression patterns of espins

In contrast to eukaryotic myosins, NCBI database searches and literature suggest that the evolution of espin is relatively recent. To date, no espin orthologues with significant homology have been reported in invertebrates or lower organisms (Sekerková *et al.*, 2004). On the other hand, the expression of espins associated with actin bundles is prominent in various vertebrate cell types. Espin is expressed in the actin-rich junctional plate of the Sertoli cell/spermatid in the rat testis (Bartles *et al.*, 1996), in the principal cells of the adult rat epididymis (Primiani *et al*., 2007), in the microvilli of the brush border epithelial cells in rat intestine and kidney (Bartles *et al.*, 1998), in the developing (E15-E20) rat lacrimal gland and lung (Sekerková *et al.*, 2006), in the rat type I spiral ganglion neurons, in the synapses in the rat cochlear nucleus, and in the differentiating mouse bone marrow stem cells (Jeon *et al.*, 2007) inoculated with *Math1*, a transcription factor known to promote hair cell differentiation (Kawamoto *et al.*, 2003). Moreover, espin expression has been detected in microvilli of many sensory cells including in the rat and mouse stereocilia of inner ear hair cells (Rzadzinska *et al.*, 2005), in the calycal

processes of photoreceptors (Based on personal communication with Andrea Dosé), the vomeronasal organ sensory neurons, solitary chemoreceptor cells, palatal taste buds, and Merkel cell mechanoreceptors (Sekerková *et al*., 2004). Moreover, espins are predicted to express in pufferfish (*Tetraodon nigroviridis*; NCBI accession number CAG03205), zebrafish (XP_695442), gray short-tailed opossum (*Monodelphis domestica*; XP_001365671), chicken (XM_417532), dog (XP_543304), cattle (XP_602703), and chimpanzee (XP_514338).

An *ex vivo* experiment was conducted on Sertoli cells to examine actin dynamics under a deprivation of male gonadotrophic hormones, testosterone and follicle-stimulating hormone (FSH) following the removal of rat pituitary gland—a procedure called hypophysectomy. The Sertoli cells are the only cells in the seminiferous epithelium that express receptors sensitive to testosterone and FSH necessary to maintain adhesion to the developing spermatids. Downregulation of the espin expression was observed in parallel to a decrease in the amount of polymerized actin within the Sertoli cell from the hypophysectomized rats. This result putatively suggests that the actin bundles of ectoplasmic specialization are disrupted following the surgery due to a concomitant decrease in espin levels and therefore a decrease in the cross-linking activity and polymerization (Show *et al*., 2004).

1.2.11 Espin 1 is the largest espin isoform

The *espin* mRNA variant 1 encodes the largest protein isoform (espin 1; NCBI accession numbers: NM_031475 [human], NM_207687 [mouse], U46007 [rat]) identified to date, with a molecular weight of ~110 kDa (Bartles *et al.,* 1996). The expression of espin 1

has been found in the testes and inner ear and is the only espin isoform that contains a predicted domain of eight or more ankyrin repeats (reviewed by Bartles, 2000) that extend approximately 300 amino acids at the N-terminus (Fig. 1-2a; Bartles *et al.,* 1996*;* Chen *et al.*, 1999; Lee *et. al.*, 2006; Loomis *et al.,* 2003; Sekerková *et al.*, 2004; SMART, accessed October 2007).

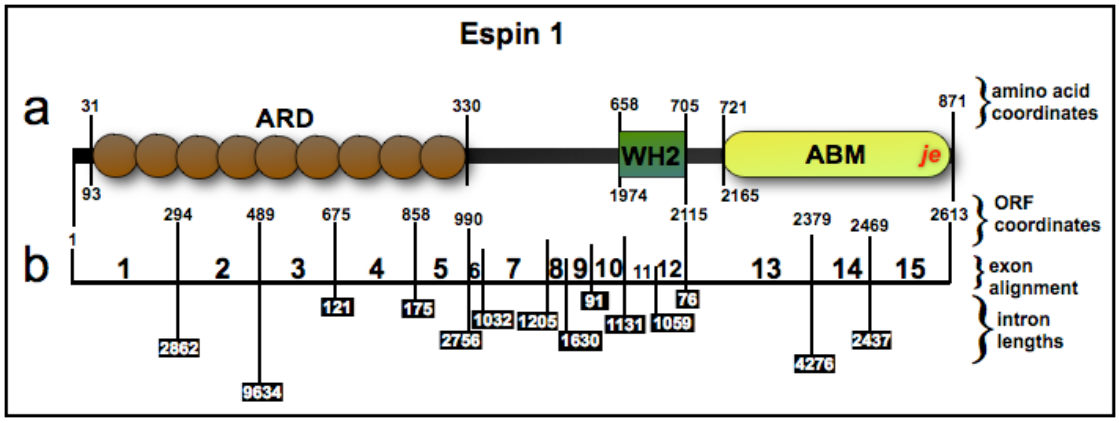

Figure 1-2 Molecular map of espin 1*. (**a**) Schematic diagram of mouse espin 1 (NCBI accession number NM_207687) illustrating orientation of the functional domains. Polypeptide amino acid (aa) and open reading frame (ORF) nucleotide (nt) coordinates are displayed (top and bottom, respectively). The aa coordinates are predicted by SMART. The ankyrin repeat domain (ARD), located at the N-terminus, is a ~300 aa long predicted between amino acid position 31 and 330. Wiskott–Aldrich syndrome protein (WASP) homology 2 (WH2; Chereau *et al.*, 2005) is located at amino acid positions 658 and 705. The C-terminus contains two actin-binding sites, which make up the actin bundling module (ABM; aa positions 722 and 871). '*Je'* denotes roughly the position of the single point mutation at the ABM that causes the phenotype of the deaf *jerker* mouse. (**b**) Coarse predicted exon alignment of the espin 1 above with illustrations of intron lengths (black boxes) between the exons. Exons 1-5 encode ARD. Exons 11 and 12 encode the WH2. Exons 13-15 encode the ABM. See text for further details. *Not to scale. **Use NCBI Spidey or elsewhere for precise alignment.

The exact function of the ankyrin repeats domain (ARD) of espin 1 is unclear. Although, homologues to this protein domain have been well characterized in which peptide sequences and structures appear to be evolutionarily conserved dating back to early eukaryotes (reviewed by Bennett and Baines, 2001; Mosavi *et al*., 2002; Mosavi *et al*., 2004; Sotomayor *et al.*, 2005). The term, ankyrin, is derived from the protein, erythrocyte ankyrin, which was first cloned from an immature erythrocyte cDNA library (Lux *et al.*,

1990). These proteins containing ankyrin repeats have been localized to membrane skeleton and found to interact with a membrane associated anion exchanger and with the cytoskeletal protein, spectrin (Bennett and Baines, 2001; Hryniewicz-Jankowska *et al*., 2002; Lambert and Bennett, 1993).

1.2.12 Functional domains of espin 1 and other espin isoforms

ABM in espin 1 and all other espin isoforms contains two actin-binding sites that participate in *in vitro* and *in vivo* actin-bundling activities (Bartles *et al.*, 1998; Chen *et al.*, 1999; Loomis *et al.*, 2003). Espin isoforms' role in cytoskeletal processes is influenced by various combinations of highly conserved domains at the upstream of the ABM. For instance, all espin isoforms except isoform 4 contain two proline-rich regions that mediate interactions with IRSp53 (insulin receptor substrate p53; a cytoskeletal protein adaptor; Loomis *et al.,* 2006; Sekerková *et al*., 2003) and profilin, a distinct actin-binding protein, (Sekerková *et al*., 2004). These isoforms also have an extra actin-binding site which may enhance actin-bundling activity in conjunction with ABM (Chen *et al*., 1999). All espin isoforms have the WH2 (Wiskott–Aldrich syndrome protein [WASP] homology 2) domain in which it binds ATP-actin monomers and participates in assembling actin filaments (Loomis *et al*., 2003; Naz *et al.*, 2004; reviewed by Takenawa and Suetsugu, 2007). This WH2 domain predicts a glycine-rich consensus sequence called P-loop motif (phosphate-binding loop; GXXXXGK[TS]) that commonly interacts with the phosphate groups of ATP or GTP (Bartles *et al*., 1996; Saraste *et al.*, 1990; Walker *et al*., 1982), suggesting that WH2 binds to ATP-bound actin through the P-loop motif.

Proteins equipped with ankyrin repeats are frequently found to mediate protein-protein or membrane-protein interactions (Bartles *et al.*, 1996; Bennett and Baines, 2001; Lin *et al.,* 1999*;* Matsuno *et al.,* 1997; Mosavi *et al*., 2002, 2004; Sedgwick and Smerdon, 1999; Witt *et al.*, 2005). Each ankyrin repeat is about 30-33 amino acids long (e.g. compare literature with SMART protein sequence alignments) with a mixture of conserved and non-conserved residues. Research has indicated that the conserved residues make up the backbone of ARD and the non-conserved regions have a tendency to serve as binding sites at the exterior interface (Mosavi *et al.*, 2002). NMR and X-ray crystallography studies indicate that ARD contains antiparallel α-helices that stack to form a "superhelical spiral" (Lee *et al.*, 2006; Mosavi *et al.*, 2002; Sotomayor *et al*., 2005). Atomic force microscopy data also indicate that ARD elicits spring-like behavior (Lee *et al.,* 2006; Li *et al.*, 2006). These observations are consistent with the postulation that one of general functions of ARD, owning to its elasticity, is to sustain mechanical stresses and deformations experienced by eukaryotic cells (Bennett and Baines, 2001; Li *et al.*, 2006; Witt *et al*., 2005).

The tips of the tallest stereocilia of OHCs interact with the tectorial membrane through the connecting extracellular matrix, in which they experience high, recurrent shear stresses amid the basilar membrane vibrations and stereocilia deflections. The tethering tip links between stereocilia pull membranes upon stereocilia deflections and occasionally cause membrane tenting (Assad *et al.*, 1989; Furness and Hackney, 1985; Kachar *et al.*, 2000; Pickles *et al.*, 1991). Espin 1^{ARD} might be a good candidate as an absorber to sustain such stereocilia tip mechanical stress. Espin 1^{ARD} could also be a

structural scaffold (reviewed by Mosavi *et al.*, 2004) for protein-protein interactions at the stereocilia tips.

Taken together, espins are not merely cross-linking proteins but rather multifunctional actin regulatory proteins in the sensory epithelia.

1.2.13 Colocalization and functional interactions between class III myosins and espin 1

The original impetus for this dissertation research on class III myosins and espin 1 in the stereocilia came from the finding that the espin 1 immunolocalization and temporal expression pattern at the stereocilia tip was virtually identical to that of myosin IIIa. Confocal images of optical sections across the tips of stereocilia clearly show the same thimble-like pattern of immunolabeling, using the anti-espin 1 or anti-myosin IIIa antibody. This finding was unprecedented since espin 1 localizes to the new compartment at the tip in contrast to other espin isoforms that are present inside the actin core and along the entire stereocilia length (Rzadzinska *et al.*, 2005). Espin 1 is different from other isoforms due to its N-terminal ARD, which suggests that this domain is involved in the localization of espin 1. These observations raised questions whether these proteins interact and if they, together, play a role in the structure and function of stereocilia.

Both myosin IIIa and espin 1 are implicated in sensorineural deafness (Walsh *et al.*, 2002; Naz *et al.*, 2004) and shown to influence stereocilia length (Schneider *et al.*, 2006; Rzadzinska *et al.*, 2005). When rat VHCs were co-transfected with engineered myosin IIIa and espin 1 plasmid DNA constructs, these two proteins colocalized to the stereocilia tips and promoted significant elongation of the stereocilia length ($P = 0.002$, ANOVA). This observation was reproducible when these two constructs were co-

expressed in heterologous COS-7 fibroblasts, in which the elongation of filopodia appeared more dramatic. The disparity in the lengthening of actin protrusions between these two cell types was no surprise since the actin treadmilling rate is faster in filopodia than in stereocilia (reviewed by Manor and Kachar, 2008).

Espin 1 and all other espin isoforms identified to date possess ABM and the actin-monomer binding domain, WH2. This WH2 domain is believed to be responsible for elevating local concentration of polymerizable actin monomers (Loomis *et al.*, 2006). Live-cell images on COS-7 cell filopodia co-transfected with myosin IIIa and espin 1^{ARD} constructs show that these two proteins actively co-transport during the formation and extension of filopodia. Biochemical assays using the GST pulldown technique have confirmed that these two proteins interact. Espin 1 is the first cargo shown to be transported by myosin IIIa. These two proteins, together, elicit a powerful, synergistic elongation of both stereocilia and filopodia. We hypothesized that the mechanism underlying this synergistic elongation is due to the transport of the actin-polymerizing factor, espin 1, toward the stereocilia tip by myosin IIIa.

Since there is no explanation why *DFNB30* individuals with a homozygous mutation in the *MYO3A* gene have had a normal ability to hear for the first twenty years and progressively become deaf from that point and on, we sought answers to whether myosin IIIb, the other member of class III myosins with a shorter tail, compensates for loss of myosin IIIa function. Our anti-myosin IIIb antibody, which only cross-reacts with mouse myosin IIIb but not rat or human myosin IIIb, revealed that myosin IIIb is also localized to the same compartment as myosin IIIa and espin 1 in the mouse inner ear hair

cell stereocilia. However, we found that the temporal expression of myosin IIIb differs. Myosin IIIb showed a peak of immunofluorescence around age P0, while myosin IIIa and espin 1 have the peak at age P8. Furthermore, we found that myosin IIIb cannot self-localize to the tips of filopodia due to the lack of actin-binding 3THDII in the tail. Myosin IIIb rather depends on espin 1 for the tip localization. Taken together, we postulate that myosin IIIb compensates for myosin IIIa in the function of hearing during the development and maturation, but not everlasting maintenance, of stereocilia.

Chapter 2: Myosin IIIa Boosts Elongation of Stereocilia by Transporting Espin 1 to the Plus Ends of Actin Filaments

2.1 Abstract

Two proteins implicated in inherited deafness, myosin IIIa (Walsh *et al*., 2002), a plus-end-directed motor (Komaba *et al*., 2003), and espin (Donaudy *et al*., 2006; Naz *et al*., 2004; Sekerková *et al*., 2006; Zheng *et al*., 2000), an actin-bundling protein containing the actin-monomer-binding motif WH2, have been shown to influence the length of mechanosensory stereocilia (Rzadzinska *et al.*, 2005; Schneider *et al*., 2006). Here we report that espin 1, an ankyrin repeat-containing isoform of espin (Sekerková *et al*., 2006), colocalizes with myosin IIIa at stereocilia tips and interacts with a unique conserved domain of myosin IIIa. We show that combined overexpression of these proteins causes greater elongation of stereocilia, compared with overexpression of either myosin IIIa alone or espin 1 alone. When these two proteins were co-expressed in the fibroblast-like COS-7 cell line they induced a tenfold elongation of filopodia. This extraordinary filopodia elongation results from the transport of espin 1 to the plus ends of F-actin by myosin IIIa and depends on espin 1 WH2 activity. This study provides the basis for understanding the role of myosin IIIa and espin 1 in regulating stereocilia length, and presents a physiological example where myosins can boost elongation of actin protrusions by transporting actin regulatory factors to the plus ends of actin filaments.

2.2 Introduction

Stereocilia, the prominent actin protrusions on the apical surfaces of sensory hair cells, emerge early during development. Their lengths are maintained at fixed heights for the lifetime of the organism. The bundle of parallel actin filaments that make up the core of each stereocilium is continually renewed, with the entire actin bundle constantly assembled at the tip, treadmilling downward, and disassembling at the base (Lin *et al.*, 2005; Rzadzinska *et al.*, 2004; Schneider *et al.*, 2002). Given that stereocilia can be up to 100 μm in length, it is likely that some form of regulated transport is necessary to localize components of the actin polymerization machinery to the plus end of actin filaments. Although several myosins have been shown to alter stereocilia length and shape depending on their expression levels (Belyantseva *et al.*, 2005; reviewed by Manor and Kachar, 2008; Prosser *et al.*, 2008; Rzadzinska *et al.*, 2004; Tokuo and Ikebe, 2004; Tokuo *et al.*, 2007), the mechanisms by which these motors or their binding partners regulate actin dynamics and stereocilia length remain unclear.

2.3 Materials and Methods[i]

2.3.1 Antibodies

Affinity-purified polyclonal antibodies (PB538 and PB539) were developed in rabbits immunized with a synthetic peptide (Princeton Biomolecules) corresponding to the amino acid sequence (LDALPVHHAARSGKLHCLR) of the first ankyrin repeat of mouse espin 1. A similarly raised antibody specific for a region conserved in all isoforms

[i]Dr. Felipe T. Salles and I contributed equally to the work. I designed DNA probes and experiments, performed cell culture, immunocytochemistry, transfections, confocal imaging, the GST pulldowns, Western blot, and data processing. Dr. Salles performed dissections, tissue culture, immunohistochemistry, transfections, and confocal imaging. Other investigators assisted with probes, electron microscopy, transfections, imaging, ATPase assays, and statistical analyses. Results were published in the *Nature Cell Biology* journal, volume 11, issue 4, pp. 430-450. (Salles, Merritt, *et al.*, 2009).

of espin (pan-espin, PB127; Rzadzinska *et al*., 2005 and anti-myosin IIIa (PB638; Schneider *et al*., 2006) antibodies have been previously described.

2.3.2 Immunofluorescence and microscopy

After CO_2 anaesthesia, rats, mice and guinea pigs were euthanized in accordance with National Institutes of Health (NIH) guidelines, and their temporal bones fixed by immersion in 4% paraformaldehyde in phosphate buffered saline (PBS; pH 7.4) for 2 h at room temperature. Sensory tissue was dissected in PBS, permeabilized with 0.5% Triton X-100 for 30 min and blocked overnight at 4 °C with 4% bovine serum albumin in PBS. Tissues were then incubated with primary antibody for 2 h, rinsed with PBS, stained with Alexa Fluor 488-conjugated secondary antibody (Molecular Probes) for 1 h, counterstained with Alexa Fluor 568 phalloidin (0.001 U μl^{-1}; Molecular Probes) and mounted using Prolong Antifade (Molecular Probes). Fluorescence confocal images were obtained with a Nikon microscope equipped with a×100 1.45 numerical aperture (NA) objective and a spinning disk confocal unit (PerkinElmer).

2.3.3 Electron microscopy

Rat organ of Corti or vestibular tissues were either rapidly frozen by contact with a liquid nitrogen cooled metal block in a LifeCell (The Woodlands) freezing apparatus or fixed, glycerinated and plunge-frozen in Freon 22 cooled in liquid nitrogen before freeze-substitution in 1.5% uranyl acetate in absolute methanol at –90 °C. Freeze-substituted tissues were infiltrated with Lowicryl HM-20 resin (Electron Microscopy Sciences) at –45 °C, polymerized with UV light, thin-sectioned and labelled with immunogold. Samples were viewed and photographed with a Zeiss 922 electron microscope. As control

for the immunogold labeling, we also used the antibody PB288, which is unrelated to espin or to myosin IIIa (Fig. 2-1d).

2.3.4 Expression plasmids

Espin 1 (NCBI accession number NM_031475) in pSPORT1 vector was obtained from imaGenes and PCR-cloned into pEGFP-C2 (Clontech) and pcDNA3.1(–) (Invitrogen) through *Eco*RI and *Kpn*I sites. The site-directed leucine to alanine mutations in the WH2 motif of espin 1 were generated using a GeneTailor site-directed mutagenesis kit (Invitrogen). The ARD between amino acid positions 16 and 363 was PCR-amplified using the mouse espin 1 template (NM_207687) and subcloned in-frame into the mCherry-C1 (Clontech) expression vector through *Xho*I and *Eco*RI sites, and pDEST 15 GST expression vector (Invitrogen) using the Gateway LR Clonase cloning method (Invitrogen). The GFP-tagged expression plasmids used were espin $1^{\Delta ARD}$ (a gift from James Bartles, Northwestern University, Chicago, IL), myosin X (a gift from Richard Cheney, UNC, Chapel Hill NC), myosin XVa (a gift from Thomas Friedman, NIDCD/ NIH), as well as full-length and deletion constructs of myosin IIIa that were generated in our laboratories. Myosin IIIa $2IQ^{\Delta K}$ constructs were generated as described previously (Dosé *et al.*, 2008; Dosé *et al.*, 2007a). Myosin IIIa $2IQ^{K50R}$ and myosin $IIIa^{K50R}$ constructs were generated by performing site-directed mutagenesis on the myosin IIIa 2IQ and myosin IIIa full-length constructs, respectively. All expression plasmids were sequence verified. Further details about the clones used are available in Table 2-2, Figures 2-6, and 2-8.

DNA construct (aa)	Species (accession no.)	Vector	Forward primer	Reverse primer
GFP-myoIIIa $^{\Delta 32}$ (1-1479)	human (AY101367)	pEGFP-C1	5′-GCTAGGATCCCACCATGTTTCCATTAATTGGAAAAACAATCATC	5’-GTCTGCGGCCGCGTGCCTGCTGGTGCCAGCCCC
GFP-myoIIIa $^{\Delta K,33}$ (21-1515)			5’-GCTAGGATCCGTAGATGATTTAGCAACCCTAGAAGTTTTGGATG	5’-GTCTGCGGCCGCGTGCCTGCTGGTGCCAGCCCC
GFP-myoIIIa ^{K50R} (1-1616)			5’-GCTAGGATCCCACCATGTTTCCATTAATTGGAAAAACAATCATC	5’-GTCTGCGGCCGCGGACTGCTGGACGAGGCGCCG
GFP-IIIa tail$^{\Delta 3THDII}$ (1376-1594)			5′-CGTAGGATCCGCATCAGAGGATTGTCACAACACCAACAGAAGTAGC	5′-GAGAGAGAGCCAGCAGCCACCCCCTACTAAGCGGCCGCATCG
GFP-IIIa^{pre3THDI} (1376-1491)			5′-CGTAGGATCCGCATCAGAGGATTGTCACAACACCAACAGAAGTAGC	5′-CTCAGGTGTCTGTAAAGGAGAGGAGCCAAAAATATTGAGAGCGGCCGCATCG
GFP-IIIa^{3THDI} (1492-1561)			5′-CGTAGGATCCCCCCCAAGACGACCCCGGAAACCCAAAAC	5′-CGATGCGGCCGCTCTTCGTTCTCTTAAACTAGGGCTATGTTCCTTTGGTCCAG
GFP-IIIa^{post3THDI} (1562-1595)			5′-CGTAGGATCCCCACAGCAAGAACTCCAGAATCAATGTATTAAGGCTAATG	5′-GAGAGAGAGCCAGCAGCCACCCCCTACTAAGCGGCCGCATCG
GFP-IIIa 3THDI$^{\Delta 33}$ (1492-1525)		pcDNA 6.2/N-EmGFP-DEST	5′-CGTAGGATCCCCCCCAAGACGACCCCGGAAACCCAAAAC	5′-CGCTGGTCTTCGTTTTTCTTCTTG
myoIIIa^{K50R} 2IQ (1-1143)		pEGFP-C1	5’-GCTAGGATCCCACCATGTTTCCATTAATTGGAAAAACAATCATC	5’-GCTACGCCGGCGAATGAATTCCTGATCAGAAGTTTGAATGGTTGTTACTGCTGTG
V5-IIIa^{3THDI} (1492-1553)	mouse (AY101368)	pcDNA/ nV5-DEST	5′-CCTCCAAGACGACCTCGGAAA	5′-TTATTTCCATTCTCTTGCATTAGAGCT
mCherry-espin 1^{ARD} (16-363)	mouse (NM_207687)	pmCherry-C1	5′-GACGTGCTGAGGTCCCTGC	5′-TTAGACCGACATGGTGGTGTTGG
GST-espin 1^{ARD}		pDEST^{TM}15		
GFP-espin 1^{ARD}		pcDNA 6.2/N-EmGFP-DEST		

Table 2-1 Novel myosin IIIa clones and associated primers used in the dissertation.

2.3.5 Cultures and transfection of COS-7 cells

COS-7 (American Type Culture Collection [ATCC], Manassas, VA) cells were trypsinized and plated on coverslips and maintained at 37 °C in Dulbecco’s Modified Eagle Medium (DMEM) with 10% fetal bovine serum (FBS). Cultures were transfected using GeneJuice transfect reagent (Novagen, EMD Chemicals, Inc, Gibbstown, NJ) and incubated for 24 h. Time-lapse videos of live cells were acquired at the maximum nominal laser power and camera gain allowed by the confocal microscope. Samples were

also fixed for 20 min in 4% paraformaldehyde in PBS, permeabilized for 30 min in 0.5% Triton X-100 in PBS, and counterstained or processed for immunofluorescence as described above.

2.3.6 Culture and transfection of rat inner ear tissue

Organ of Corti and vestibular tissues were dissected from postnatal day 0–4 rats and attached to coverslips previously coated with Cell-Tak (150 μg μl^{-1}; BD Biosciences). Cultures were maintained in DMEM/F12 (Invitrogen) with 5–7% FBS and ampicillin (1.5 μg ml^{-1}; Sigma) and kept at 37 °C and 5% CO_2. For transfections, 50 μg of DNA was precipitated onto 25 mg of 1 μm gold particles and loaded into the Helios Gene Gun cartridges (BioRad). Tissue explants were transfected with the gene gun set at 95 psi of helium and maintained in culture for 18–48 h. Samples were fixed and counterstained for confocal microscope viewing as described above. The efficiency of transfection ranged from 0–9 hair cells per explant.

2.3.7 Image analysis

Image analysis was performed with ImageJ software (NIH). To estimate the relative increase in stereocilia length, we compared the heights of the tallest row of well-preserved stereocilia of cochlear and vestibular hair cells transfected (H_T) with the average height of all their respective neighboring (usually between 3–5) non-transfected cells (H_{NT}) within the field of view of our camera/confocal setup (30 × 45 μm). The average ratio of stereocilia length was calculated as $1 = \frac{H_T}{H_{NT}}$. ANOVA was performed

using MATLAB (Mathworks). Cross-correlation analysis for the intensity plot in Fig. 3 was performed using Microsoft Excel.

2.3.8 Western blotting

100-mm dishes of transfected semi-confluent COS-7 cells were rinsed in PBS and scraped in 160 µl of lysis buffer: PBS, 1% Triton-X, 5 mM DTT, 1 mM Pefabloc, 5 µg ml^{-1} pepstatin A, 5 µg ml^{-1} leupeptin, 2 mM EDTA, 0.2 mM PMSF and 1% mammalian protease inhibitor cocktail (Sigma). After addition of 1× loading sample buffer and dithiothreitol (Invitrogen), samples were boiled and 10 µl of lysates were loaded in 4–12% Bis-Tris minigel (Invitrogen). Western blots were incubated overnight at 4 °C with 4 µg ml^{-1} of the primary antibody. Horseradish peroxidase-conjugated goat anti-rabbit antibodies (Santa Cruz) and ECL chemiluminescence system (Amersham Biosciences) were used for detection.

2.3.9 GST pulldown assays

Protein expressions of glutathione S-transferase (GST) alone or fused to ARD (GST–ARD) were optimized under L-arabinose induction in BL21-AI bacteria (Invitrogen). GST proteins were purified from bacterial extracts using glutathione–Sepharose 4B beads according to the manufacturer's instructions (Amersham Biosciences). GFP–myosin $IIIa^{\Delta K}$, $\_^{pre3THDI}$, $\_^{3THDI}$ and $\_^{post3THDI}$ proteins were extracted from 24-h COS-7 transfectants by brief sonication and 20-min ultracentrifugation at 145,000 g in ice-cold lysis buffer (1% Triton X-100, 5 mM DTT, 150 mM NaCl, 50 mM Tris pH 7.4, 2 mM EDTA, 3 mM Pefabloc SC, 1× Pefabloc [Roche] and 1× mammalian protease inhibitor cocktail [Sigma]). To test for myosin IIIa interactions, the same amount of GST–espin

1^{ARD} or GST alone was bound to 4B beads for 1 h at 4 °C followed by incubation with the GFP-tagged myosin IIIa fragment in CLB for 2 h. The beads were then washed four times with lysis buffer. Bound proteins were separated by electrophoresis on NuPAGE Bis-Tris 4-12% gels (Invitrogen) and analyzed by western blotting using rabbit polyclonal anti-GFP and anti-GST antibodies (Invitrogen).

2.3.10 ATPase assays

The steady-state actin-activated ATPase activity of baculovirus expressed myosin IIIa $2IQ^{K50R}$ and wild-type were assessed in an NADH-coupled assay (Dosé *et al.*, 2008; Dosé *et al.*, 2007a). ATPase activity of fully phosphorylated myosin IIIa was compared with unphosphorylated myosin IIIa after a 60-min incubation at room temperature in the presence and absence of 200 μM ATP, respectively. The kinase activity of the myosin IIIa 2IQ constructs was assayed using 32P-ATP or western blotting with anti-phosphothreonine antibodies (Dosé *et al.*, 2008; Dosé *et al.*, 2007a).

2.4 Results

2.4.1 Espin 1 and myosin IIIa localized to tips of stereocilia of inner ear hair cells

Using antibodies specific for the ARD of espin 1 (Fig. 2-1), we show by confocal microscopy that espin 1 is localized at stereocilia tips (Fig. 2-2) with a tip-to-base gradient distribution (Fig. 2-3) similar to that previously described for myosin IIIa.

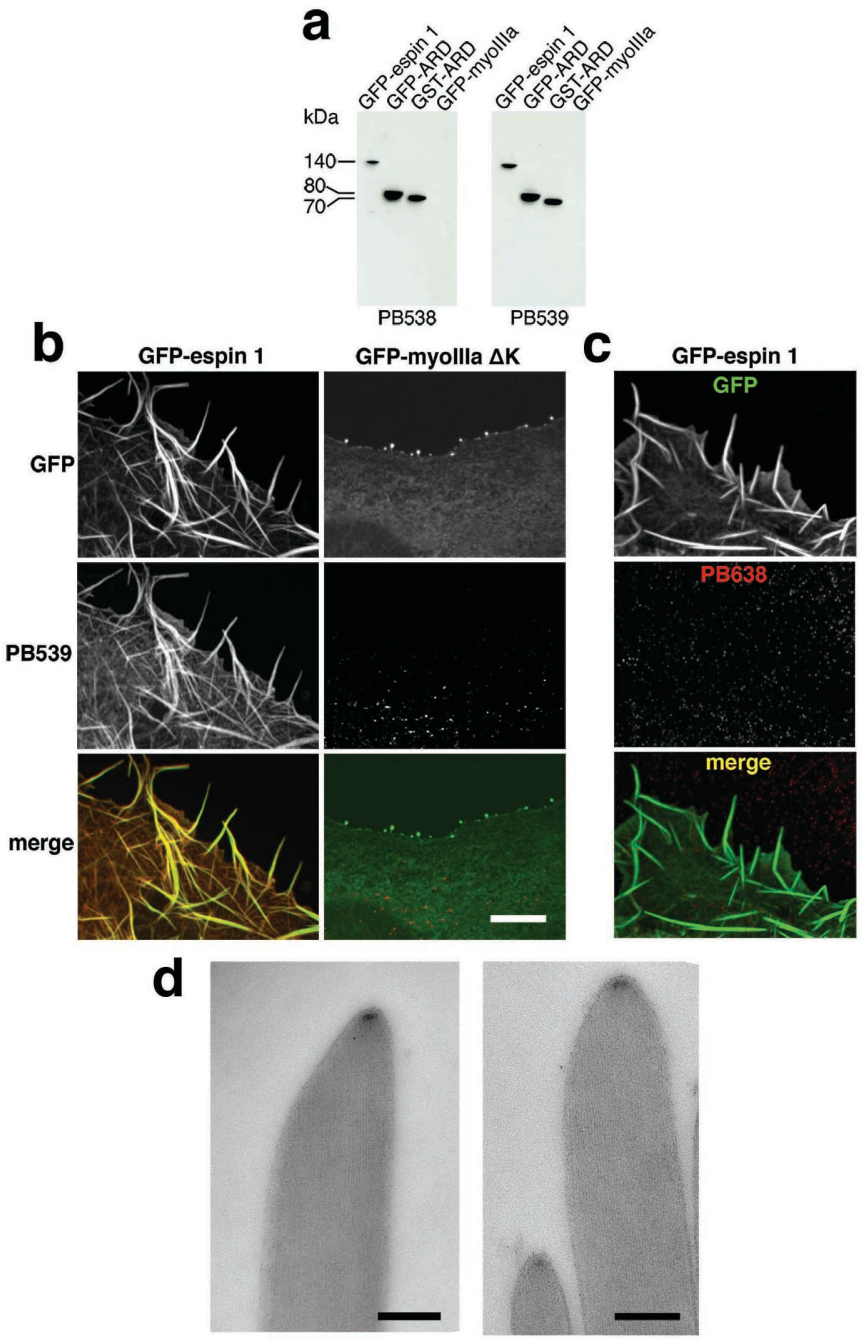

Figure 2-1 Specificity of the antibodies generated against the ARD of espin 1. (**a**) Immunoblots of lysates from COS-7 cells transfected with GFP-espin 1, GFP-espin 1^{ARD}, and GFP-myoIIIa$^{\Delta K}$ as well as lysates from bacteria expressing GST-espin 1^{ARD} show that both PB538 and PB539 specifically recognize the ARD of espin 1. (**b**) GFP-espin 1 (left column) overexpressed in COS-7 cells is recognized by PB539. The same antibody shows no labeling in COS-7 cells with overexpressing GFP-myoIIIa$^{\Delta K}$ only (right column). (**c**) In the negative control, our myosin IIIa specific antibody (PB638) fails to recognize GFP-espin 1 in COS-7 cells. GFP constructs are in green and Alexa Fluor 568-conjugated secondary antibody is red. Scale bar is 5 μm. (**d**) Control experiments for the post embedding immunogold labeling in directly frozen freeze-substituted adult rat cochlear hair cells shows no gold labeling at the tip of stereocilia when using the PB288 antibody, unrelated to espin 1 and myosin IIIa. Scale bars, 200 nm. (Dr. Sousa assisted with Western blotting; Dr. Kachar performed electron microscopy)

Immunofluorescence of espin 1 was more intense in the longer stereocilia where the characteristic tip-to-base fluorescence intensity gradient also had a longer decay length (Fig. 2-3a, b). In contrast to other espin isoforms, which are present inside the actin core and along the entire stereocilia length (Rzadzinska *et al.*, 2005), espin 1 was excluded from the actin cores and formed a thimble-like distribution at the tips of stereocilia (Fig. 2-2g, h). Immunofluorescence in developing hair cells of the rat organ of Corti showed that espin 1 can be detected at the tips of stereocilia during their elongation and maturation phases (Fig. 2-2d–f).

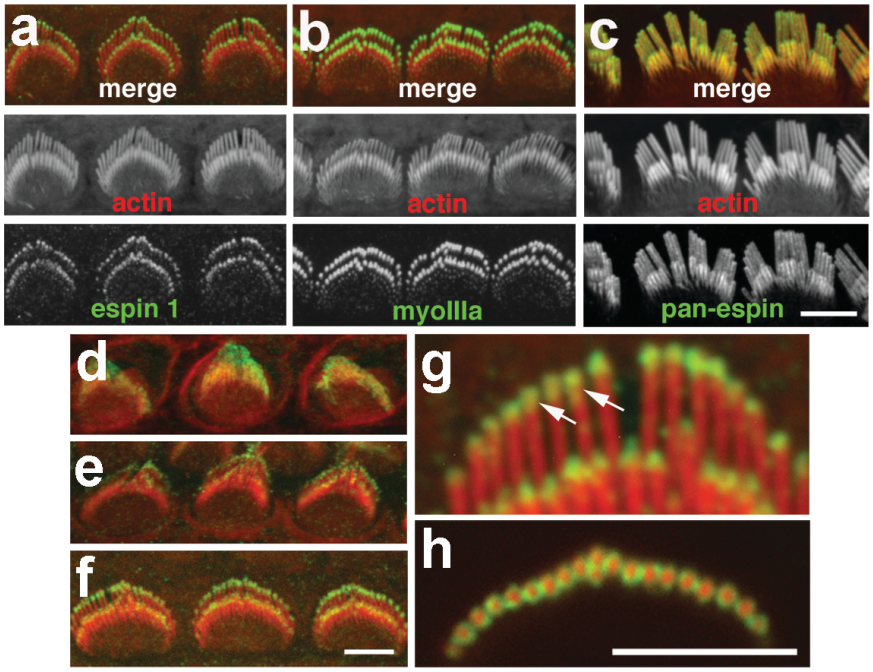

Figure 2-2 Espin 1 distribution in stereocilia is similar to myosin IIIa distribution. (**a–c**) Confocal images show that espin 1 (green, **a**) localized at the tips of stereocilia in rat cochlear hair cells at postnatal day (P) 6 matches the localization observed for myosin IIIa (green, **b**). In contrast, pan-espin labeling (green) is seen along the entire stereocilia (**c**). (**d–f**) Immunofluorescence of rat cochlear hair cells at different developmental time-points shows that espin 1 targets stereocilia tips as early as P0 (**d**) and undergoes progressive compartmentalization at the tips during P2 (**e**) and P4 (**f**), reaching a peak of intensity at about P6 as shown in b. (**g, h**) Longitudinal (**g**) and cross-section (**h**) images reveal a thimble-like distribution of espin 1 (green) at the tips of stereocilia in P8 rat cochlear hair cells. Scale bars, 5 µm. Antibodies: espin 1 (PB539), myosin IIIa (PB638) and pan-espin (PB127). In all immunofluorescence images, the immunolabeling was visualized using Alexa-488-conjugated secondary antibody and F-actin (red) is visualized using Alexa 568-phalloidin. (Dr. Salles assisted with immunohistochemistry)

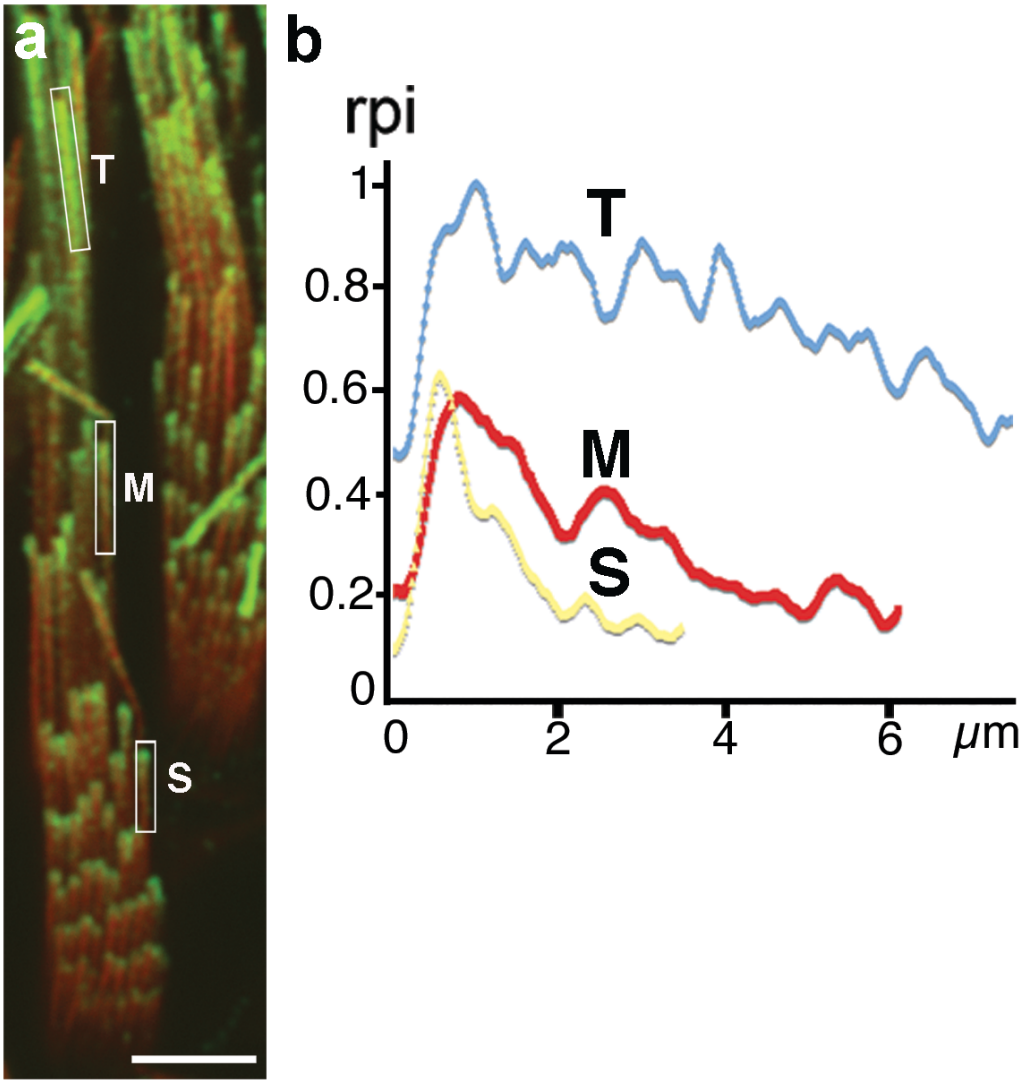

Figure 2-3 Tip-to-base gradient distribution of espin 1 in vestibular stereocilia. (**a**) Espin 1 (green) localization in guinea pig vestibular stereocilia reveals a tip-to-base gradient that is more extended in longer stereocilia (inset T) than medium (inset M) and short (inset S) stereocilia. (**b**) Measurements of green (espin 1) and red (actin) relative pixel intensity (rpi) of fluorescence along the stereocilia for each rectangular inset in g confirm this tip-to-base concentration gradient of espin 1 immunofluorescence. (Dr. Salles assisted with immunohistochemistry)

Immunoelectron microscopy confirms that the localization of espin 1 is confined to the space between the stereocilia actin core and the enveloping plasma membrane (Fig. 2-4a), except perhaps at the very tip of the actin bundle, where there appears to be labeling closer to the center of the core (Fig. 2-4b). we also confirmed pan-espin localization throughout the stereocilia (Fig. 2-4c).

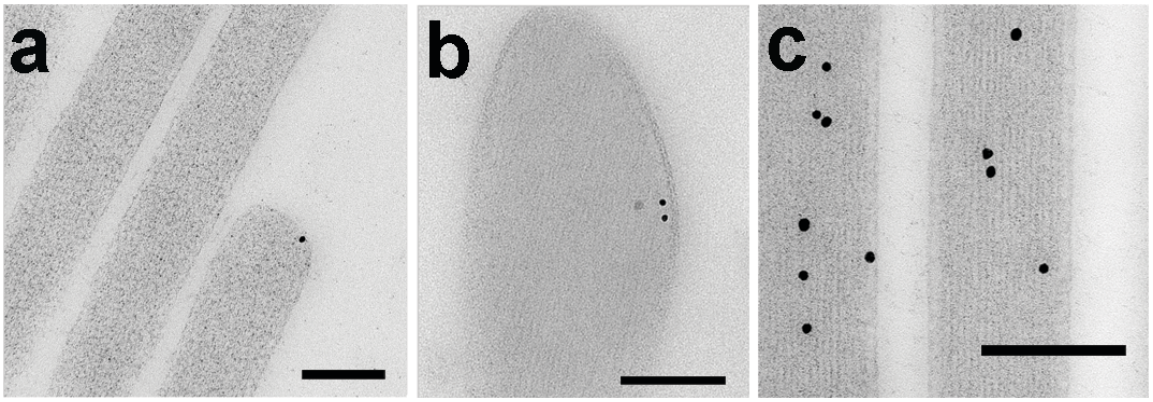

Figure 2-4 Electron micrographs of thin section of rat stereocilia. (**a–c**) Immunogold labelling shows espin 1 localized at the tip of stereocilia around the actin core (**a, b**), whereas labelling with a pan-espin antibody shows localization throughout the entire stereocilia actin cores (**c**) in plunge frozen vestibular (**a, c**) or directly frozen cochlear (**b**) tissues obtained from adult rats. Scale bars, 200 nm. (Dr. Kachar performed electron microscopy)

To confirm the localization of espin 1 at the tips of stereocilia, we overexpressed GFP–espin 1 in organotypic cultures of hair cells. Transfected hair cells show that GFP–espin 1 localizes at the tips of stereocilia, showing a tip-to-base gradient of intensity (Fig. 2-5a, b) comparable to the immunolocalization (Fig. 2-3). These localization patterns — tip-to-base gradients and thimble-like distributions (Schneider *et al*., 2006), as well as the temporal expression pattern (Waguespack *et al*., 2007) — closely match those of myosin IIIa. We hypothesized that targeting espin 1 to stereocilia tips, which is the site of actin polymerization (Rzadzinska *et al*., 2004; Schneider *et al*., 2002), influences actin polymerization and stereocilia elongation. Analysis of the heights of stereocilia of cochlear and vestibular hair cells transfected with GFP–espin 1 showed that stereocilia were elongated when espin 1 was overexpressed (Fig. 2-5g), consistent with our hypothesis.

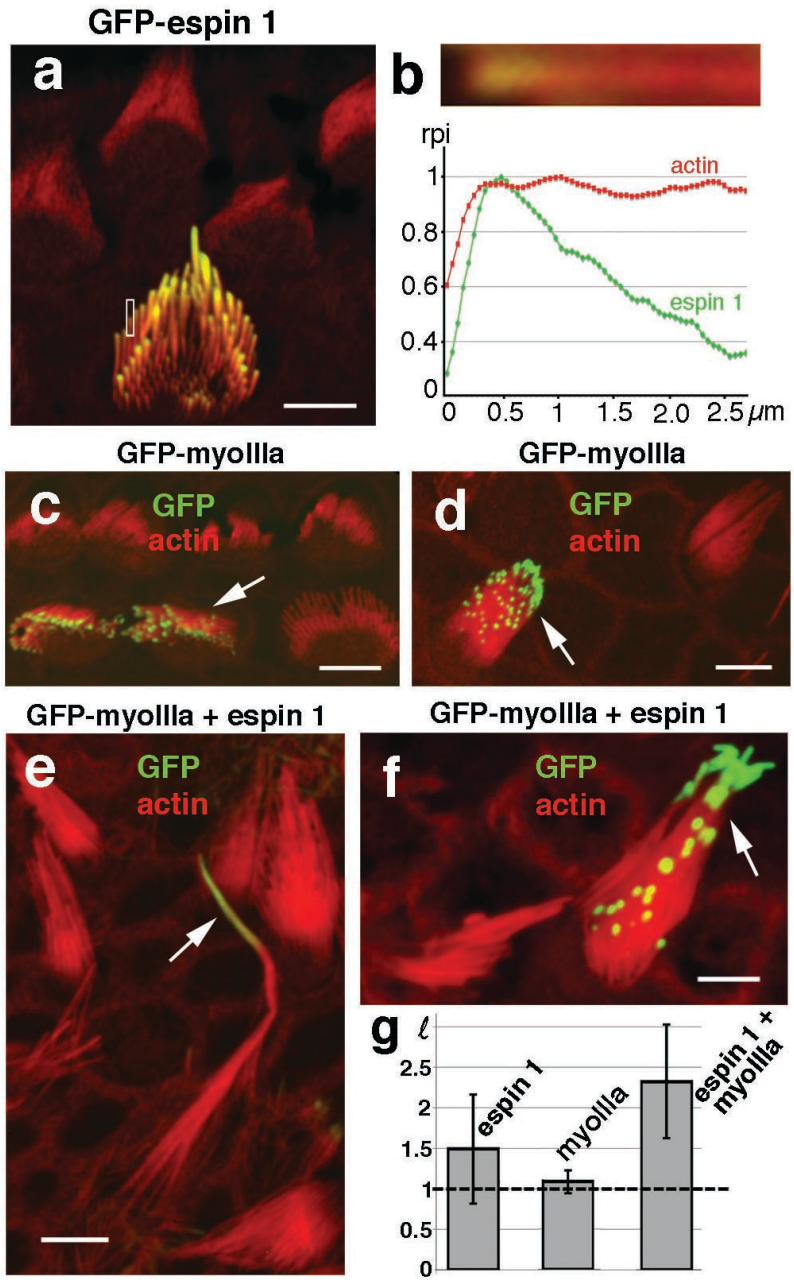

Figure 2-5 Espin 1 alone or when overexpressed with myosin IIIa elongates stereocilia. (**a**) GFP–espin 1 localizes to stereocilia tips in a tip-to-base gradient distribution in transfected cultured organ of Corti hair cells. (**b**) High magnification close-up view (upper panel) and measurement of the relative pixel intensity (rpi, lower panel) of GFP–espin 1 and actin (Alexa 568-phalloidin) fluorescence along the distal portion of the stereocilia shown in the rectangular inset in a matches the tip-to-base concentration gradient observed for endogenous espin 1 (Fig. 1h). (**c–f**) Organ of Corti (**c**) and vestibular (**d**) hair cells transfected with GFP–myosin IIIa show tip localization similar to that of espin 1. Co-transfection of vestibular hair cells with GFP–myosin IIIa (arrow, green) and untagged espin 1 together (**e, f**, images of two different cells) produce longer stereocilia than in hair cells transfected with GFP–espin 1 alone (**a**) or with GFP–myosin IIIa alone (**c, d**). (**g**) The average ratios of stereocilia length (**l**) between transfected (H_T) and neighboring non-transfected (H_{NT}) cells, l = $\frac{H_T}{H_{NT}}$. GFP–espin 1 alone = 1.5 ± 0.67, n = 19 (~50% increase); GFP–myosin IIIa alone = 1.1 ± 0.14, n = 16 (~10% increase); and GFP–myosin IIIa and espin 1 = 2.3 ± 0.69, n = 14, (~130% increase). Note that a value of L = 1 (indicated by the dotted line in the graph) corresponds to a zero percent increase in length. Data are mean ± s.d.; the mean value for the hair cells co-transfected with espin 1 and myosin IIIa was significantly higher than that of the cells transfected with espin 1 alone (P = 0.002, ANOVA); the mean bundle heights for hair cells transfected with myosin IIIa alone were not significantly higher than the controls (P = 0.149, ANOVA). Scale bars, 5 μm. (Dr. Salles and Mr. Manor assisted with transfection and measurements, respectively)

2.4.2 Co-expression of GFP-myosin IIIa and espin 1 enhanced stereocilia elongation in transfected hair cells

The striking similarity of the tip-to-base gradient localization of both espin 1 and myosin IIIa prompted us to investigate whether myosin IIIa helps localize espin 1 to the tips of stereocilia and whether they have a combined role in the regulation of stereocilia length. We compared stereocilia length in hair cells transfected with espin alone, myosin IIIa alone and with a combination of both plasmids (Fig. 2-5). Hair cells transfected with myosin IIIa and espin 1 combined showed an increase in stereocilia length, higher than the increase observed for myosin IIIa alone and espin 1 alone (Fig. 2-5). It is important to note that any analysis of lengthening due to overexpression of myosin IIIa and espin 1 in hair cells must take into account intrinsic limitations due to natural variations in stereocilia length and, importantly, the fact that stereocilia are already quite elongated and express substantial amounts of endogenous espin 1 and myosin IIIa.

2.4.3 Myosin IIIa transported espin 1 to filopodia tips in COS-7 cells

We tested whether myosin IIIa can effectively interact with and transport espin 1 in COS-7 cells, using filopodia as a model to study actin protrusions. Myosin IIIa and espin 1 are not naturally expressed at detectable levels in COS-7 cells (Schneider *et al.*, 2006). Myosin IIIa has been shown to induce filopodial actin protrusions and localize to their tips in cultured cells particularly well when its kinase domain is removed (myosin IIIa$^{\Delta K}$; Schneider *et al.*, 2006; Les Erickson *et al.,* 2003) suggesting that the kinase could serve to downregulate the functional activity of myosin IIIa. We examined the distribution of co-expressed mCherry–ARD of espin 1 (mCherry–espin 1^{ARD}) with GFP-tagged myosin IIIa$^{\Delta K}$ (Fig. 2-6).

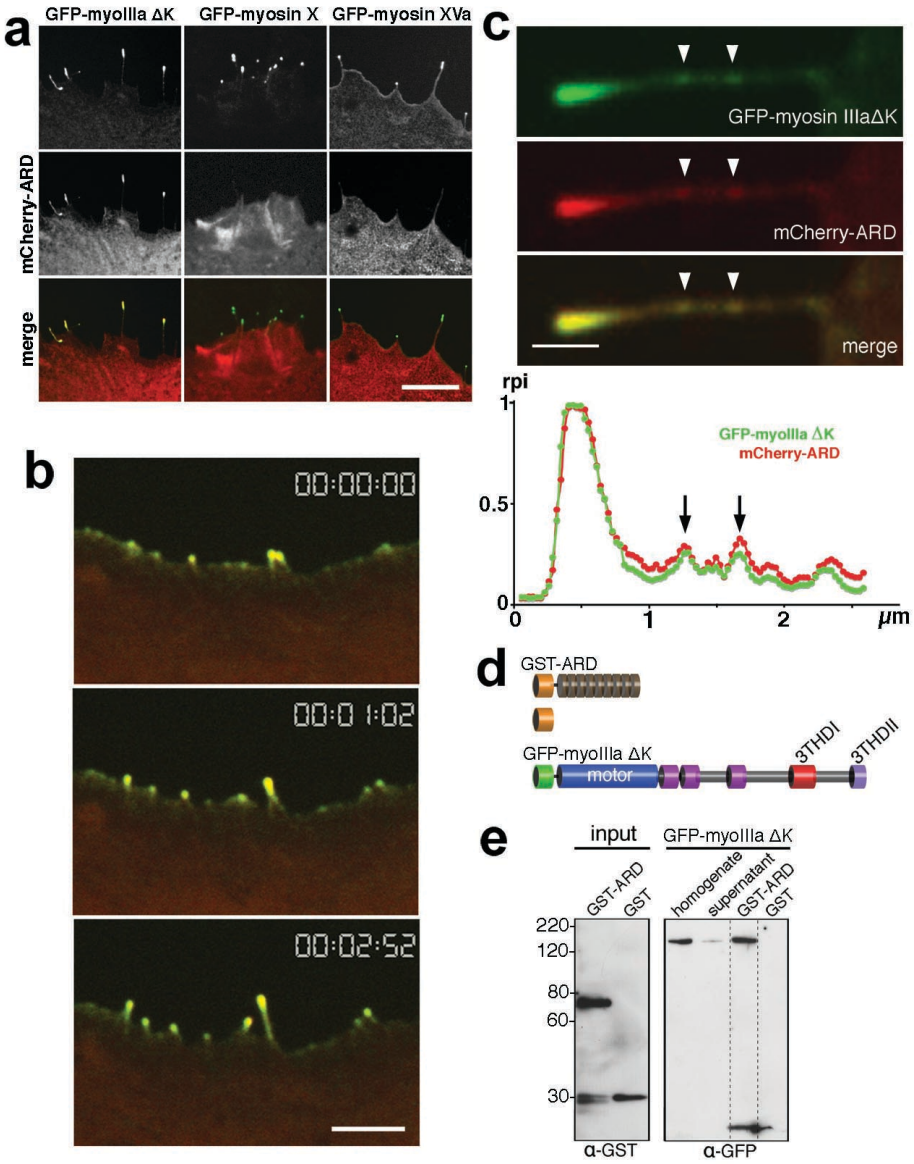

Figure 2-6 Espin 1 interacts with myosin IIIa through its ankyrin repeats domain (ARD) in transfected COS-7 cells. (**a**) mCherry-tagged espin 1^{ARD} shows filopodia tip localization when co-transfected with GFP–myoIIIa$^{\Delta K}$ but failed to localize at the filopodia tips when co-transfected with GFP–myosin X or GFP–myosin XVa. Scale bar, 5 μm. (**b**) Selected video images from a time-lapse video (Movie 2-1) show co-transport of GFP–myoIIIa$^{\Delta K}$ and mCherry–espin 1^{ARD} during the formation and extension of filopodia in COS-7 cells. Scale bar, 2.5 μm. (**c**) Single representative frame from a time-lapse video of a single filopodium (Movie 2-2) graph with the normalized relative pixel intensity of the fluorescence along the filopodium show co-distribution (cross-correlation of the green and red intensity values = 0.990 for this frame; the average cross-correlation for six randomly selected frames from the same video was 0.99) of GFP–myoIIIa$^{\Delta K}$ and mCherry–espin 1^{ARD} forming a tip-to-base gradient and colocalization of the green and red fluorescence puncta (arrowheads) corresponding to the co-transport of GFP–myoIIIa$^{\Delta K}$ and mCherry–espin 1^{ARD} trafficking into and out of the tip of the filopodia. Scale bar, 0.5 μm. **(d)** Schematic representation of the constructs analyzed in this figure. GST, glutathione S-transferase; GFP, green fluorescence protein; myosin IIIa$^{\Delta K}$, myosin IIIa with a deletion of it kinase domain; 3THDI and 3THDII, myosin IIIa tail homology domains 1 and 2, respectively. (**e**) Western blots of GST pulldowns show that purified GST-tagged espin 1^{ARD} co-precipitates with GFP–myosin IIIa$^{\Delta K}$, but not with GST alone. Precipitates were detected using anti-GST and anti-GFP antibodies. (Dr. Salles and Mr. Manor assisted with live-cell imaging and measurements)

We also co-expressed mCherry–espin 1^{ARD} with GFP-tagged myosin X and GFP-tagged myosin XVa. As all of these myosins accumulate at the tips of filopodia (Belyantseva *et al.*, 2005; Bohil *et al*., 2006; Tokuo and Ikebe, 2004), they provide a well-defined spatial compartment where any potential interaction can be clearly visualized. Co-transfections showed that mCherry–espin 1^{ARD} is efficiently targeted to the tips of filopodia initiated by myosin $IIIa^{\Delta K}$, but not by myosins X or XVa (Fig. 2-6a), demonstrating a specific colocalization of ARD with myosin IIIa. Live imaging of COS-7 cells transfected with GFP–myosin $IIIa^{\Delta K}$ and mCherry–espin 1^{ARD} showed dynamic colocalization at the filopodia tips from the early steps of their initiation and elongation (Fig. 2-6b; Movie 2-1).

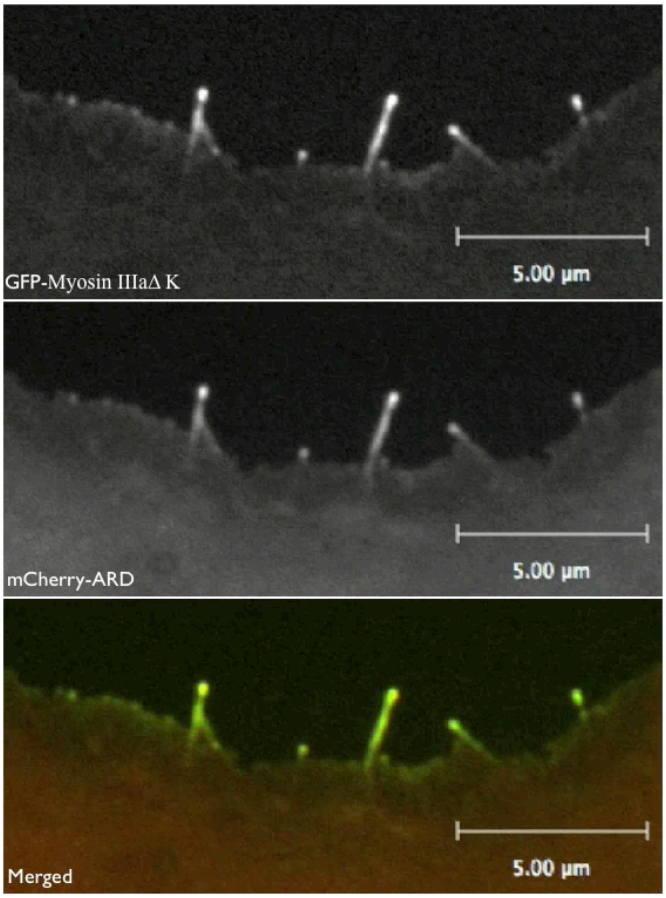

Movie 2-1 Time-lapse imaging of the simultaneous expression of GFP-myosin $IIIa^{\Delta K}$ (top), mCherry-espin 1^{ARD} (middle) in live COS-7 cells, and images merged (bottom). GFP-myosin $IIIa^{\Delta K}$ induces extension of filopodia and transports mCherry-espin 1^{ARD}, accumulating at the tips of the actin protrusions. Cell was imaged 24 h after transfection. Video acquisition was performed for ten minutes with exposure times of 7.9 seconds for each frame (alternating 3.9 seconds for each of the green and red color channel). The movie can be viewed at the following URL address: http://www.nature.com/ncb/journal/v11/n4/extref/ncb1851-s1.mov. (Dr. Salles performed live-cell imaging)

Live imaging also showed matching forward and rearward intra-filopodial movements of the GFP–myosin IIIa$^{\Delta K}$ and mCherry–espin 1^{ARD} fluorescence puncta while maintaining steady-state tip-to-base distributions (Fig. 2-6c; Movies 2-2, 2-3), similar to the distributions of myosin IIIa and espin 1 observed in stereocilia (Figs. 2-3, 2-5).

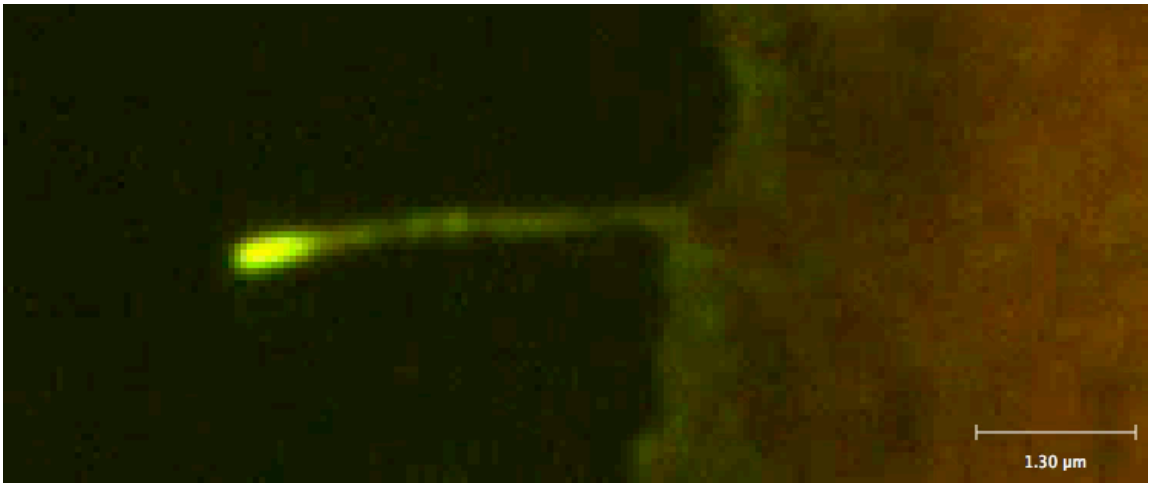

Movie 2-2 GFP-myosin IIIa$^{\Delta K}$ (green) and mCherry-espin 1^{ARD} (red) co-expressed in COS-7 cells accumulate in a tip-to-base gradient in the resulting filopodia, while maintaining a dynamic bidirectional intra-filopodial observed as fluorescence puncta moving towards and away the filopodia tips. The colocalization of the moving puncta was demonstrated by the comparison of the plots of pixel intensity profiles for the green and the red channels in individual frames and the cross correlation analysis shown in figure 2-4 c. Cell was imaged 24 h after transfection. Video acquisition was performed with exposure times of 4.2 seconds for each frame (alternating 2 seconds for each of the green and red color channel). The movie can be viewed at the following URL address: http://www.nature.com/ncb/journal/v11/n4/extref/ncb1851-s2.mov. (Dr. Salles performed live-cell imaging)

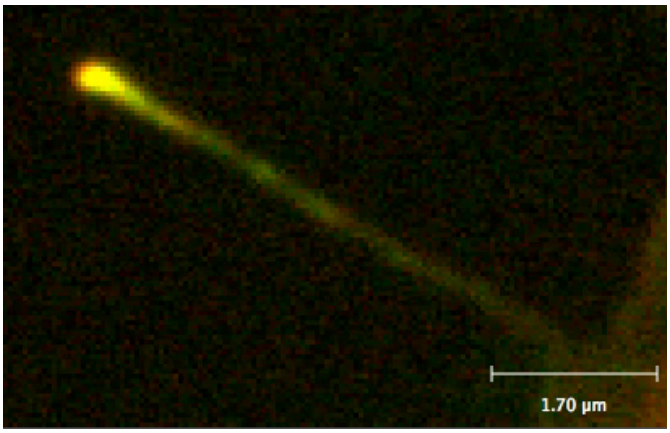

Movie 2-3 GFP-myosin IIIa$^{\Delta K}$ (green) and mCherry-espin 1^{ARD} (red) co-expressed in COS-7 cells accumulate in a tip-to-base gradient in the resulting filopodia, while maintaining a dynamic bidirectional intra-filopodial observed as fluorescence puncta moving towards and away the filopodia tips. Cell was imaged 24 h after transfection. Video acquisition was performed with exposure times of ~4 seconds for each frame (alternating exposure times of 1.5 seconds for the green channel and 2.3 seconds for the red channel). The total duration of the recoding was 5 min. The movie can be viewed at the following URL address: http://www.nature.com/ncb/journal/v11/n4/extref/ncb1851-s3.mov. (Dr. Salles performed live-cell imaging)

The intensity profiles for mCherry–espin 1^{ARD} and GFP–myosin $IIIa^{\Delta K}$ within each frame of the video (Fig. 2-6c) are closely correlated (cross-correlation = ~0.990), supporting the view that these two proteins traffic together in the filopodia. The interaction between espin 1^{ARD} and myosin $IIIa^{\Delta K}$ was confirmed with a GST pulldown assay (Fig. 2-6e). The dynamic localization of espin 1^{ARD} at filopodia tips when co-transfected with myosin IIIa, but not with myosin X or with myosin XVa, along with our GST pulldown assay results, led us to hypothesize that myosin IIIa transports espin 1 to the tips of stereocilia.

2.4.4 Myosin IIIa interacted with espin 1 through its conserved domain, 3THDI, in C-terminal tail

We next asked which specific region of myosin IIIa is involved in the interaction with espin 1. Myosin IIIa has the two conserved binding domains, 3THDI and 3THDII (Dosé *et al.*, 2003). We first co-transfected COS-7 cells with espin 1 and GFP–myosin IIIa and showed that the two proteins colocalize at actin bundles as well as at filopodia tips (Fig. 2-7a, b). This pattern of colocalization was abolished when we used a GFP–myosin IIIa construct that lacks the portion of the tail containing both 3THDI and 3THDII (GFP–myoIII$a^{\Delta 32}$; Figs. 2-7a,b and 2-8).

Figure 2-7 Myosin IIIa interacts with espin 1 through its 3THDI domain. (**a**) Schematic representation of the espin 1 and myosin IIIa constructs analyzed in this figure. ABM, actin binding module; WH2, Wiskott-Aldrich homology domain 2; GFP–myosin $IIIa^{\Delta 32}$, myosin IIIa lacking exon 32 which causes a frame shift rendering the protein without the 3THDI and 3THDII domains. (**b**) Co-expression of untagged espin 1 shows that GFP–myosin IIIa, GFP–IIIa $tail^{\Delta 3THDII}$, and GFP–myosin $IIIa^{3THDI}$ (green) colocalize with espin 1 (red) along actin filament bundles. In contrast, GFP–myosin $IIIa^{\Delta 32}$, GFP–myosin $IIIa^{pre3THDI}$, and GFP-myosin $IIIa^{post3THDI}$ are dispersed in the cytoplasm, despite the presence of espin 1 bundles. Scale bar, 5 μm. (**c**) Western blots of GST pulldowns confirm that the 3THDI region of myosin IIIa is necessary and sufficient for binding to espin 1^{ARD}, as pre3THDI and post3THDI show no binding to GST–espin 1^{ARD}. Precipitates were detected using anti-GST and anti-GFP antibodies.

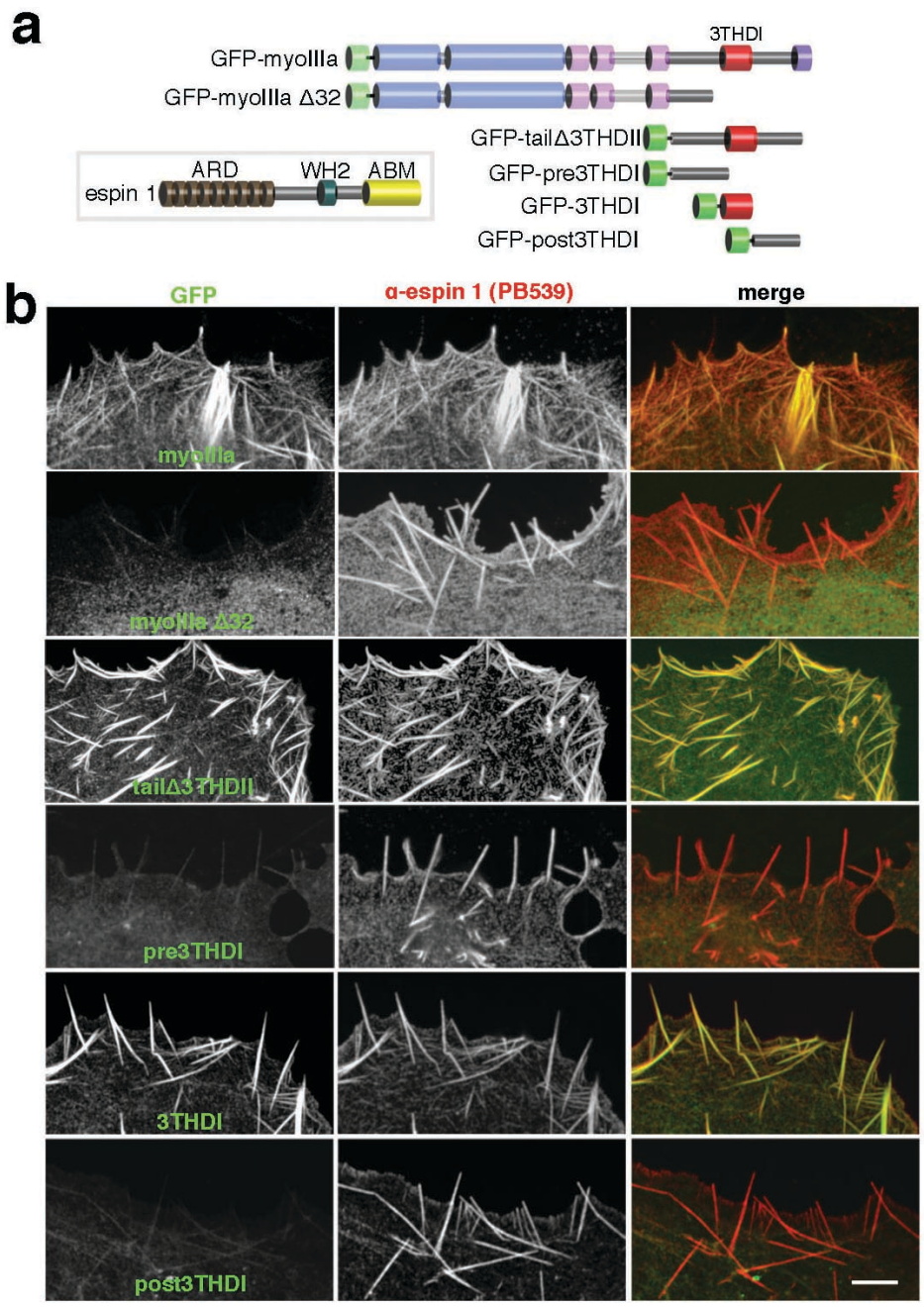
a
3THDI
GFP-myoIIIa
GFP-myoIIIa Δ32
GFP-tailΔ3THDII
GFP-pre3THDI
GFP-3THDI
GFP-post3THDI
ARD
WH2
ABM
espin 1
b
GFP
α-espin 1 (PB539)
merge
myoIIIa
myoIIIa Δ32
tailΔ3THDII
pre3THDI
3THDI
post3THDI
c
input
GFP-pre3THDI
input
GFP-3THDI
input
GFP-post3THDI
GST-ARD
GST
homogenate
supernatant
GST-ARD
GST
80
60
40
30
α-GST
α-GFP

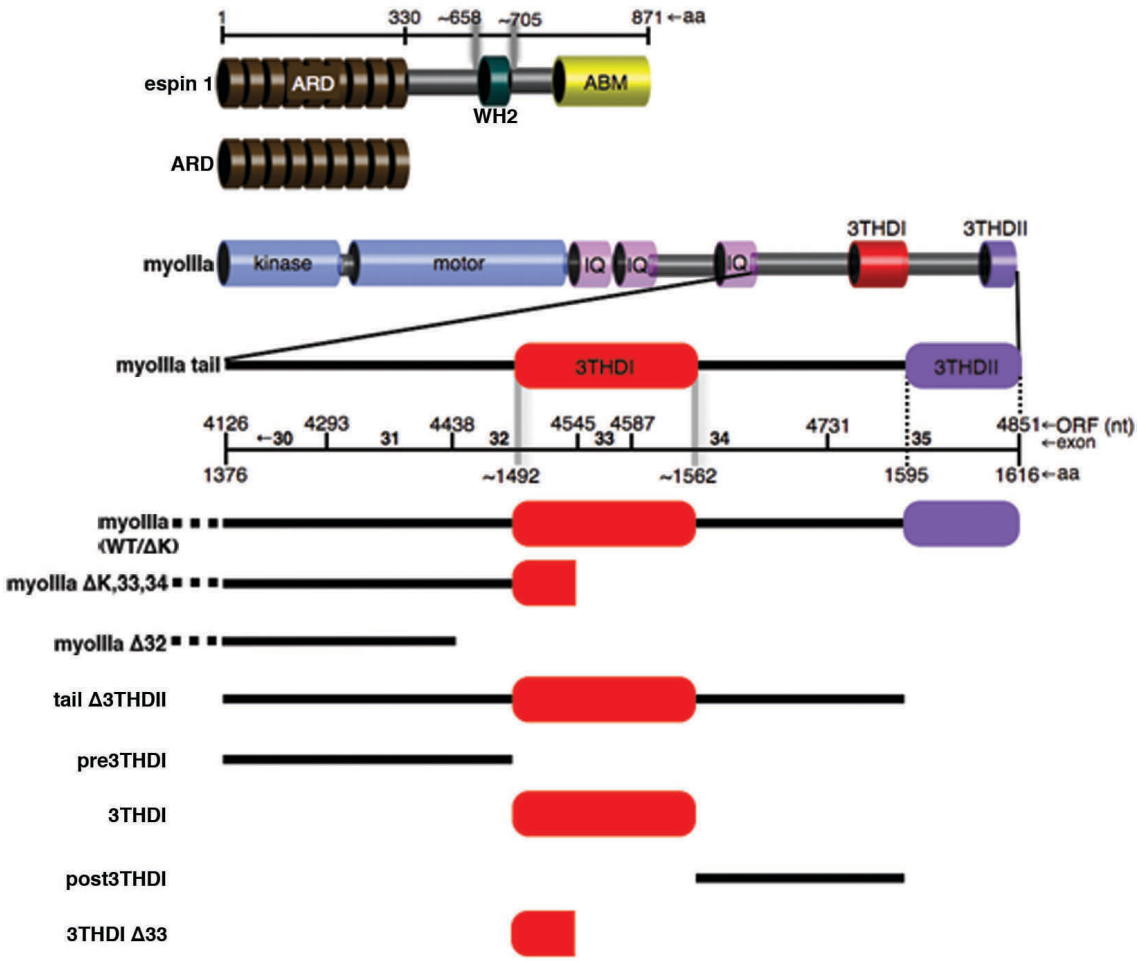

Figure 2-8 Schematic map of wild-type and deletion constructs. Only the myosin IIIa coding regions are shown. Full-length espin 1 is 871 amino acid-long in mouse and 854 amino acid-long in human (mouse espin 1 is illustrated here). The tail domain of myoIIIa encompasses 3THDI, 3THDII, and the third IQ domain, however; only 3THDI and 3THDII were considered in this study. Myosin IIIa$^{\Delta 32}$ lacks exon 32, which causes a frame shift eliminating 3THDI and 3THDII, and introduces 26 new amino acids. Myosin IIIa$^{\Delta 33,34}$ lacks exons 33 and 34, which causes a frame shift approximately one-third of the way through 3THDI and therefore eliminates the rest of 3THDI and 3THDII, and introduces 72 new amino acids.

We next co-transfected COS-7 cells with espin 1 and with a GFP-tagged myosin IIIa tail portion lacking 3THDII (GFP–IIIa tail$^{\Delta 3THDII}$; Fig. 2-7a, b) and narrowed down the region of interaction to the 3THDI and its immediate flanking regions. We observed colocalization of espin 1 with GFP–myosin IIIa tail that contained only the 3THDI domain (GFP–3THDI; Fig. 2-7a, b), but not with regions of only the myosin IIIa tail

immediately amino-terminal (pre3THDI) or carboxy-terminal (post3THDI) to the 3THDI domain (Fig. 2-7a, b). This suggests that the 3THDI domain is necessary for the myosin IIIa–espin 1 interaction. Together these data suggest that espin 1 and myosin IIIa interact specifically through their ARD and 3THDI domains, respectively. We verified this interaction *in vitro* using a GST pulldown assay and showed that GST–espin 1^{ARD} binds to GFP–myosin $IIIa^{3THDI}$, but not to the $-^{pre3THDI}$ or $-^{post3THDI}$ regions (Fig. 2-7c).

2.4.5 Myosin IIIa and espin 1 synergistically elongated filopodia in COS-7 cells

The fact that stereocilia length can be influenced by either espin 1 (Rzadzinska *et al.*, 2005; Zheng *et al.*, 2000) or myosin IIIa (Schneider *et al.*, 2006), along with the observation that they both localize to the same compartment at stereocilia tips and interact biochemically, suggests a combined functional role for the myosin IIIa–espin 1 complex in the elongation of stereocilia F-actin. We discovered that COS-7 cells co-transfected with myosin $IIIa^{\Delta K}$ and espin 1 (Fig. 2-9a–c) show filopodial actin protrusions that can be up to ten times longer (mean length = 14.3 ± 9.1 μm; number of cells, n_c = 18; number of filopodia, n_f = 56) than those transfected with myosin $IIIa^{\Delta K}$ alone (1.7 ± 0.83 μm, n_c = 12, n_f = 49), or with espin 1 alone (1.3 ± 0.28 μm, n_c = 13, n_f = 104). Mean lengths of filopodia of COS-7 cells transfected with an empty GFP vector was 1.26 ± 0.7 μm (n_c = 10, n_f = 59). The synergistic effect between myosin IIIa and espin 1 is specific for myosin IIIa, as elongation was not enhanced when espin 1 was co-expressed with either myosin X (2.40 ± 1.50 μm, n_c = 16, n_f = 165) or myosin XVa (2.08 ± 1.63 μm, n_c = 15, n_f = 134).

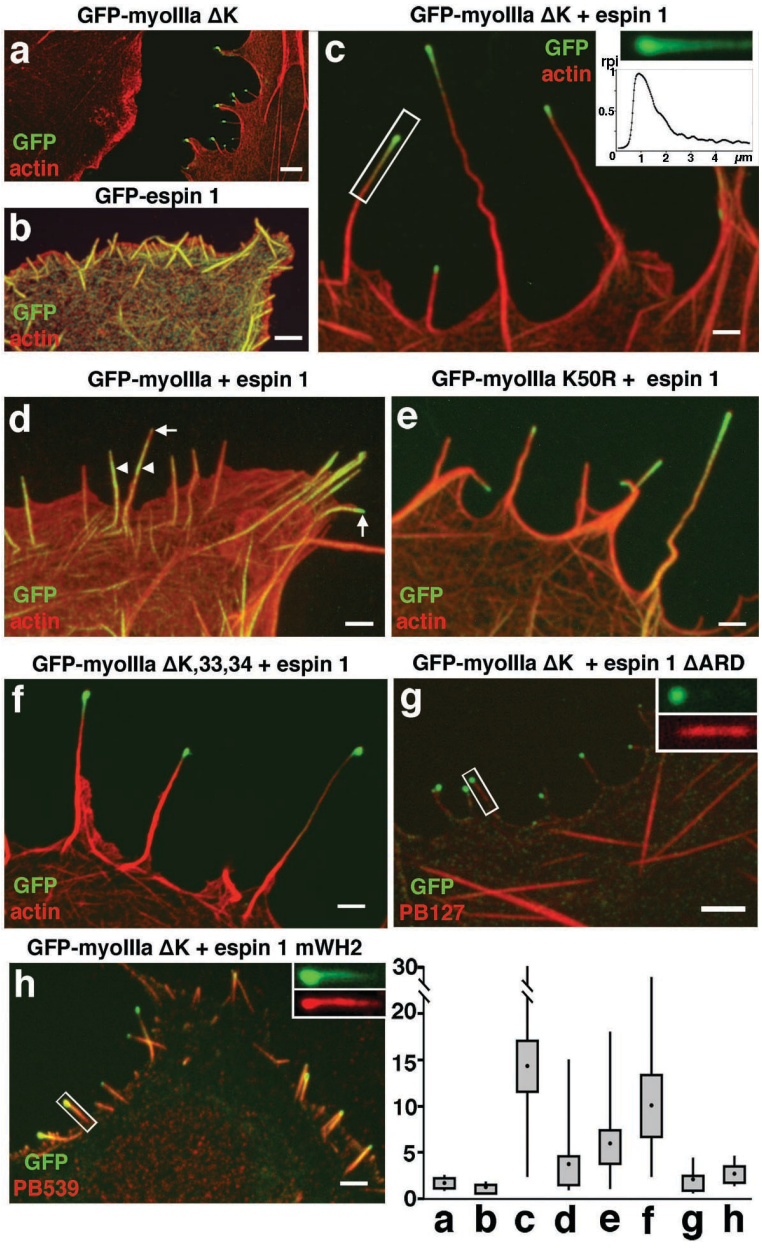

Figure 2-9 Myosin IIIa and espin 1 synergistically elongate filopodia in COS-7 cells through espin 1 WH2 activity. (**a**–**c**) Overexpression of either GFP–myosin IIIa$^{\Delta K}$ (**a**) or GFP–espin 1 (**b**) resulted in formation of short filopodia (mean lengths = 1.7 ± 0.83 μm and 1.3 ± 0.28 μm, respectively). In contrast, co-expression of GFP–myosin IIIa$^{\Delta K}$ (green) and espin 1 (**c**) had a synergistic effect that generated extremely long filopodia (14.3 ± 9.1 μm). F-actin (red) was visualized using Alexa 568-phalloidin. Graph (inset) of the relative pixel intensity (rpi) of the GFP–myosin IIIa$^{\Delta K}$ distribution in the single filopodium indicated by the rectangle in **c** shows the characteristic tip-to-base decaying gradient. (**d**) Co-expression of full-length GFP–myosin IIIa and espin 1 produced a more limited tip localization of these proteins and elongation of filopodia (3.7 ± 3.2 μm) when compared with co-expression of GFP–myosin IIIa$^{\Delta K}$ and espin 1. (**e**) The enhanced elongation phenotype was restored to a limited extent (5.93 ± 3.10 μm) when COS-7 cells were co-transfected instead with GFP–myosin IIIa^{K50R} and espin 1. **(f)** The enhanced elongation phenotype was similar to **c** when the cell was co-transfected with GFP–myosin IIIa$^{\Delta K,33,34}$ and espin 1 (10.02 ± 4.7 μm). (**g**) Co-expression of GFP–myoIIIa$^{\Delta K}$ and espin 1 lacking ARD (espin 1$^{\Delta ARD}$, labeled with the pan espin antibody, red) failed to elongate filopodia (2.05 ± 1.8 μm) and to show tip localization of espin 1$^{\Delta ARD}$ (inset). **(h)** Co-expression of GFP–myosin IIIa$^{\Delta K}$ and espin 1 with a mutated WH2 domain (espin 1^{mWH2}, labeled with an anti-espin 1 antibody, red) failed to elongate filopodia (2.65 ± 1.5 μm) despite the fact that espin 1^{mWH2} localized to the tip and formed the tip-to-base gradient matching the distribution of the GFP–myoIIIa$^{\Delta K}$ (inset). Scale bars, 2.5 μm. Measurements of filopodia lengths for each of the combinations shown in the panels above are presented as box-plots; upper and lower whiskers represent the range, the top and bottom of the box represent the upper and lower 25th percentile, and the filled squares represent the mean values. (Dr. Salles and Mr. Manor assisted with transfection and measurements)

We used myosin IIIa without the kinase domain to observe the behavior of the dephosphorylated and more functionally active myosin. To exclude the possibility that deletion of the kinase domain produces aberrant behavior, we developed a kinase-dead construct, myosin IIIa^{K50R} (Fig. 2-10a). This construct allowed us to examine the role of autophosphorylation in the regulation of motor function, which in turn enabled us to investigate the role of myosin IIIa motor function in espin 1 tip-localization activity. We have determined that inactivation of the myosin IIIa kinase in a myosin IIIa 2IQ construct reduces K_{ATPase}, yet it does not affect maximal ATPase activity (Table 2-1; Fig. 2-10).

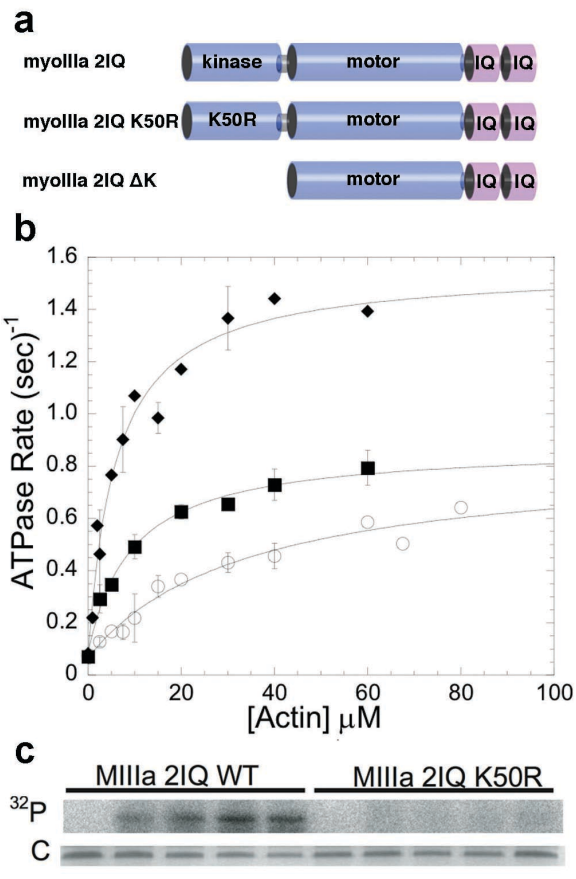

Figure 2-10 Actin-activated ATPase activity of myosin IIIa 2IQ constructs. (**a**) A diagram of the myosin IIIa 2IQ constructs examined. (**b**) The results for myosin IIIa 2IQ^{K50R} (squares) are compared to that of myosin IIIa 2IQ wild-type (Dosé *et al.*, 2007a; open circles) and myosin IIIa 2IQ$^{\Delta K}$ (Ricci *et al.*, 2006; diamonds). The steady-state ATPase rate of 0.1 μM myosin was measured using the NADH coupled assay in the presence of 1 mM ATP and a range of actin concentrations. The error bars represent the standard deviation from the mean and include data from 3-4 protein preparations. The enzymatic parameters determined from the fits to the data are summarized in the Table 2-1. Full phosphorylation of myosin IIIa 2IQ results in a ~40% reduction in ATPase activity compared to unphosphorylated myosin IIIa 2IQ, in the presence of 20 μM actin (data not shown). A previous study reported the kinetic mechanisms of the myosin IIIa 2IQ$^{\Delta K}$ and myosin IIIa 2IQ WT (Dosé *et al.*, 2007a) constructs, which demonstrated the specific steps in motor ATPase cycle that are altered by the presence of the kinase domain. (**c**) The kinase activity of 1 μM myosin IIIa 2IQ WT was monitored by ^{32}P incorporation (200 μM [^{32}P]ATP) over a 60 minute period (lanes 1-5 are 0, 5, 15, 30, and 60 minute time points, respectively). The results are compared to myosin IIIa 2IQ^{K50R} that demonstrated little or no kinase activity under identical conditions (lanes 6-10 are 0, 5, 15, 30, and 60 minute time points, respectively). The top panel, labeled ^{32}P, is the phosphorimage demonstrating the degree of ^{32}P incorporation while the bottom panel, labeled C, is the same gel coomassie stained to demonstrate that the total protein concentration in each lane is similar. (Drs. Yengo and Moore performed the ATPase assay)

Motor ATPase Parameters	MIIIa 2IQ	MIIIa 2IQ$^{\Delta K}$	MIIIa 2IQ^{K50R}
[a]V_0 (sec)$^{-1}$	0.07 ± 0.03	0.08 ± 0.02	0.07 ± 0.05
[b]k_{cat} (sec)$^{-1}$	0.77 ± 0.08	1.5 ± 0.1	0.76 ± 0.08
[c]K_{ATPase} (μM)	34 ± 11	6.0 ± 1.4	11.9 ± 3.7

Table 2-2 Steady-state motor ATPase parameters of the myosin IIIa 2IQ constructs. [a]Steady-state ATPase activity in the absence of actin measured with the NADH coupled assay. [b]Maximum rate of actin-activated ATPase measured with the NADH coupled assay. The values for K_{ATPase} and *k*cat were determined from the fit of the data in Figure 2-8 to the equation: (V_0 + (k_{cat} [actin]) / (K_{ATPase} + [actin])). [c]Actin concentration at which the actin-activated ATPase rate is one-half maximal from the NADH assay. (Drs. Yengo and Moore performed the measurements)

We next evaluated the role of kinase activity in myosin IIIa tip localization in COS-7 cells using GFP-tagged constructs. Full-length myosin IIIa^{K50R} localized more efficiently to the tips of filopodia in COS-7 cells (39% at tips n_c = 137) than wild-type (5% at tips n_c = 200), although not as strikingly as myosin IIIa$^{\Delta K}$ (93% at tips n = 105). Furthermore, co-expression of myosin IIIa^{K50R} and espin 1 (Fig. 2-9e) produced longer filopodia (mean length = 5.93 ± 3.10 μm, n_c = 15, n_f = 89) than those produced by co-expression of wild-type myosin IIIa and espin 1 (3.7 ± 3.2 μm, n_c = 15, n_f = 63; Fig. 2-9d), but not as long as those seen with myosin IIIa$^{\Delta K}$ and espin 1 co-expression. These data show that myosin IIIa motor ATPase activity parallels the ability of myosin IIIa to localize to filopodia tips and to elongate filopodia when co-expressed with espin 1. Interestingly, espin 1 co-expressed with a myosin IIIa$^{\Delta K}$ lacking the tail domain downstream of exon 32 (myosin IIIa$^{\Delta K,33,34}$; Fig. 2-8) resulted in slightly shorter filopodia (10.0 ± 4.74 μm, n = 64; Fig. 2-7f) than co-expression with myosin IIIa$^{\Delta K}$. Using COS-7

cell co-expression and GST pulldown assays, we confirmed that the upstream portion of 3THDI (3THDI$^{\Delta 33}$, Fig. 2-11) binds to espin 1.

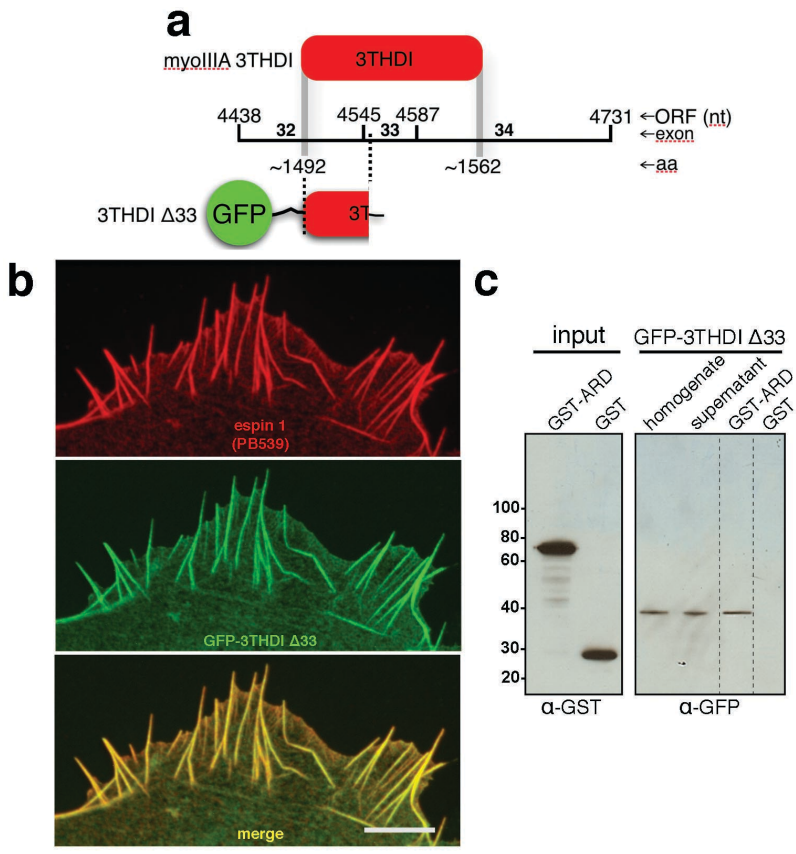

Figure 2-11 The first 24 amino acids of the 3THDI domain are sufficient for binding espin 1. (**a**) The mapping of the GFP-IIIa 3THDI$^{\Delta 33}$ fusion protein is illustrated. (**b**) GFP-3THDI$^{\Delta 33}$ (green) colocalizes with espin 1 (red, labeled with PB539). PB539 (red) is labeled with Alexa Fluor 568-conjugated secondary antibody. Scale bar is 5 µm. (**c**) GST pull-down shows that GFP-IIIa 3THDI$^{\Delta 33}$ interacts with espin 1^{ARD} but not with GST.

The 3THDII of myosin IIIa has been shown previously to be an actin-binding site (Les Erickson *et al.*, 2003). Previous studies reported that myosin IIIa lacking the 3THDII actin-binding domain does not localize to filopodia tips (Les Erickson *et al.*, 2003; Schneider *et al.*, 2006), but here we show that when co-expressed with espin 1, myosin IIIa goes to the tip and promotes filopodia elongation (Fig. 2-9f). It seems that the association with espin 1, which does have actin-binding sites, compensates for the

missing actin-binding site in the myosin IIIa without the 3THDII domain. Co-expression of espin 1 and myosin IIIa results in enhanced localization of espin 1 at filopodia tips (Fig. 2-12).

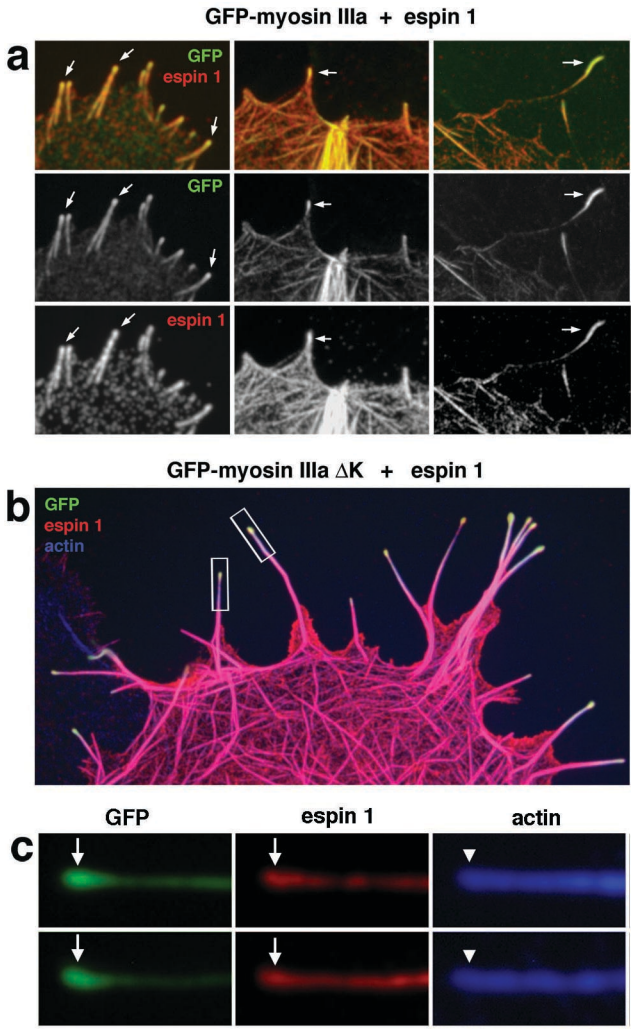

Figure 2-12 Colocalization of myosin IIIa and espin 1 at filopodia tips. (**a**) Close up views of COS-7 cells show that espin 1 (red) colocalizes with GFP-myoIIIa$^{\Delta K}$ (green) at the filopodia tips when these two proteins are co-expressed in COS-7 cells. (**b**) Espin 1 (red) colocalizes with GFP-myoIIIa$^{\Delta K}$ (green) at the filopodia tips (actin is labeled Alexa fluor 647 shown in blue) when these two proteins are co-expressed in COS-7 cells. (**c**) Close up views of the regions outlined by rectangles in (**b**) show the increased concentration of GFP-myosin IIIa$^{\Delta K}$ (arrows, green) and espin 1 (arrows, red) but not actin (arrowheads, blue) at the filopodia tips. Bars = 3 μm. (Dr. Salles assisted with immunocytochemistry and imaging)

When myosin IIIa$^{\Delta K}$ was co-expressed with espin 1 lacking the ARD domain, both espin tip localization and filopodia elongation were abolished (Fig. 2-9g). These results show

that the actin crosslinking activity of espin 1 is not solely responsible for the enhanced elongation of filopodia or stereocilia observed in our experiments. We conclude that espin 1 promotes enhanced elongation of filopodia only when transported to the polymerization end of actin filaments by myosin IIIa. The finding that espin 1 elongates filopodia only when localized to the F-actin plus ends by myosin IIIa suggests that WH2-dependent polymerization activity is involved in elongation. We tested this hypothesis by substituting the first two of three highly conserved Leu residues of the espin 1 WH2 motif (L655A, L656A), which have been shown to be essential for its actin-monomer-binding activity (Quinlan *et al.*, 2005; Loomis *et al.*, 2006). In COS-7 cells co-transfected with the WH2-mutated espin 1 construct (espin 1^{mWH2}) and myosin $IIIa^{\Delta K}$ (Fig. 2-9h), the average length of filopodia (2.65 ± 1.50 μm, $n_c = 10$, $n_f = 75$) remained comparable to the protrusions induced by myosin $IIIa^{\Delta K}$ alone. The lack of enhanced elongation despite the colocalization of espin 1^{mWH2} and myosin $IIIa^{\Delta K}$ at the tips of filopodia (Fig. 2-9h) demonstrates that the WH2 motif is essential for the effect of espin 1 in elongation.

2.5 Discussion

2.5.1 Myosin IIIa–espin 1 complexes are dynamically associated with the treadmilling actin core

The steady-state distribution of myosin IIIa in a tip-to-base gradient is probably dynamically maintained. The length of myosin IIIa distribution should be inversely proportional to the net velocity of myosin towards the tip (Naoz *et al.*, 2008), which will be slower for faster treadmilling actin cores (that is, in longer stereocilia [Rzadzinska *et al.,* 2004] and filopodia [Mallavarapu and Mitchison, 1999]). This prediction is also consistent with our observation that wild-type myosin IIIa, which has relatively low

activity, has decreased tip localization in the filopodia, compared with the more active kinase mutant forms of myosin IIIa used in our experiments (Fig. 2-9). However, in stereocilia where the actin treadmilling is much slower, the wild-type myosin IIIa self-localizes effectively to the tip (Schneider *et al.*, 2006; Fig. 2-5). Similarly, the observed steady-state tip-to-base gradient distribution of espin 1 is not compatible with a model where espin 1 passively diffuses and binds to myosin IIIa resident at the tip, as this would result in a homogenous distribution along the entire length of the stereocilia with no detectable concentration gradient at steady-state. The gradient distribution of espin 1 at steady-state is reminiscent of a myosin VI-driven gradient for the stereocilia membrane protein PTPRQ, and is best explained by a model that includes binding, directed transport and diffusion of myosins and their cargo (Sakaguchi *et al.,* 2008). A more detailed consideration of this dynamic process that also accounts for actin treadmilling and plus-end directed motors predicts a similar distribution, which can be several microns long for longer stereocilia (Naoz *et al.,* 2008). Thus, we favor a model where myosin IIIa–espin 1 complexes are dynamically associated with the treadmilling actin core. This model suggests that espin 1 is transported to the tips of stereocilia by myosin IIIa, where it remains bound to the surface of the actin core for a period of time. Interestingly, abolishing or reducing myosin IIIa kinase activity enhances the affinity of myosin IIIa for actin, providing further evidence that the kinase domain has a role in regulating myosin IIIa motor kinetics and actin-binding properties (Dosé *et al.*, 2008; Kambara *et al.*, 2006). While the myosin IIIa–espin 1 complex is tightly bound to actin, it travels back towards the base of the stereocilia along with the treadmilling actin core. In support of this model,

live video imaging in transfected COS-7 cells shows fluorescent puncta of GFP–myosin IIIa$^{\Delta K}$ and mCherry–espin 1^{ARD} (Movie 2-4) that move rearwards at rates matching the rates reported for actin treadmilling in filopodia (~0.5 μm min^{-1}; Mallavarapu and Mitchison, 1999). We suggest that these puncta are stably bound to the surface of the treadmilling actin filament bundle.

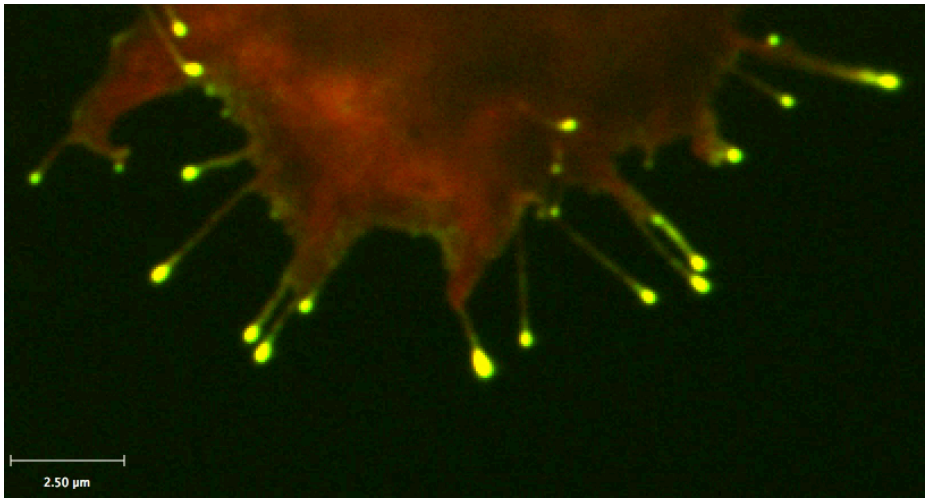

Movie 2-4 GFP-myosin IIIa$^{\Delta K}$ (green) and mCherry-espin 1^{ARD} (red) co-expressed in COS-7 cells accumulate in a tip-to-base gradient in the resulting filopodia, while maintaining dynamic intra-filopodial movements. Cell was imaged 24 h after transfection. Video acquisition was performed with exposure times of 7.9 seconds for each frame (alternating 3.9 seconds for each of the green and red color channel). Because of the longer exposure time than in the stream acquisition shown in **Movie 2-2** this movie highlights the slower moving fluorescence puncta, which were estimated to be moving at ~0.5 μm/min in the retrograde direction. The movie is located at the following URL address: http://www.nature.com/ncb/journal/v11/n4/extref/ncb1851-s4.mov. (Dr. Salles performed live-cell imaging)

2.5.2 Myosin IIIa may possess other unidentified cargoes

Notably, the stereocilia tips are also the site of mechanoelectrical transduction (MET; Ricci *et al.*, 2006), that the myosin IIIa developmental expression level is correlated with maturation of MET in stereocilia (Waguespack *et al.*, 2007), and that myosin IIIa has been shown to transport components of the photoreceptor transduction machinery in *Drosophila* (Porter *et al.,* 1993a; Wes *et al.*, 1999). We cannot exclude the possibility that the localization and dynamics of the myosin IIIa–espin 1 complex are also

affected by interactions with other proteins at the stereocilia tip. Furthermore, ankyrin repeats have been shown to be promiscuous binders of membrane proteins (Mosavi *et al.*, 2004). It is possible that the turnover and dynamic localization of the espin 1–myosin IIIa complex are influenced by interactions with components of the MET machinery, and vice-versa.

Chapter 3. Myosin IIIb, Myosin IIIa Paralogue, Depends on its Espin 1 Cargo for Tip Localization and Elongation of Stereocilia

3.1 Abstract

Myosin IIIa is an actin-dependent motor protein that co-transports with espin 1 to the stereocilia tips of vertebrate inner ear hair cells and influences the length of mechanosensory stereocilia. Myosin IIIb is a second class III myosin isoform known to express in hair cells and photoreceptors. Encoded by a separate gene, myosin IIIb is different from myosin IIIa in their C-terminal tail. Myosin IIIb lacks a second actin-binding domain, 3THDI in the tip of the C-terminal tail. Research on myosin IIIb is limited relative to the well-characterized myosin IIIa. Several mutations in the human myosin IIIa gene (*MYO3A*) lead to a non-syndromic progressive deafness that starts at the second decade of life. There is speculation that myosin IIIb partially compensates for the loss of function of myosin IIIa. We report differences between myosins IIIb and IIIa in localization, expression, and actin elongation in the hair cell stereocilia and filopodia of COS-7 cell. Myosin IIIb localizes to the same stereocilia tip compartment as myosin IIIa in both vestibular and cochlear hair cells but less prominent in the shortest and tallest rows of cochlear stereocilia bundle. Peak myosin IIIb localization is detected at stereocilia tips of cochlear hair cells ~eight days earlier than myosin IIIa. Similar to a functionally active myosin IIIa kinase deletion mutant, an overexpression of GFP-myosin IIIb kinase mutant results in stereocilia tip localization and stereocilia elongation. Synergistic elongation of COS-7 filopodia is observable when the GFP-myosin IIIb

mutant is co-expressed with espin 1. Unlike myosin IIIa which contains 3THDII, the espin 1 cargo is essential for the mobility of myosin IIIb along the actin filaments. This observation reveals a new kind of cargo-dependent movement of a myosin. Furthermore, myosin IIIa is downregulated by overexpression of GFP-myosin IIIb in the vestibular, but not in the cochlear, stereocilia tips. Taken together, we argue that myosin IIIb can partially compensate for the functions of myosin IIIa in stereocilia.

3.2 Introduction

The inner ear hair cell's mechanosensory bundle is composed of tens to hundreds of stereocilia arranged in a staircase pattern of increasing lengths. Stereocilia possess remarkably well-defined structures which are dynamically regulated by the activities of unconventional myosins, actin-binding, and membrane-associated proteins for the lifetime of the cell (reviewed by Manor and Kachar 2008). The emergence and coordinated elongation of stereocilia at the apical surfaces of hair cells occurs early during the development of hearing. The length of each mature stereocilium is established while the bundle of tightly packed, parallel actin filaments in the stereocilium core is continually renewed. This renewal of the actin bundle is achieved by continuous polymerization at the tip and depolymerization at the base that maintains a steady-state length of the stereocilium (Lin *et al*., 2005; Rzadzinska *et al*., 2004; Schneider *et al*., 2002). Although the exact molecular description for regulating the actin molecular treadmill and the steady-state length of stereocilia remains rudimentary, several recent studies have provided insight towards understanding the molecular processes involved in

the elongation and maintenance of stereocilia (Manor and Kachar, 2008; Naoz *et al.*, 2008).

The actin-based, plus-end directed motor protein, myosin IIIa (Dosé *et al.*, 2003), and the actin regulatory protein, espin 1 (Sekerková *et al*., 2006a), have each been implicated in sensorineural deafness (*DFNB30*, Walsh *et al*., 2002; *DFNB36*, Naz *et al*., 2004, respectively), and have been shown to colocalize to the tips of stereocilia and COS-7 cell filopodia. When overexpressed, these proteins synergistically elongate both stereocilia and filopodia (Figs. 2-5 and 2-9). The colocalization and cell transfection data as well as live-cell imaging (Figs. 2-5, 2-12; Movies 2-1, 2-2, 2-3, and 2-4), biochemical (Fig. 2-6), and molecular data (Figs. 2-6, 2-7, 2-9, 2-10, 2-11) collectively indicate that myosin IIIa and espin 1 interact through their tail homology domain I (3THDI) and ankyrin repeats domain (ARD), respectively, co-transport to the plus ends of actin filaments, and participate in the elongation of stereocilia.

Myosins IIIa and IIIb are the two class III myosins, each of which, have a unique N-terminal kinase domain (Ng *et al*., 1996; Komaba *et al*., 2003: Dosé *et al*., 2007a; Kempler *et al*., 2007; Katti *et al*., 2009) and the 3THDI. Myosin IIIb has a shorter C-terminal tail that lacks the actin-binding tail homology domain II (3THDII; Fig. 1-1; Dosé *et al.*, 2003). Interestingly, 3THDII has been shown to be essential for the tip localization of myosin IIIa in HeLa cell filopodia (Les Erickson *et al*., 2003), but not in stereocilia (Schneider *et al*., 2006), or in COS-7 cell filopodia co-expressing espin 1 (Fig. 2-7). Myosins IIIb and IIIa are encoded by separate genes that are alternatively spliced across tissues and vertebrate species (Dosé and Burnside, 2000; Dosé and Burnside,

2002; Katti *et al*., 2009). The expression of these proteins is limited to sensory epithelia —i.e. photoreceptors (Dosé *et al*., 2003; Katti *et al*., 2009), inner ear hair cells (Gillespie *et al*., 2009; Schneider *et al*., 2006; Walsh *et al.*, 2002), and olfactory bulbs (Katti *et al.*, 2009)—and a few other non-sensory tissues (Dosé and Burnside, 2002; Dosé *et al*., 2003; Katti *et al*., 2009; Lin-Jones *et al*., 2009). Mutations in the *MYO3A* gene lead to late-onset, progressive deafness at the beginning of the second decade and beyond. These mutations do not affect vision or balance (Dosé and Burnside, 2002; Walsh *et al*., 2002). A possible explanation is that, in the cochlea, myosin IIIb compensates for the loss of myosin IIIa during the early years of hearing and consistently in the vestibular system (Walsh *et al*., 2002; Les Erickson *et al*., 2003; Schneider *et al*., 2006; Katti *et al*., 2009; Lin-Jones *et al*., 2009).

Since the compensation for a loss-of-function *MYO3A* mutation does not last a lifetime, a protein candidate for this compensation has to be slightly different from myosin IIIa in terms of structure, function, localization, and/or developmental expression. Myosin IIIb is a good candidate to serve as a myosin IIIa compensator since it is paralogous to myosin IIIa sharing an overall amino acid identity of ~50% (Dosé *et al*., 2003; Katti *et al*., 2009), and is predicted to contain the same functional domains—i.e. kinase and motor domain in the head region, IQ domains in the neck region, and the highly conserved 3THDI in the tail region. In humans, myosin IIIb differs from myosin IIIa in the C-terminal tail region by lacking a predicted IQ (SMART, accessed August 2009) and the 3THDII domain. Myosin IIIb is expressed in the inner ear and retina and

localizes to several of the same subcellular compartments as myosin IIIa (Schneider *et al*., 2006; Gillespie *et al*., 2009; Katti *et al*., 2009).

Espin 1, recently identified as another molecular component involved in length regulation at the tips of stereocilia (section 2.4.2), has an N-terminal ARD that has been shown to bind to the myosin IIIa 3THDI (Fig. 2-7). Ankyrin repeats are highly conserved motifs found in many proteins that have been implicated in binding various membrane-associated proteins. These ankyrin-repeats containing proteins are thought to serve as adaptors between the membrane and the cytoskeleton (Bennett, 1992; Hryniewicz-Jankowska *et al*., 2002). Unlike smaller espin isoforms lacking the N-terminal ARD, which are present along the entire stereocilia length (Rzadzinska *et al.*, 2005), espin 1 colocalizes with myosin IIIa exclusively at the tips of stereocilia (Figs. 2-2 and 2-3; Schneider *et al.*, 2006). All espin isoforms are encoded by a single gene and share a WH2 actin-monomer binding domain which is implicated in actin bundle elongation (Loomis *et al*., 2006), and the ~125 amino-acid long C-terminal ABM (Fig. 1-2; Bartles, 2000) required for cross-linking actin filaments and microvillar elongation (Sekerková *et al*., 2004). Mutations in the human espin gene, *ESPN,* have been associated with both autosomal recessive (Naz *et al*., 2004) and dominant deafnesses (Donaudy *et al.*, 2006), in which the recessive form affects both hearing and vestibular function. Furthermore, a well-characterized recessive null mutation in the mouse *Espn* gene (*Espn*$^{je/je}$; deaf jerker mouse) has been directly linked to stereocilia degeneration and vestibular dysfunction (Rzadzinska *et al*., 2005).

We compared the spatiotemporal expression of myosins IIIb and IIIa in the stereocilia tips during the stereocilia development. Interestingly, a peak in the myosin IIIb expression was observed at postnatal day (P) zero—about eight days earlier than myosin IIIa. The myosin IIIb expression subsequently recedes to background levels concomitantly with a peak in myosin IIIa expression at P8. Subsequent cell biology and molecular experiments were employed to further investigate similarities and differences between myosins IIIb and IIIa in terms of their phenotype, interaction with espin 1, and influence on stereocilia elongation. Data accumulated from these experiments provide the basis for understanding different roles of class III myosin isoforms and may lead to answers to the question of how individuals with loss-of-function mutations in the *MYO3A* gene can hear for the first two decades.

3.3 Materials and Methods[ii]

3.3.1 Antibodies

The affinity-purified polyclonal antibody (PB791) was developed in rabbits immunized with a synthetic peptide (Princeton Biomolecules) matching the amino acid sequence (GESNRGHEETSRNC) in the tail region of mouse myosin IIIb (Fig. 3-6a). The antibodies specific for an N-terminal region conserved in mouse espin 1 (PB539; section 2.3.1) and a C-terminal region in mouse myosin IIIa (PB638; Schneider *et al*., 2006) have been previously described.

[ii] I designed probes and experiments, performed cell culture, immunocytochemistry, transfections, confocal imaging, GST pulldowns, and data processing. Dr. Felipe Salles performed dissections, tissue culture, immunohistochemistry, and transfections. Mr. Uri Manor quantified the fluorescence data. Drs. Andrea Dosé and Mark Schneider designed three DNA probes. The localization and overexpression of myosins IIIb, IIIa, and espin 1 were investigated mainly in mouse inner ear hair cells and heterologous COS-7 cells. The interaction between these two proteins were tested by the GST pulldown technique. In progress, Merritt *et al.*

3.3.2 Immunofluorescence and microscopy

Mice were euthanized by CO_2 overdose according to National Institutes of Health (NIH) guidelines, and their temporal bones perfused with 4% paraformaldehyde (PFA) in phosphate buffered saline (PBS; pH 7.4) through the round window and fixed for 2 hours at room temperature. Inner ear epithelia were dissected in PBS, permeabilized with 0.5% Triton X-100 for 30 min and blocked overnight at 4 °C with filtered 4% bovine serum albumin in PBS. Epithelia were then incubated with primary antibody for 2 hours, rinsed with PBS three times, stained with Alexa Fluor 488-conjugated secondary antibody (Molecular Probes) for 1 hour, rinsed with PBS three times, counterstained with Alexa Fluor 568 phalloidin (0.001 U μl^{-1}; Molecular Probes), rinsed with PBS three times, and mounted using ProLong Gold antifade reagent (Invitrogen). Fluorescence confocal images were obtained with a Nikon microscope equipped with a ×100 1.45 numerical aperture (NA) objective and a spinning disk confocal unit (PerkinElmer).

3.3.3 Expression plasmids

Full length mouse myosin IIIb (NCBI accession number BC156281) in pENTR223.1 vector was obtained from Open Biosystems and the insert recombined with pcDNA 6.2/N-EmGFP-DEST vector by LR clonase using the Gateway Technology (Invitrogen). Full length human myosin IIIb variant 2 (NM_138995) was obtained from Origene and the insert was subcloned by PCR and ligated to pCR8/GW/TOPO entry vector (Invitrogen). The insert was subsequently recombined with pcDNA 6.2/N-

EmGFP-DEST vector by LR clonase. Wild-type and WH2 mutant (mWH2) human espin 1 inserts in the untagged vector (pcDNA3.1(-); Invitrogen) have been described earlier (section 2.3.4). Constructs encoding myosin IIIb and espin 1 deletion mutants (except GFP-hMyoIIIb$^{\Delta TAIL}$) were PCR subcloned into pCR8/GW/TOPO entry vector and recombined with pcDNA 6.2/N-EmGFP-DEST, pDEST 15 GST, and/or pcDNA/nV5-DEST expression vector by LR clonase. GFP-hMyoIIIb$^{\Delta TAIL}$ deletion mutant construct was directionally subcloned into the pEGFP-C tag expression vector (BD Biosciences Clontech, CA) via 5′ *Not*I and 3′ *Spe*I restriction sites. All expression plasmids were verified by sequencing, immunofluorescence, and immunoblot. Further details about the clones used are found in Table 3-1 and Figures 1-1, 1-2, 3-6 and 3-7.

DNA construct (aa)	Species (accession no.)	Vector	Forward primer	Reverse primer
GFP-hMyoIIIb (1-1341)	human (NM_138995)	pcDNA 6.2/N-EmGFP-DEST	5′- ATGAAACATC TGTATGGATTATT TCAC	5′-TTTAATGTTGA GCAAAAGAGTCT CC
GFP-hMyoIIIb$^{\Delta K}$ (345-1341)			5′-GATGATTTGGT CAACCTAGAGGT T	5′-ATGTTGAGCA AAAGAGTCTCCT TT
GFP-hMyoIIIb$^{\Delta TAIL}$ (1-1141)		pEGFP-C2	5′-GCTAGCGGCC GCCACCATGCTT GGACTTGAATCA CTTCCAGATCCC ACAGACAC	5′-GCCACATTCCC CCGTCGCAGCAG GTACGACTAGTG CTA
mMyoIIIb-GFP (1-1333)	mouse (BC156281)	pcDNA 6.2/N-EmGFP-DEST	n/a	n/a
GFP-mMyoIIIb$^{\Delta 3THDI,post}$ (1-1247)			5′-GCAGCAGCCT CGGAGGTGAG	5′-TTATGCTCGCT GCTTCTGGGAGA GACCTTC
GFP-mMyoIIIb$^{\Delta K}$ (303-1333)			5′-GTTGCTAAAA CCAGGCATGAAA GGATG	5′-TCAGTGTTGA GCAAAGGGGTCT TCTC
GFP-mMyoIIIb^{TAIL} (909-1333)			5′-GAGGCTCACA TTCACACAGTTC TCCA	
GFP-mMyoIIIb^{pre3THDI} (909-1333)				5′-TTATGCTCGC TGCTTCTGGGAG AGACCTTC
GFP-mMyoIIIb^{3THDI} (909-1333)			5′- CCTCGCAGAC GGTGTCAGCAGC CC AAAATG	5′- TCACCCAGGG GACAGGCATTTG TAATACTGGTC
GFP-mMyoIIIb^{post3THDI} (909-1333)			5′-GCCTGTGCCC CTGAGGAAAC	5′-TCAGTGTTG AGCAAAGGGGT CTTCTC
GFP-espin 1$^{\Delta ABM}$	human (NM_031475)		5′- ATGGCCCTGG AGCAGGCGCTGC AG	5′- TTACCGGACT GGTGACAGTGCA GGTGACACAGA AGGCAG
V5-espin 1$^{\Delta ABM}$		pcDNA/ nV5-DEST		

Table 3-1 Novel myosin IIIb and espin 1 clones and associated primers used in the dissertation.

3.3.4 Cultures and transfection of COS-7 cells

COS-7 cells (ATCC) were trypsinized, plated on coverslips and maintained at 37 °C in DMEM with 10% FBS. Cultures were transfected using either GeneJuice

(Novagen) or Lipofectamine transfection reagent (Invitrogen) according to manufacturer's instructions and incubated for 24 hours. Samples were then fixed for 20 min in 4% PFA in PBS, permeabilized for 30 min in 0.5% Triton X-100 in PBS, and counterstained or processed for immunofluorescence as described earlier.

3.3.5 Culture and transfection of rat inner ear tissue

Organ of Corti and vestibular tissues were dissected from postnatal day 0–8 rat and attached to coverslips previously coated with Cell-Tak (150 μg μl^{-1}; BD Biosciences). Cultures were maintained in DMEM/F12 (Invitrogen) with 5–7% FBS and ampicillin (1.5 μg ml^{-1}; Sigma) and kept at 37 °C and 5% CO_2. For transfections, 50 μg of DNA was precipitated onto 25 mg of 1 μm gold particles and loaded into the Helios Gene Gun cartridges (BioRad). Tissue explants were transfected with the gene gun set at 95 psi of helium and maintained in culture for 18–48 hours. Samples were fixed and counterstained for confocal microscope viewing as described above. The efficiency of transfection ranged from 0–9 hair cells per explant.

3.3.6 Quantification

Physical quantities of stereocilia and filopodia were measured using confocal microscopy and NIH ImageJ.

Relative pixel intensity of protein fluorescence was quantified by the difference in the fluorescence intensity between a region over the stereocilia bundle and an arbitrary background region (Waguespack *et al.*, 2007) divided by the fluorescence intensity of phalloidin (red). All relative pixel intensity numbers were normalized.

To estimate the relative increase in stereocilia length (Fig. 3-8), we compared the heights of the tallest row of well-preserved stereocilia of cochlear and vestibular hair cells transfected (H_T) with the average height of all their respective neighboring (usually between 3–5) non-transfected cells (H_{NT}) within the field of view of our camera/confocal setup (30 × 45 μm). The average ratio of stereocilia length was calculated as $1 = \frac{H_T}{H_{NT}}$.

ANOVA was performed using MATLAB (Mathworks).

Measurements of average filopodia lengths of transfected COS-7 cells (Figs. 3-11 and 3-13) were made using NIH ImageJ by measuring the distance from the periphery of the cell to the filopodia tip.

The mean pixel intensity of immunofluorescence in non-transfected hair cells versus transfected hair cells (Fig. 3-10) was quantified by taking the ratio of the absolute immunofluorescence intensities of the non-transfected and transfected hair cell bundles. n = 10 non-transfected/transfected vestibular hair cell pairs, and n = 3 for cochlear hair cell pairs.

3.3.7 Western blotting

100-mm dishes of transfected semi-confluent COS-7 cells were rinsed in PBS and scraped in 300 μl of ice-cold cell lysis buffer (CLB): dH_2O, 1% Triton-X, 5 mM dithiothreitol, 150 mM NaCl, 50 mM Tris, 2 mM EDTA, 1 mM Pefabloc, 1x Pefabloc protector, and 1% mammalian protease inhibitor cocktail (Sigma). After addition of 1× loading sample buffer (Invitrogen), samples were boiled and sample reducing agent (Invitrogen) added. 10 μl of lysates were loaded in NuPAGE 4–12% Bis-Tris mini-gel

(Invitrogen). Western blots were blocked overnight at 4 °C with 5% nonfat milk (Bio-Rad, Hercules, CA) and incubated with primary antibody for 2 hours. Horseradish peroxidase-conjugated goat anti-rabbit antibodies (Santa Cruz) and ECL chemiluminescence system (Amersham Biosciences) were used for detection.

3.3.8 GST pulldown assays

Protein expressions of glutathione S-transferase (GST) alone or fused to ARD (GST–espin 1^{ARD}) and protein purification are previously described (2.5 Materials and Methods). Briefly, GST proteins were isolated from bacterial lysates using glutathione–Sepharose 4B beads (Amersham Biosciences). GFP–mMyosin $IIIb^{\Delta K}$, $-^{pre3THDI}$, $-^{3THDI}$ and $-^{post3THDI}$ fusion proteins were extracted from 24-hour transfected COS-7 cells by brief sonication in ice-cold CLB and 30-min ultracentrifugation at 145,000 g. To test for myosin IIIb interactions, the same amount of GST–espin 1^{ARD} or GST alone was bound to 4B beads for 1 hour at 4 °C followed by incubation with the same amount of a GFP-tagged myosin IIIb fragment in CLB for 1 1/2 hours. The beads were then washed three times with CLB. 10 µl of co-precipitates were loaded, separated by electrophoresis on NuPAGE Bis-Tris 4-12% gels, and analyzed by Western blotting using rabbit polyclonal anti-GFP and anti-GST antibodies (Invitrogen).

3.4 Results

3.4.1 Myosin IIIb localized to stereocilia tips earlier than myosin IIIa during stereocilia development

We used three affinity purified antibodies, anti(α)-myosin IIIb (PB791), α-myosin IIIa (PB638), and α-espin 1 (PB539), to compare localizations of myosins IIIb, IIIa, and espin 1 in the hair cell during the stereocilia development from the mouse cochlea and

vestibular epithelia and in the transfected heterologous COS-7 cell line. The specificity of these antibodies has been confirmed via Western blotting and COS-7 cell transfection (Figs. 3-1, 2-1, and 4-4; Schneider *et al.*, 2006). The α-myosin IIIb antibody was generated against a fourteen-amino acid peptide corresponding to the pre3THDI region (-^{pre3THDI}) in the carboxl(C)-terminal tail of mouse myosin IIIb (Fig. 3-6a; section 3.3.1). The α-myosin IIIa antibody was generated against a seventeen-amino acid peptide corresponding to the actin-binding 3THDII domain in the C-terminal tail region of mouse myosin IIIa (Schneider *et al.*, 2006). Lastly, the α-espin 1 antibody was generated against a twenty-amino acid peptide corresponding to the first ankyrin repeat of espin 1^{ARD} (Fig. 3-7a; section 2.3.1). The α-myosin IIIa and α-espin 1 antibodies cross-reacted with human and rat orthologues (Figs. 2-1, 2-2, and 2-5; Schneider *et al.*, 2006). Conversely, the α-myosin IIIb antibody did not cross-react with a human or rat orthologue (data not shown). Since the α-myosin IIIb antibody reacted only with mouse myosin IIIb, mouse inner ear epithelia or mouse plasmid DNA constructs were used in all α-myosin IIIb immunofluorescence preparations.

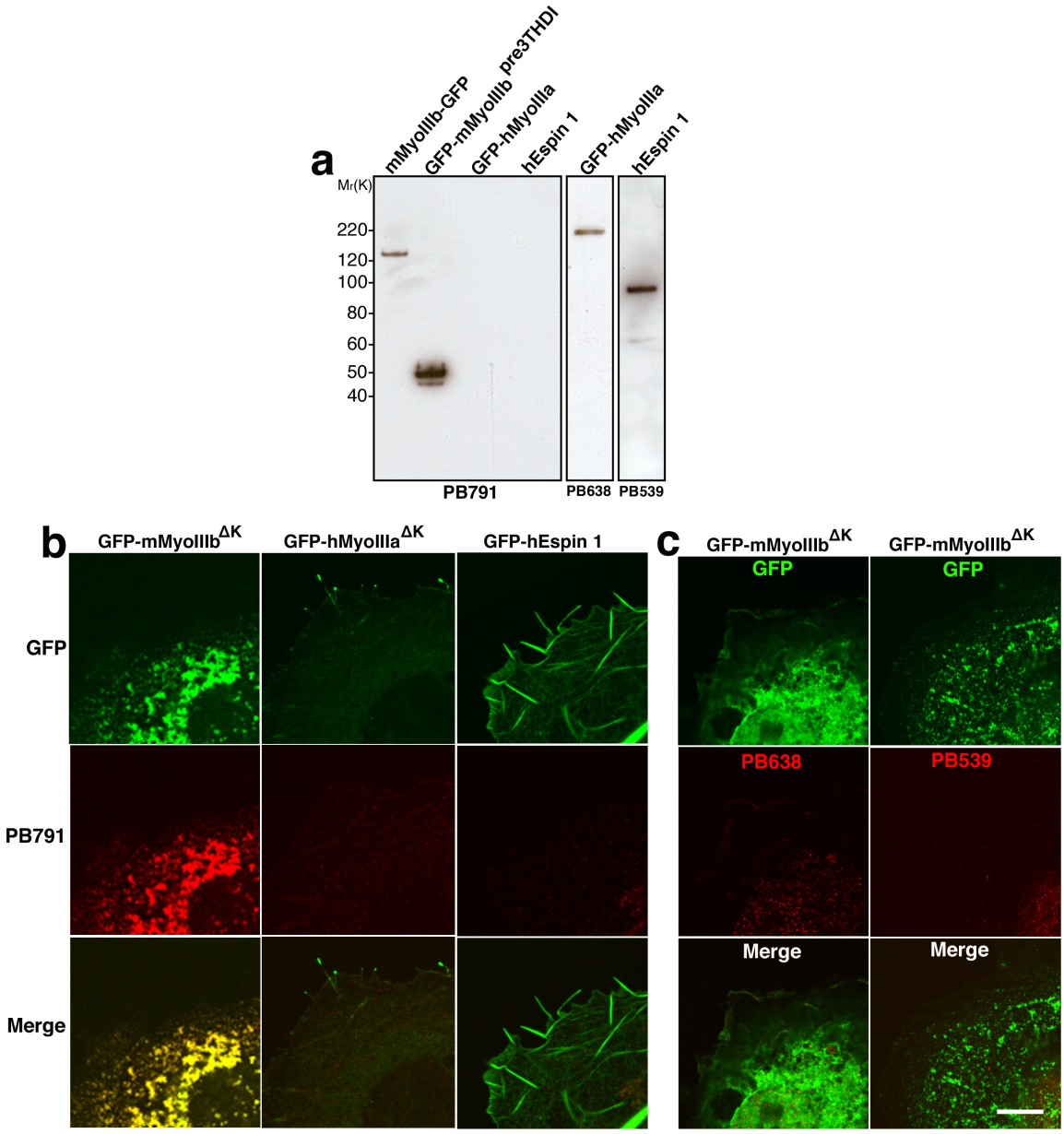

Figure 3-1 Specificity of the affinity-purified antibody, PB791, generated against the C-terminal tail of myosin IIIb. (**a**) Immunoblots of COS-7 cell lysates transfected with mMyoIIIb-GFP, GFP-mMyoIIIb^{pre3THDI}, GFP-hMyoIIIa, and hEspin 1 show that PB791 specifically recognizes the tail of myosin IIIb but not myosin IIIa or espin 1. The presence of myosin IIIa and espin 1 is confirmed by anti-myosin IIIa (PB638) and anti-espin 1 (PB539) antibodies. See Figure 3-6a for the mapping of the PB791 epitope. (**b**) GFP-mMyoIIIb$^{\Delta K}$ (left column) overexpression in COS-7 cells is recognized by PB791. The same antibody shows no labeling in COS-7 cells with overexpressing GFP-hMyoIIIa$^{\Delta K}$ (middle column) or GFP-hEspin 1 (right column). (**c**) In the negative controls, PB638 (left column) and PB539 (right column), fail to recognize GFP-mMyoIIIb$^{\Delta K}$ in COS-7 cells. GFP constructs are in green and Alexa Fluor 568-conjugated secondary antibody is red. Scale bar, 5 μm.

The myosin IIIb tip localization results in our immunofluorescence experiments (Fig. 3-2a) were nearly indistinguishable from the myosin IIIa (Fig. 3-2b) and espin 1 (Fig. 3-2c) localizations at the stereocilia tips of both the cochlear and vestibular hair cells. However, fluorescent puncta of myosin IIIb was often less visible in the stereocilia rows besides the middle stereocilia row (Fig. 3-3). This phenotype is different from myosin IIIa where the puncta are more visible in the taller and shorter rows (e.g. compare Figs. 3-2a with b; Schneider *et al.*, 2006).

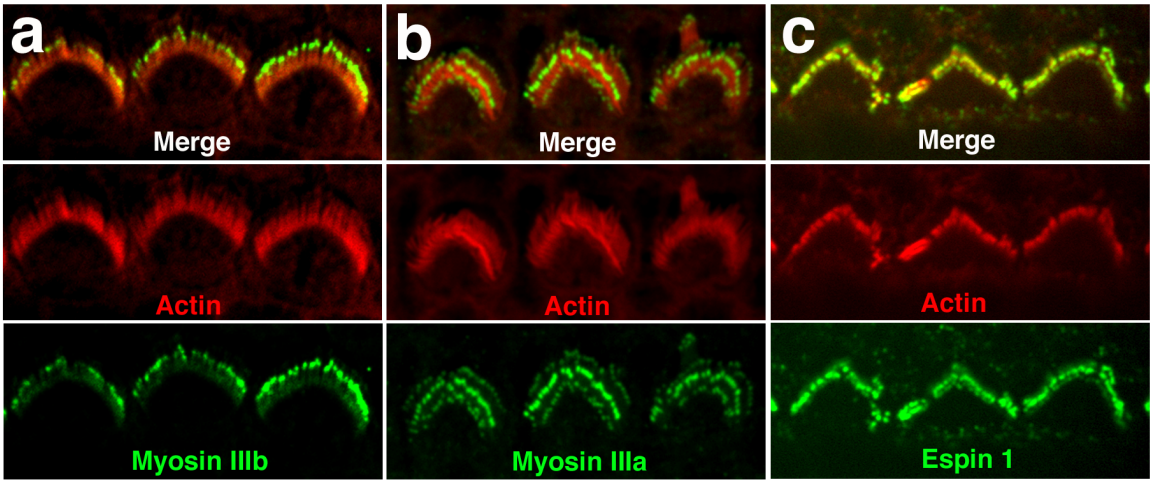

Figure 3-2 Myosin IIIb localization at the stereocilia tips is the same as myosin IIIa and espin 1 localizations. (**a, b, c**) Confocal images show that myosin IIIb (**a**, green) localizes at the tips of stereocilia in mouse cochlear hair cells which matches the localization observed for myosin IIIa (**b**, green) and espin 1 (**c**, green) but reaches a peak fluorescent intensity at about postnatal day (P) 2 as opposed to myosin IIIa and espin 1 at P6. Primary antibodies used: α-myosin IIIb (PB791), α-myosin IIIa (PB638), and α-espin 1 (PB539). In all immunofluorescence images, the immunolabeling was visualized using Alexa-488-conjugated secondary antibody and the filamentous actin (red) was visualized using Alexa 568 phalloidin. (Dr. Salles assisted with immunohistochemistry)

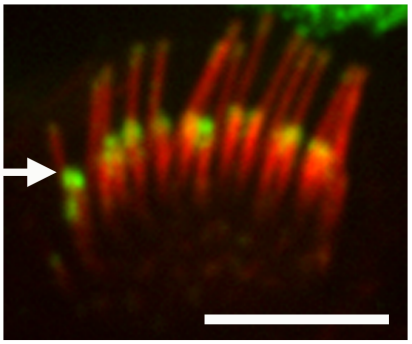

Figure 3-3 Prominent myosin IIIb immunofluorescence in the middle row of stereocilia bundle of mouse inner hair cell at P2. Myosin IIIb puncta are mostly observable at the stereocilia tips in the middle row (arrow). Myosin IIIb demonstrates the thimble-like pattern, a resemblance of myosin IIIa.

In the basal turn of the rodent cochlea, stereocilia appear from the apical surface of the IHCs and OHCs at embryonic day (E) ~18. By ~P21, the stereocilia bundles fully matured (Lim and Anniko, 1985; Tilney *et al.*, 1988; Kaltenbach *et al.*, 1994). The maturation of IHCs at the cochlear base precedes the maturation of OHCs, and development advances toward the cochlear apex over several days (Zine and Romand, 1996; Waguespack *et al.*, 2007). In the immature hair cells of the basal regions of the P0 mouse cochlea, myosin IIIb immunolabeling was observed at the tips of the emerging stereocilia (Fig. 3-4c; P2 shown in Fig. 3-4a), in contrast to the paucity of myosin IIIa immunolabeling during that age (Fig. 3-4b). The levels of myosin IIIb immunoreactivity at the stereocilia tips progressively declined through P4, P6, and P8 (Fig. 3-4a) against the maturational phase of the stereocilia and the increasing immunoreactivity levels of myosin IIIa (Fig. 3-4b). The relative pixel intensity (rpi) of myosin IIIb immunofluorescence intensity was found to be inversely correlated to the myosin IIIa fluorescence intensity from P0 to P8 (Fig. 3-4c). No fluorescence signal of myosin IIIb was detected in mouse adult cochlear hair cells during P40 with or without the antigen retrieval step (data not shown). In the mouse vestibular stereocilia, myosin IIIb immunoreactivity was detectable from P0 through P8 and in adults (Fig. 3-5). These results indicate that the difference in myosin IIIb and IIIa expression is in the cochlear hair cells but not in the vestibular hair cells.

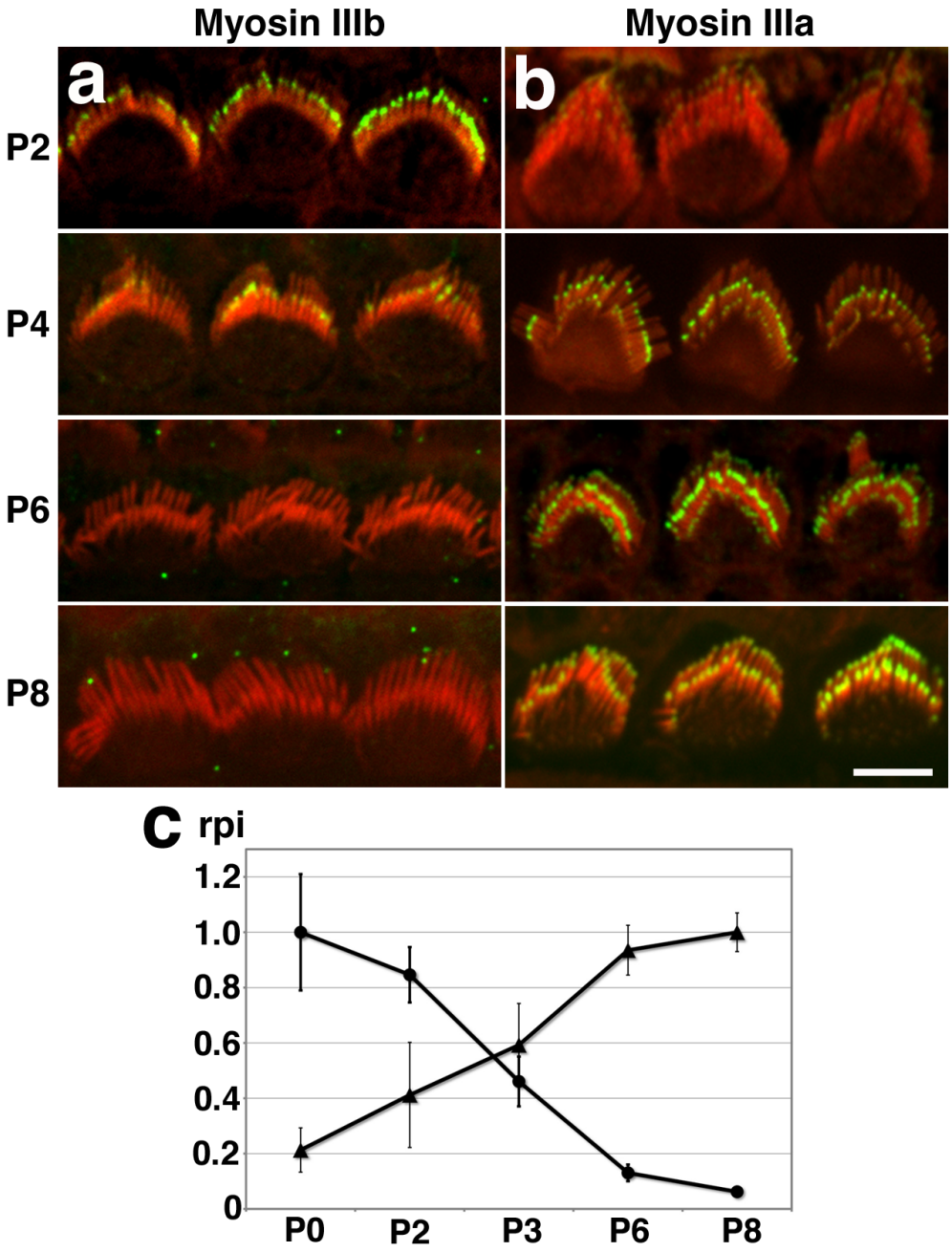

Figure 3-4 Myosin IIIb has a different phase of immunoreactive protein expression from myosin IIIa. (**a**) Immunofluorescence of mouse cochlear hair cells at different developmental time points shows that myosin IIIb compartmentalizes at stereocilia tips at P2 and regresses during P4, P6, and P8 reaching a low immunofluorescence intensity. (**b**) Myosin IIIa immunofluorescence in mouse cochlear hair cells at different developmental time points shows that myosin IIIa targets stereocilia tips at P2 and undergoes progressive compartmentalization at the tips during P4 and P6, reaching a peak of immunofluorescence intensity at about P8. (**c**) The graph illustrates relative pixel intensity (rpi) measurements of myosin IIIb (circle) and myosin IIIa (triangle) immunofluorescence in the stereocilia bundle versus different developmental time-points from P0 to P8. The difference in the temporal immunoreactive expression pattern between myosins IIIb and IIIa is reflected by the opposite slopes of the best linear fits (R-squares of 0.96 and 0.97). The error bars represent the standard error of the mean (± s.e.m). (Dr. Salles and Mr. Manor assisted with immunohistochemistry, imaging, and quantification)

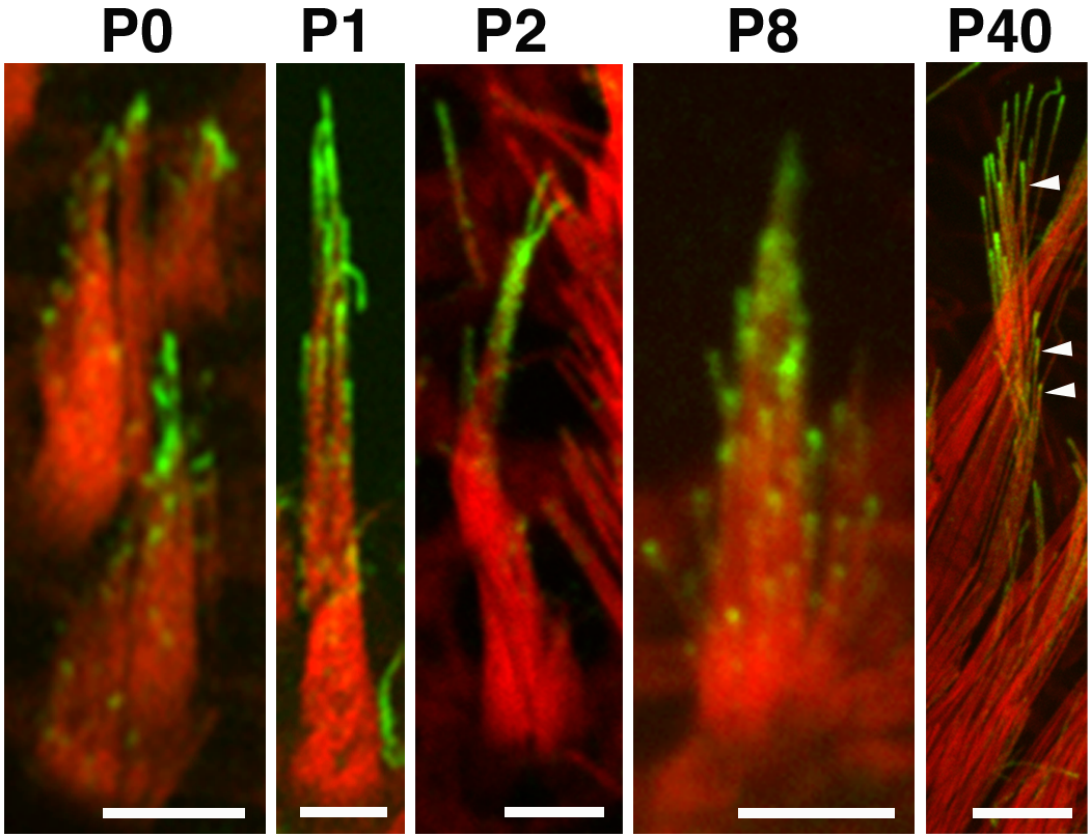

Figure 3-5 Spatiotemporal expression of myosin IIIb in mouse vestibular stereocilia. Myosin IIIb (green) localizes at the stereocilia tips of the mouse vestibular hair cell at P0, P1, P2, P8, and P40, indicating a stable presence of myosin IIIb in the vestibular stereocilia. Myosin IIIb localization reveals a tip-to-base gradient that is more extended in longer stereocilia than shorter stereocilia (arrowheads). Scale bars, 5 μm. Primary antibody used: α-myosin IIIb (PB791). In all immunofluorescence images, the immunolabeling was visualized using Alexa-488-conjugated secondary antibody and the filamentous actin (red) was visualized using Alexa 568 phalloidin. (Dr. Salles assisted with immunohistochemistry)

3.4.2 The profile of myosin IIIb overexpression in the stereocilia

We further explored the phenotype and function of myosin IIIb via protein overexpression in transfected hair cells and COS-7 cell line. Wild-type and mutant myosins IIIb, IIIa, and espin 1 plasmid DNA constructs were generated in the laboratory for the purpose of cell transfection and GST pulldown experiments. Figures 3-6 and 3-7 illustrate diagrammatic panels of those engineered constructs. The integrity of the constructs has been confirmed by sequencing (data not shown), Western blotting (Figs.

3-6b and 3-7b), and immunofluorescence (Figs. 2-5, 2-6, 2-7, 2-9, 2-12, 3-6, 3-7, 3-8, 3-9, and 3-12).

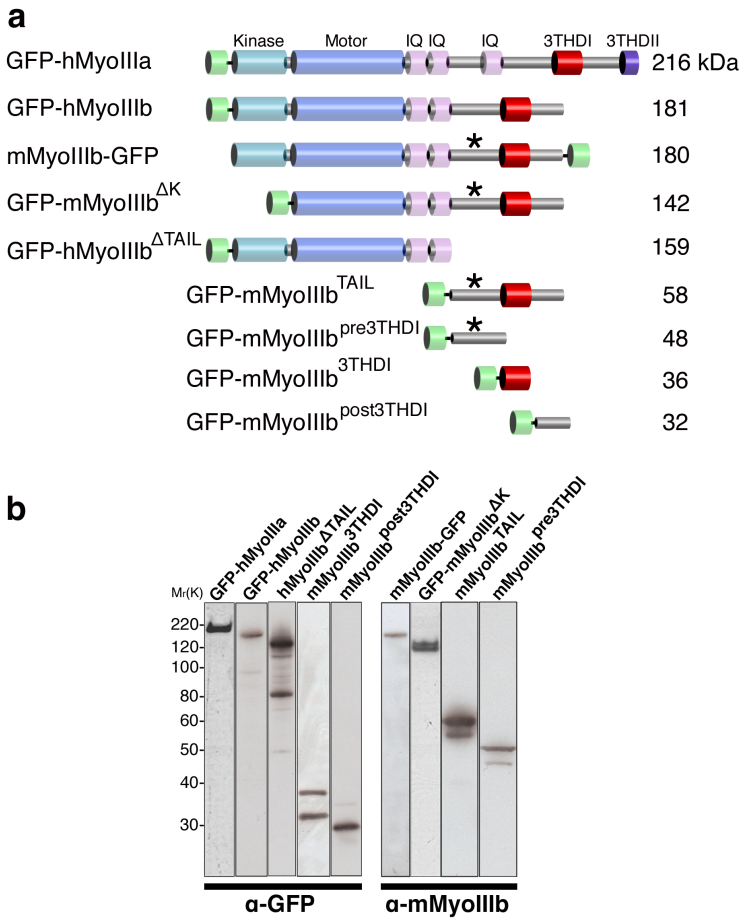

Figure 3-6 Full length and mutant myosin III constructs. (**a**) Schematic map of myosin IIIa and IIIb wild-type and deletion mutant constructs fused to GFP. Full length human myosin IIIa (NCBI accession number AY101367), myosin IIIb (NM_138995), and mouse myosin IIIb (BC156281) are shown respectively at the top. Asterisks (*) denote the epitope position in the mouse myosin IIIb molecule recognized by the anti(α)-mMyoIIIb (PB791) antibody (Fig. 3-1). GFP-mMyosin IIIb delta (Δ) kinase deletion mutant (GFP-mMyoIIIb$^{\Delta K}$) lacks the N-terminal kinase domain. GFP-hMyosin IIIb Δtail deletion mutant (GFP-hMyoIIIb$^{\Delta TAIL}$) lacks the entire C-terminal tail. The last four constructs at the bottom are derived from the mouse myosin IIIb DNA template. GFP-mMyoIIIb^{TAIL} encodes exclusively the C-terminal tail encompassing the 3THDI domain. GFP-mMyoIIIb^{pre3THDI} encodes a divergent amino acid region between second IQ motif and 3THDI. GFP-mMyoIIIb^{3THDI} encodes exclusively the conserved 3THDI domain. GFP-mMyoIIIb^{post3THDI} encodes the last 27 amino acids downstream of the 3THDI. Predicted molecular weights (kDa) of the constructs are indicated at the right. See Tables 2-1 and 3-1 as well as Figure 1-1 for further details about the constructs depicted here. (**b**) Western blots of myosin IIIa and IIIb expression constructs. COS-7 cell lysates were prepared from transfected cultures and an equal volume of protein lysate (10 µl) was separated by SDS-PAGE and processed for immunoblot analysis using α-GFP and α-mMyoIIIb antibodies (indicated at bottom). The α-GFP antibody was used instead to stain those GFP-hMyoIIIb constructs (lanes on left) not recognizable by the α-mMyoIIIb antibody as well as the GFP-hMyoIIIa construct. M_r(K), relative molecular weights in kilodaltons, is indicated vertically on the left. Construct names are indicated diagonally on the top. Although more than one band was detected in several construct lanes likely due to protein degradation or background, all construct lanes demonstrate a positive band that matches with the corresponding expected molecular weight of the protein construct.

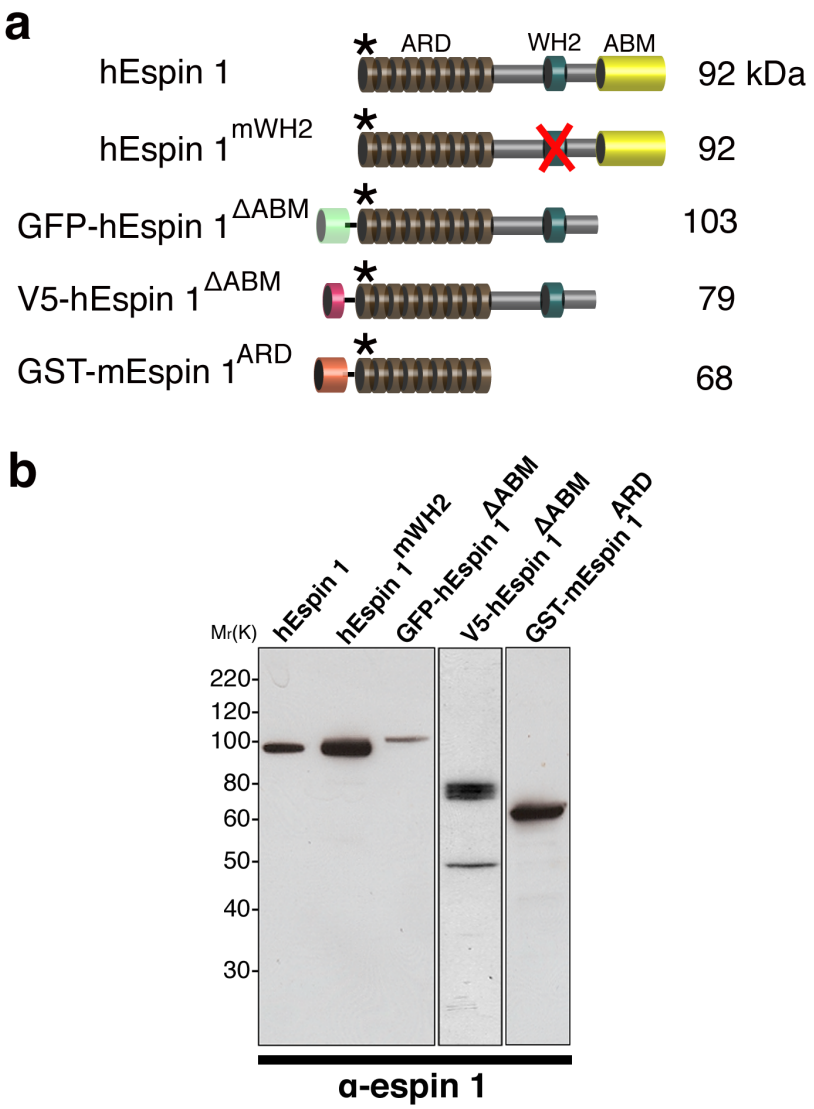

Figure 3-7 Full length and mutant espin 1 constructs. (**a**) Schematic map of wild-type, deletion mutant, and base substitution espin 1 mutant constructs. These espin constructs were derived from the human espin variant 1 (hEspin 1; NCBI accession number NM_031475) or the mouse espin variant 1 (mEspin 1; NM_207687) cDNA template. Asterisks (*) denote the epitope position in the espin molecules recognized by the α-espin 1 (PB539) antibody (Fig. 2-1; section 2.3.1). hEspin 1 is an untagged full length construct. hEspin 1^{mWH2} is the same as hEspin 1 except that two leucine residues in the WH2 motif are substituted with alanine residues (L655A, L656A; section 2.3.4). GFP-hEspin $1^{\Delta ABM}$ and V5-hEspin $1^{\Delta ABM}$ are espin 1 deletion mutants that lack the ABM (Actin Bundling Module). GST-mEspin 1^{ARD} is a GST construct fused to the ARD (Ankyrin Repeats Domain) of mouse espin 1. See Tables 2-1 and 3-1 as well as Figure 1-2 for further details about the constructs depicted here. (**b**) Western blot of espin 1 expression constructs. COS-7 cell lysates were prepared from transfected cultures and an equal volume of protein lysate (10 µl) was separated by SDS-PAGE and processed for immunoblot analysis using α-espin 1 antibody (indicated at bottom). M_r(K), relative molecular weights in kilodaltons, is indicated vertically on the left. Construct name is indicated horizontally on the top. All construct lanes demonstrate a positive band that matches with the corresponding expected molecular weight of the protein construct.

To examine the ability of hair cells to properly compartmentalize exogenous myosin IIIb to the tips of stereocilia and the effect of myosin IIIb on stereocilia elongation, we transfected rat vestibular hair cells at P2 with wild-type mouse GFP-tagged myosin IIIb (GFP-mMyoIIIb; Fig. 3-8a) or with mouse GFP-tagged myosin IIIb lacking the kinase domain (GFP-mMyoIIIb$^{\Delta K}$; Fig. 3-8b).

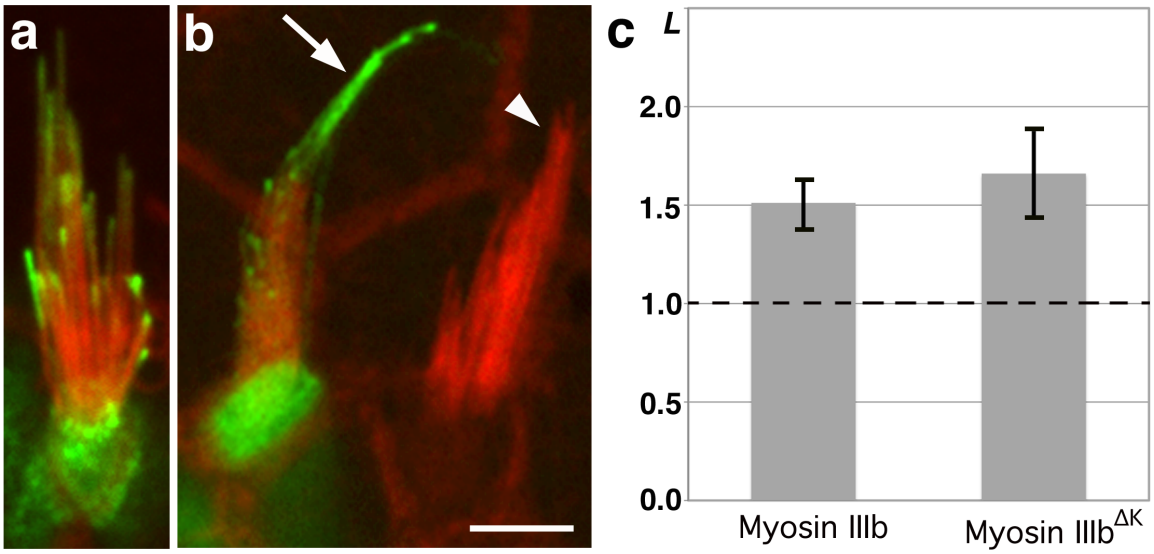

Figure 3-8 Myosin IIIb$^{\Delta K}$ overexpression results in stereocilia elongation of rat vestibular hair cells (VHCs). (**a, b**) Both GFP–mMyoIIIb (**a**) and GFP-mMyoIIIb$^{\Delta K}$ (**b**) accumulate at stereocilia tips in transfected P2 VHCs. Stereocilia of the GFP-mMyoIIIb$^{\Delta K}$ transfected cells appears significantly longer (arrow) than those of non-transfected (arrowhead) cells *(P* = 0.001, ANOVA). (**c**) The average ratios of stereocilia length (*L*) between transfected (H_T) and neighboring non-transfected (H_{NT}) hair cells, $l = \frac{H_T}{H_{NT}}$. GFP-mMyoIIIb = 1.511 ± 0.125 (~51% increase); *n* = 6. GFP-mMyoIIIb$^{\Delta K}$ = 1.66 ± 0.216 (~66% increase); *n* = 13. Note that a value of *L* = 1 (indicated by the dotted line in the graph) corresponds to a zero percent increase in length. Error bars represent ± s.e.m. Scale bar, 5 µm. (Dr. Salles and Mr. Manor assisted with transfection and quantification, respectively)

Myosin IIIb was concentrated at the tip of each stereocilium within 18 hours after hair cell transfection. Analysis of the lengths of VHC stereocilia transfected with GFP-mMyoIIIb$^{\Delta K}$ showed that stereocilia were elongated (Fig. 3-8c). The reason for the removal of kinase (ΔK) in the GFP-mMyoIIIb$^{\Delta K}$ construct has been explained in chapter 2 (section 2.4.5) and by Schneider *et al.* (2006). Briefly, since myosin III is more active

without its kinase domain (Dosé *et al.*, 2008), removing it helps in studying the function of myosin III.

To determine whether stereocilia tip localization of myosin IIIb depends on its C-terminal tail, a construct lacking the tail region (GFP-hMyoIIIb$^{\Delta TAIL}$) was used to transfect rat hair cells. Those hair cells positive for GFP-hMyoIIIb$^{\Delta TAIL}$ expression showed diffuse fluorescence in the cytoplasm with no apparent fluorescence in the stereocilia (Fig. 3-9b; n = 17). This finding suggests that the 3THDI domain, implicated as the espin 1 cargo binding domain, in the C-terminal tail is necessary for the tip localization.

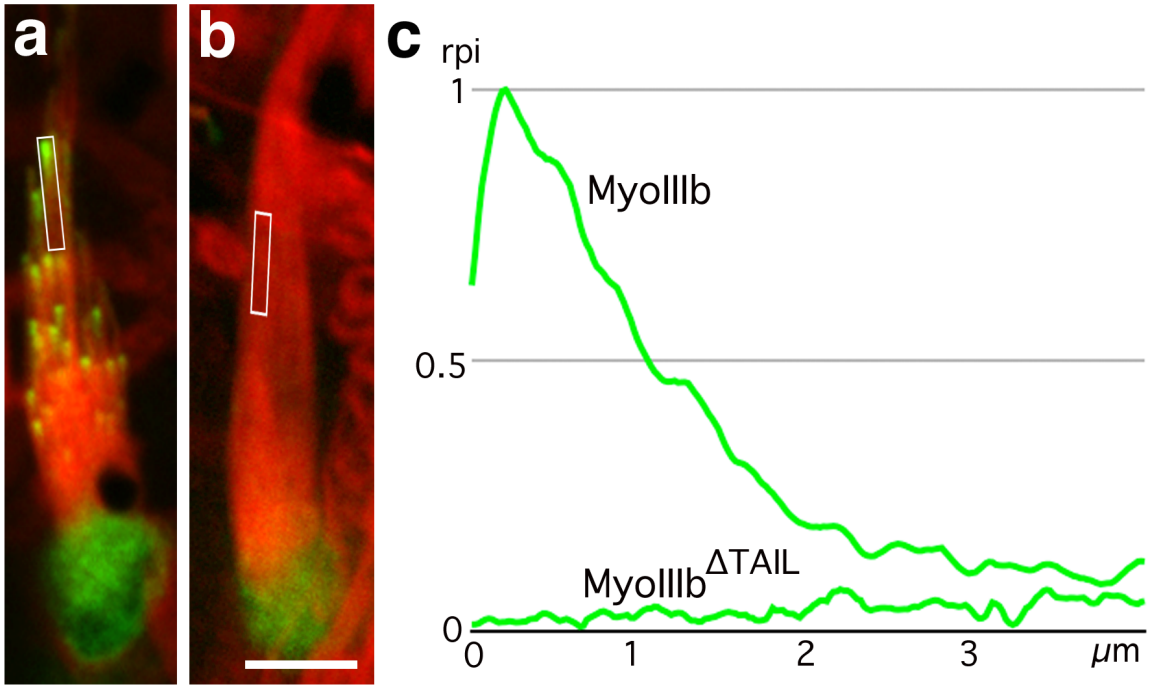

Figure 3-9 C-terminal tail of myosin IIIb is required for stereocilia tip localization. (**a**) GFP-mMyoIIIb accumulates at the stereocilia tips of rat vestibular hair cells. Tip-to-base concentration gradient of myosin IIIb fluorescence is observed (rectangular inset). (**b**) GFP-hMyoIIIb$^{\Delta TAIL}$ fails to target the stereocilia tips suggesting that endogenous espin 1 cannot bind to myosin IIIb lacking the tail region. (**c**) Measurements of GFP-mMyoIIIb and GFP-hMyoIIIb$^{\Delta TAIL}$ relative fluorescence intensity (rpi) along the stereocilium in each rectangular inset (**a** and **b**) illustrate the distribution of these GFP fusion proteins. The tip-to-base concentration gradient of myosin IIIb fluorescence is reflected by the MyoIIIb slope. (Dr. Salles assisted with hair cell transfection)

To test the effect of myosin IIIb overexpression in the stereocilia tips on the myosin IIIa expression, rat cochlear hair cells and VHCs at age of P8 were transfected with GFP-mMyoIIIb and immunostained with the α-myoIIIa antibody. Myosin IIIa immunolabeling was observed at the stereocilia tips of the GFP-mMyoIIIb transfected cochlear hair cells (Fig. 3-10a) but not of the transfected VHCs (Fig. 3-10b).

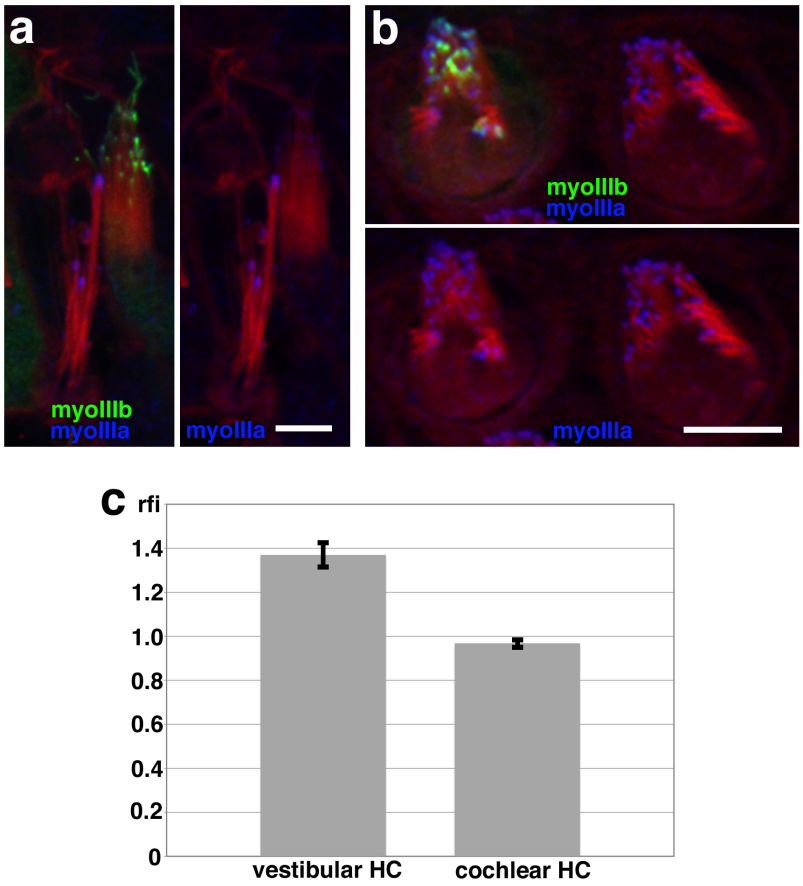

Figure 3-10 GFP-myosin IIIb overexpression downregulates myosin IIIa localization in stereocilia tips of vestibular hair cells. (**a**) Rat vestibular hair cells transfected with GFP–mMyoIIIb (green) and immunostained with anti-myosin IIIa antibody (PB638; blue). The myosin IIIa immunofluorescence intensity is attenuated in the stereocilia tips of GFP–mMyoIIIb transfected cells (upper right stereocilia bundle) compared to that of stereocilia tips of non-transfected cell (bottom left). (**b**) Rat cochlear hair cells transfected with GFP–mMyoIIIb (green) and immunostained with anti-myosin IIIa antibody (PB638; blue). There is no difference in the immunofluorescence intensity of myosin IIIa (bottom image) between the transfected (left) and non-transfected cell (right). Scale bars, 5 µm. (**c**) The mean ratios of myosin IIIa immunofluorescence intensity (rfi) between non-transfected (rpi_{NT}) hair cells and neighboring transfected (rpi_T) hair cells (n = 10, both GFP-mMyoIIIb transfected and non-transfected vestibular hair cells; n = 3 for both transfected and non-transfected cochlear hair cells; $P < 0.005$, ANOVA). The error bars represent ± s.e.m. (Dr. Salles and Mr. Manor assisted with hair cell transfection and measurements)

The mean pixel intensity ratio of the myosin IIIa immunofluorescence of transfected VHC to non-transfected VHC was greater than in cochlear hair cells (Fig. 3-10c). These data suggest that the overexpression of GFP-mMyoIIIb$^{\Delta K}$ downregulates the myosin IIIa localization in VHC stereocilia tips, but not in cochlear hair cell stereocilia tips. This is an implication that myosins IIIb and IIIa share the same compartment in the stereocilia tips and that myosin IIIb potentially has roles overlapping with myosin IIIa in vestibular more than cochlear hair cells.

3.4.3 Tip localization of myosin IIIb depended on its espin 1

We next evaluated the distribution and elongation effect of GFP-mMyoIIIb$^{\Delta K}$ on filopodia in transfected COS-7 cells (Fig. 3-11). Control immunostains of COS-7 confirmed that myosin IIIb is not expressed endogenously (Fig. 3-1b). When COS-7 cells were overexpressed with GFP-mMyoIIIb$^{\Delta K}$ alone, the motor protein failed to localize to the filopodia tips (Fig. 3-11a) presumably due to the absence of the actin-binding 3THDII in the tail region of myosin IIIb (Fig. 3-6). This phenotype is consistent with the phenotype of COS-7 cells transfected with GFP-hMyoIIIa$^{\Delta K\text{-}33\text{-}34}$ (Schneider *et al.*, 2006), which has deletions of exons 33 through 35, and lacks 3THDII (see exon map Fig. 1-1c). Conversely, the filopodia tip localization phenotype was rescued when the COS-7 cells were transfected with GFP-mMyoIIIb$^{\Delta K}$ and hEspin 1 (Fig. 3-11c). The synergistic elongation of COS-7 filopodia has been previously observed when co-transfected with myosin IIIa and espin 1 (Fig. 2-7). Here, COS-7 cells co-transfected with GFP-mMyoIIIb$^{\Delta K}$ had similar elongation phenotype, in which the mean filopodia length is

twice longer than those transfected with GFP-mMyoIIIb$^{\Delta K}$ alone or hEspin 1 alone (Fig. 3-11d).

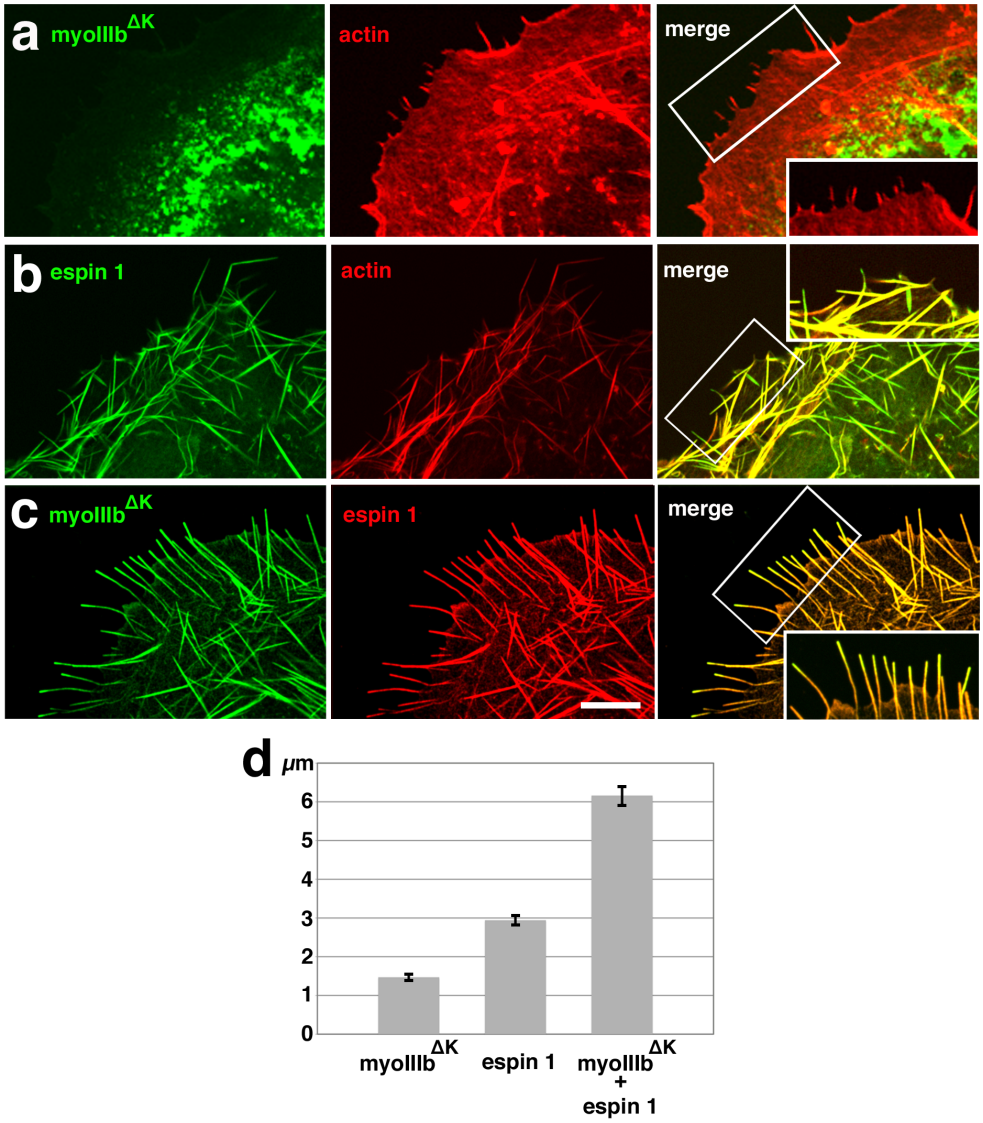

Figure 3-11 The filopodia tip localization of myosin IIIb depend on espin 1. (**a**) GFP-mMyoIIIb$^{\Delta K}$ localizes to the cytoplasm but not filopodia tips of the transfected COS-7 cell. (**b**) GFP-hEspin 1 localize to the actin bundles including the filopodia tips. COS-7 cells in both **a** and **b** rows were counterstained with phalloidin Alexa 568. (**c**) GFP-mMyoIIIb$^{\Delta K}$ and hEspin 1 colocalize to the filopodia tips. COS-7 cell was stained with anti-espin 1 antibody (PB539; red). The right column across the rows show close ups of filopodia tips from the images on the left (rectangles). Scale bar, 5 μm. (**d**) Measurements of average filopodia lengths of transfected COS-7 cells. GFP-mMyoIIIb$^{\Delta K}$ alone = 1.47 ±0.07, n_f = 93, n_c = 18; GFP-espin 1 alone = 2.94 ±0.11, n_f = 162, n_c = 10; and GFP-mMyoIIIb$^{\Delta K}$ and GFP-espin 1 = 2.94 ±0.11, n_f = 177, n_c = 27. Data are ± s.e.m.; the mean value for the COS-7 co-transfected with myosin IIIb$^{\Delta K}$ and espin 1 was significantly higher than that of the cells transfected with GFP-mMyoIIIb$^{\Delta K}$ or espin 1 alone (P = 0.002, ANOVA). Co-transfection n_f and n_c denote number of filopodia and number of cells, respectively. (Mr. Manor assisted with measurements)

3.4.4 Myosin IIIb interacted with espin 1 through its conserved domain, 3THDI, in C-terminal tail

To confirm the colocalization of myosin IIIb and espin 1 and to eliminate the question of whether the affinity of the mMyoIIIb$^{\Delta K}$ deletion mutant for espin 1 is artificial due to protein misfolding, COS-7 cells were transfected with full length myosin IIIb fused to GFP (GFP-mMyoIIIb) and untagged full length espin 1. These proteins colocalize to actin bundles of the cell (Fig. 3-12a, top row). This interaction between myosin IIIb and espin 1 was confirmed by a GST pull-down assay, which the GFP-mMyoIIIb$^{\Delta K}$ fusion protein co-precipitated with the GST-mEspin 1^{ARD} (Fig. 3-12b, upper left pane) but not with the GST alone. Since the conserved 3THDI domain of myosin IIIa binds to the ARD of espin 1 (Fig. 2-7), we sought to confirm the region of interaction on myosin IIIb to be 3THDI. COS-7 cells were co-transfected with hEspin 1 and with a GFP-tagged myosin IIIb tail portion encoding either 3THDI (GFP–mMyoIIIb^{3THDI}) or its immediate flanking regions (GFP-mMyoIIIb^{pre3THDI} or GFP-mMyoIIIb^{post3THDI}). Colocalization of GFP-mMyoIIIb^{3THDI} with espin 1 was exclusively observed (Fig. 3-12a, third row) as there was no espin 1 colocalization for the regions immediately amino-terminal, GFP-mMyoIIIb^{pre3THDI} (Fig. 3-12a, second row), or carboxy-terminal, GFP-mMyoIIIb^{post3THDI} (Fig. 3-12a, fourth row), to the myosin IIIb 3THDI domain. The myosin IIIb^{3THDI}-espin 1^{ARD} interaction was verified *in vitro* using the GST pulldown technique, which GST–espin 1^{ARD} binds to GFP–mMyoIIIb^{3THDI}, but not to the GFP-mMyoIIIb^{pre3THDI} or -^{post3THDI} regions (Fig. 3-12b). These data indicate that espin 1 and myosin IIIb interact through their ARD and 3THDI, respectively. This suggests that the

function of 3THDI as a cargo-binding site for espin 1 is conserved across class III myosins.

Figure 3-12 Myosin IIIb interacts with espin 1 in transfected COS-7 cells and *in vitro*. These two proteins interact through 3THDI of myosin IIIb and ARD of espin 1. (**a**) Co-expression of untagged hEspin 1 shows that mMyoIIIb-GFP (first row; green) and GFP-mMyoIIIb^{3THDI} (third row) colocalize with hEspin 1 (red) in filopodia. Conversely, GFP-mMyoIIIb^{pre3THDI} (second row), and GFP-mMyoIIIb^{post3THDI} (fourth row) are diffused in the cytoplasm, despite the presence of hEspin 1 bundles. (**b**) Western blots of GST pull-downs confirm that myosin IIIb interacts (dotted lanes) with espin 1 and that the 3THDI region of myosin IIIb is necessary for binding to espin 1^{ARD}, as mMyoIIIb^{pre3THDI} and mMyoIIIb^{post3THDI} show no binding to espin 1^{ARD}. Precipitates were detected using anti-rabbit polyclonal α-GST and α-GFP antibodies. The double bands of GFP-myosin III fusion proteins are probably due to a degradation or modification of the GFP moiety (e.g. proteolysis, phosphorylation, dephosphorylation, or oxidation) as the GFP alone control showed the same double band pattern (data not shown).

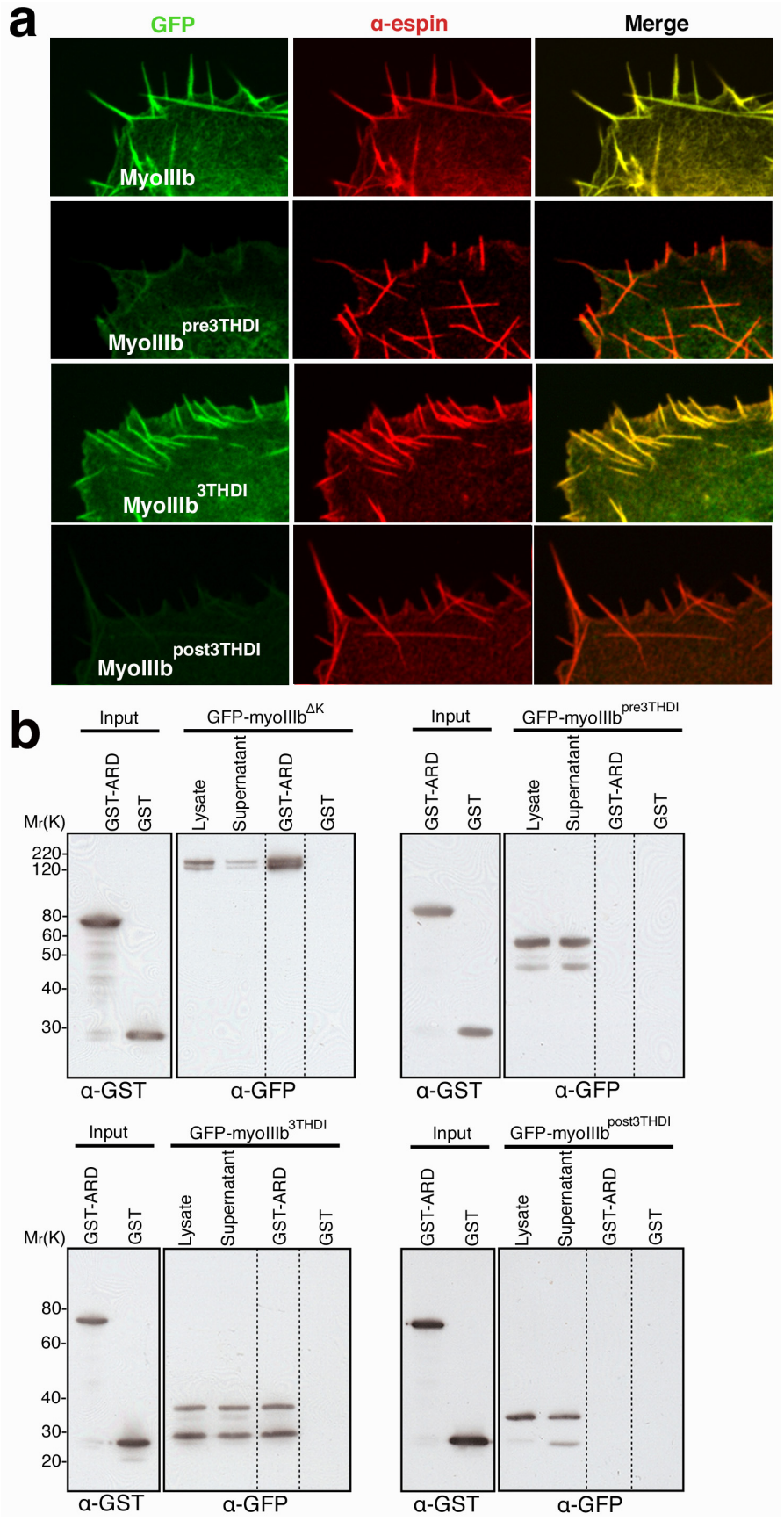
a
GFP
α-espin
Merge
MyoIIIb
MyoIIIb pre3THDI
MyoIIIb 3THDI
MyoIIIb post3THDI
b
Input
GFP-myoIIIb ΔK
GFP-myoIIIb pre3THDI
GFP-myoIIIb 3THDI
GFP-myoIIIb post3THDI
GST-ARD
GST
Lysate
Supernatant
Mr(K)
220
120
80
60
50
40
30
20
α-GST
α-GFP

3.4.5 The actin bundling module of espin 1 is required for filopodia tip localization and synergistic elongation phenotype of myosin IIIb

Synergistic elongation of filopodia was observed when COS-7 cells were co-transfected with myosin IIIa and espin 1 (Fig. 2-9). We next ask whether myosin IIIb:espin 1 has a combined functional role, similar to that of myosin IIIa:espin 1, in the elongation of COS-7 cell filopodia. COS-7 cells co-transfected with GFP-mMyoIIIb$^{\Delta K}$ and espin 1 (Fig. 3-13a; also seen in Fig. 3-11c) yielded long filopodial actin protrusions (mean length = 6.7 μm ± 0.27, n_c = 45, n_f = 178; n_c = number of cells, n_f = number of filopodia; Fig. 3-13g). Although GFP-hMyoIIIa$^{\Delta K}$ and hEspin 1 co-expression produced longer filopodia (13.0 ± 1.1 μm, n_c = 23, n_f = 70; Fig. 3-13g) than with GFP-mMyoIIIb$^{\Delta K}$, their synergistic phenotype is similar in terms of combined elongation with espin 1 (Fig. 3-13a, d).

We further investigated the function of myosin IIIb and espin 1 co-expression in filopodia elongation by testing the dependency of myosin IIIb on espin 1's functional domains, ABM and WH2. We showed that myosin IIIb interacts with espin 1 through its 3THDI domain and espin 1's ARD (section 3.4.4). Since espin 1 binds to actin filaments through its ABM (Bartles *et al.*, 1996), we predicted that the deletion of ABM from espin 1 (hEspin 1$^{\Delta ABM}$) will abolish the localization of myosin IIIb toward the filopodia tips and the synergistic elongation phenotype. This prediction was confirmed when COS-7 cells were co-transfected with GFP-mMyoIIIb$^{\Delta K}$ and V5-hEspin 1$^{\Delta ABM}$ (Fig. 3-13b, g), in which these two proteins colocalized diffusely in the cytoplasm but neither targeted filopodia tips nor elongated filopodia (1.36 ± 0.06 μm, n_c = 17, n_f = 88). Conversely, co-

transfection of GFP-hMyoIIIa$^{\Delta K}$ with V5-hEspin 1$^{\Delta ABM}$ showed filopodia tip targeting (Fig. 3-13e) and produced modest elongation (2.5 ± 0.17 µm, n_c = 95, n_f =78; Fig. 3-8g).

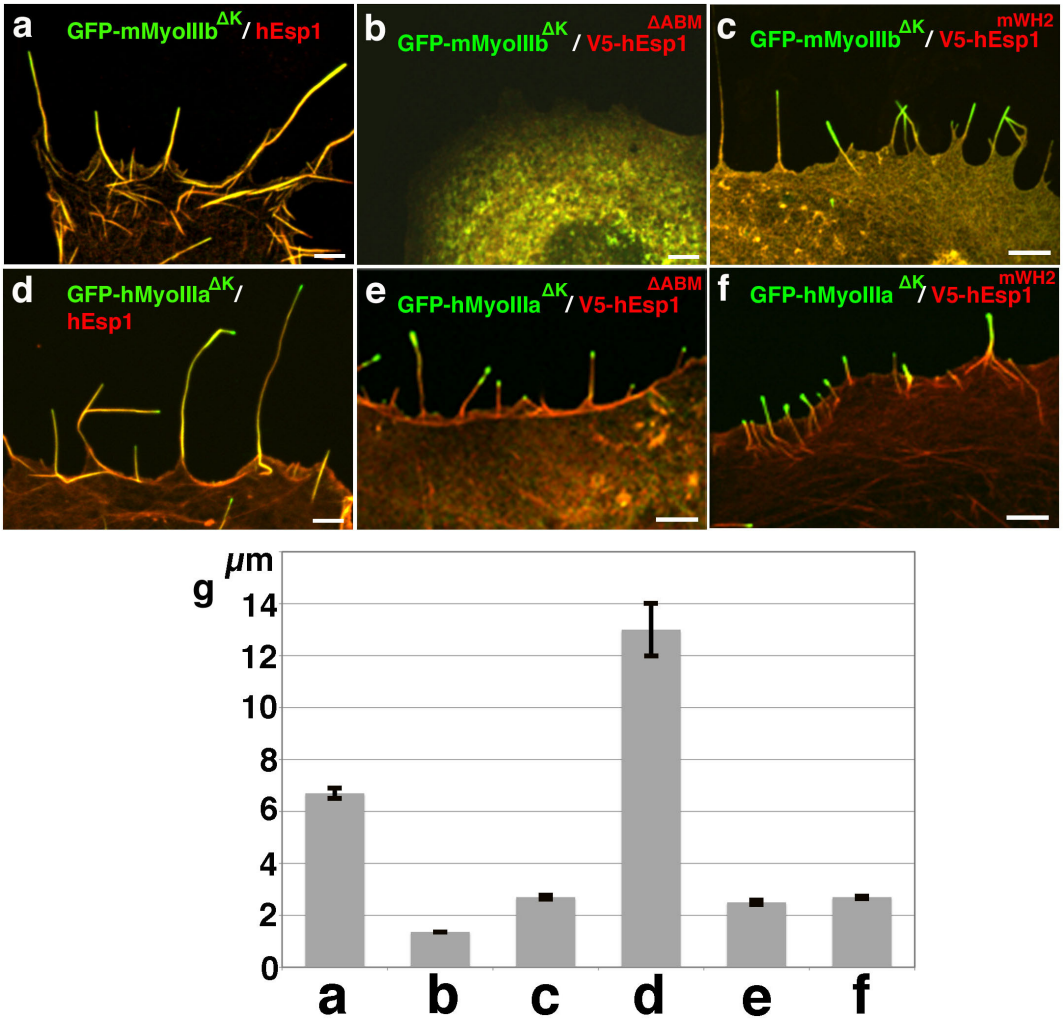

Figure 3-13 The actin bundling module (ABM) of espin 1 is required for the COS-7 filopodia tip localization and elongation phenotype of myosin IIIb, but not of myosin IIIa. Both ABM and WH2 domains of espin 1 are required for enhanced filopodia elongation. (**a**) GFP-mMyoIIIb$^{\Delta K}$ and espin 1 synergistically elongate filopodia (mean length = 6.7 ± 9.1 µm). (**b**) GFP-mMyoIIIb$^{\Delta K}$ and V5-hEspin 1$^{\Delta ABM}$ fail to elongate filopodia but instead colocalize to the cytoplasm indicating that the ABM of espin 1 is essential for the tip localization of myosin IIIb (1.36 ± 0.006 µm). (**c**) GFP-mMyoIIIb$^{\Delta K}$ and hEspin 1^{mWH2} colocalize to filopodia tips and generate relatively short filopodia indicating that WH2 is essential for the synergistic elongation (2.7 ± 0.15 µm). (**d—f**) GFP-hMyoIIIa$^{\Delta K}$ and hEspin 1 synergistically elongates filopodia (13.0 ± 1.1 µm) (**d**) while GFP-hMyoIIIa$^{\Delta K}$ and V5-hEspin 1$^{\Delta ABM}$ (**e**) or GFP-hMyoIIIa$^{\Delta K}$ and V5-hEspin 1^{mWH2} (**f**) Co-expression produces shorter filopodia indicating that ABM and WH2 are not essential for the tip localization of myosin IIIa but are essential for the synergistic phenotype (2.5 ± 0.17 µm and 2.7 ± 0.15 µm, respectively). Scale bars, 2.5 µm. (**g**) Measurements of filopodia lengths for each of the combinations shown in the panels above. The gray columns represent the mean filopodia length (µm) and the error bars represent the ± s.e.m. (Mr. Manor assisted with quantification)

We conclude that the ABM of espin 1 is required for the tip localization and elongation phenotype of myosin IIIb, but not for myosin IIIa. We postulated that the elongation of filopodia is also influenced by WH2 polymerization activity of espin 1 based on the results from COS-7 cell co-transfection with myosin IIIa$^{\Delta K}$ and the WH2-mutated espin 1 construct (hEspin 1^{mWH2}; Fig. 2-9h). Here, we tested whether GFP-mMyoIIIb$^{\Delta K}$ can target filopodia tip with hEspin 1^{mWH2} and mimic the GFP-hMyoIIIa$^{\Delta K}$-hEspin 1^{mWH2} co-expression phenotype. As a result, GFP-mMyoIIIb$^{\Delta K}$ was able to colocalize with hEspin 1^{mWH2} at the filopodia tip (Fig. 3-13c) and does not enhance filopodia elongation (2.7 ± 0.15 μm, n_c = 15, n_f = 61), which is identical to the phenotype of control GFP-hMyoIIIa$^{\Delta K}$-hEspin 1^{mWH2} (2.7 ± 0.15 μm, n_c = 22, n_f =147; Fig. 3-13f, g). Taken together, these results as well as those results in Chapter 2 suggest that both myosins IIIb and IIIa regulate stereocilia length by transporting the actin polymerizing factor, espin 1, to the plus end of actin filaments.

3.4.6 The myosin III-espin 1 complexes as regulators of stereocilia length

It has been established that all three actin-associated proteins, myosins IIIb, IIIa, and espin 1 localize to the actin plus ends of stereocilia tips of inner hair cells. Espin 1 is a cargo of myosins IIIb and IIIa in which these proteins coalesce into previously unrecognized molecular complexes that participate in actin cross-linking and polymerization activities. We developed sketch models of stereocilia length regulation as a function of these novel myosin IIIb/ and myosin IIIa/espin 1 complexes at the stereocilia tips (Fig. 3-14).

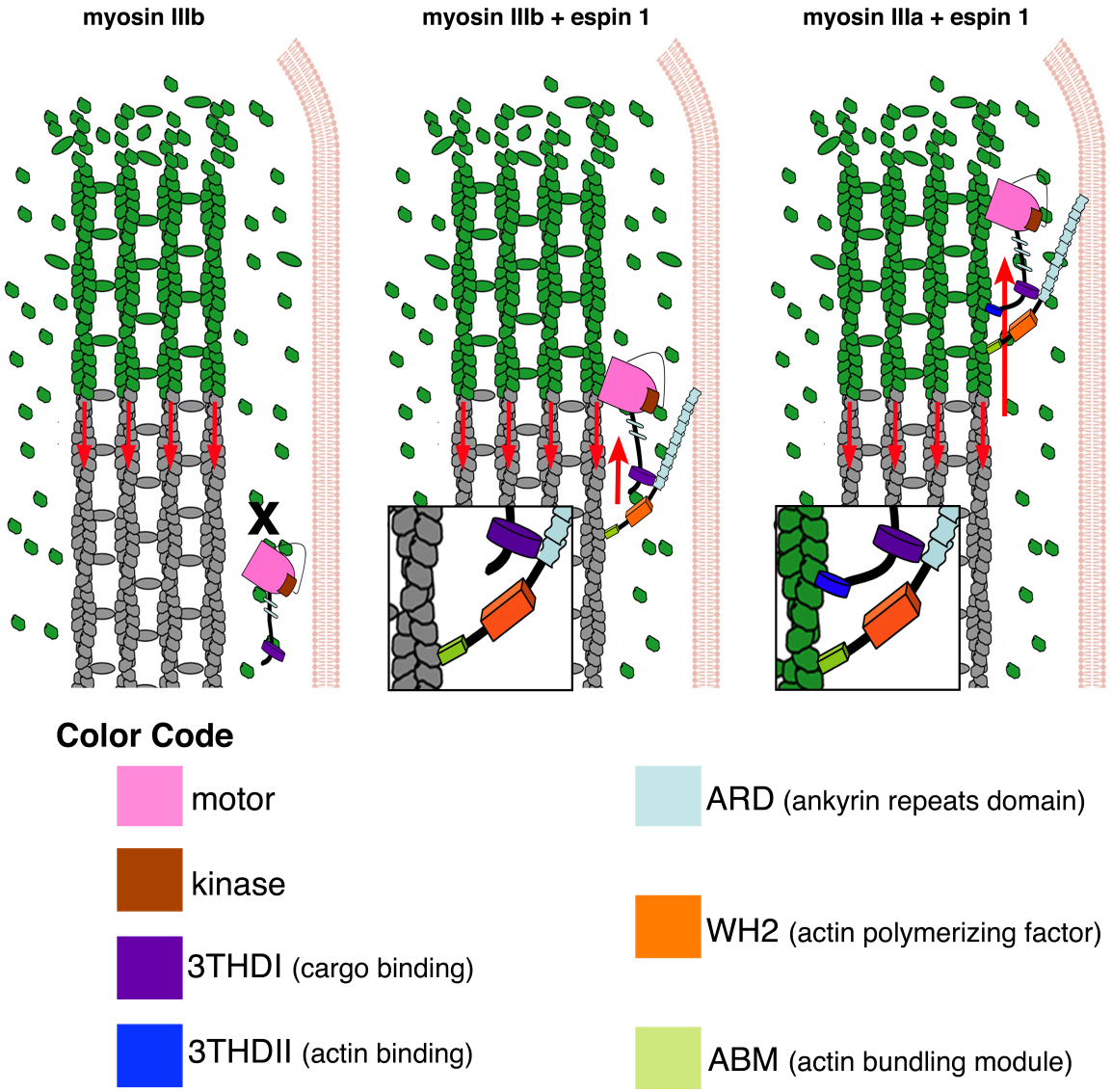

Figure 3-14 Models of myosin III/espin 1 complexes involved in the dynamic elongation of the stereocilia. Diagrams illustrating myosin IIIb alone in stereocilia (left) as well as the interactions between myosin IIIb and espin 1 (middle) and between myosin IIIa and espin 1 (right) along the actin filaments. Myosin IIIb (middle), lacking the C-terminal actin binding 3THDII domain, depends on espin 1 through 3THDI (purple) and ABM (green; middle inset) for localization toward the plus end of actin filaments. In contrast, myosin IIIa, having its own actin binding 3THDII in the C-terminus, can localize to the tip with or without espin 1. The actin polymerizing factor, WH2 (orange), of espin 1 is transported by myosin IIIb or IIIa to the stereocilia tip and stays near the actin polymerization site. The four arrows represent the actin treadmilling downward. Short and long upward arrows represents difference in the net velocity between the myosins IIIb and IIIa complexes (discussed in section 3.5.5). Each color code on the left depicts a functional domain of myosin IIIb or myosin IIIa and on the right a functional domain of espin 1.

Myosin IIIb is dynamically bound to the actin core through two anchors: the *cis* motor domain (pink) and the *trans* espin 1^{ABM} (yellow). Conversely, myosin IIIa is bound to the actin core through three anchors that include the actin-binding 3THDII domain (blue). Both myosins IIIb

and IIIa walk toward the plus end of actin filaments as the actin core treadmills downward (Fig. 3.14). However, myosin IIIb, not IIIa, essentially depends on the espin 1 cargo for motility since it lacks the 3THDII domain.

3.5 Discussion

3.5.1 Myosins IIIb and IIIa share the same compartment at the stereocilia tips but their temporal expression differs

We show that, in mice, myosin IIIb has the same immunolocalization pattern as myosin IIIa and espin 1 at the stereocilia tips in both cochlear and vestibular hair cells. Brightest fluorescent puncta of myosin IIIb were often seen in the middle row of stereocilia bundle of cochlear OHCs, (Fig. 3-3), somewhat similar to that of myosin IIIa (3-2b; Schneider *et al.*, 2006). The tip-to-base gradient distribution in the stereocilia of VHCs, as seen in the myosin IIIa and espin 1 immunostains (Fig. 2-3b), was also seen in the myosin IIIb immunostains (Figs. 3-5 and 3-9c). Both myosins III exhibit the same thimble-like pattern at the stereocilia tips (Fig. 3-3). Otherwise, myosins IIIb and IIIa display a different developmental course of protein expression in the cochlear stereocilia tips. The peak immunoreactivity of myosin IIIb appears at least eight postnatal days earlier than that of myosin IIIa (Fig. 3-4). The dynamics of myosins IIIb and IIIa expression within the stereocilia tip compartment during stereocilia development suggest that these two proteins' activities do not completely overlap in the cochlea.

3.5.2 Myosin IIIb potentially compensates for myosin IIIa in stereocilia tips

We extend our findings on the pattern of myosin IIIb spatiotemporal expression by studying myosin IIIb overexpression in rat inner hair cells using GFP-myosin IIIb wild-type and mutant constructs. Comprehensive data on cell transfection with myosin IIIa (Schneider *et al.*, 2006) and espin 1 (chapter 2) have shown characteristic targeting to

stereocilia/filopodia tip and elongation activities. Comparably, exogenous GFP-mMyoIIIb (Fig. 3-8a) and GFP-mMyoIIIb$^{\Delta K}$ (Fig. 3-8b) are found to be compartmentalized at the tips of vestibular stereocilia. GFP-mMyoIIIb$^{\Delta K}$ also influences the length of stereocilia (Fig. 3-8c).

Since myosins IIIb and IIIa target the same compartment, we checked whether myosin IIIb overexpression affects the tip localization of myosin IIIa. A distinct fluorescence protocol, using a combination of hair cell transfection and immunostaining, was used to juxtapose GFP-mMyoIIIb$^{\Delta K}$ and myosin IIIa at the stereocilia tips of rat hair cells. Overexpression of GFP-mMyoIIIb$^{\Delta K}$ abolishes immunolocalization of myosin IIIa in vestibular stereocilia tips (Fig. 3-10a) but not in cochlear stereocilia tips (Fig. 3-10b, c) demonstrating the ability of the cochlear hair cell to co-compartmentalize these myosin III isoforms. Conversely, the myosin IIIa compartmentalization is downregulated by myosin IIIb in the vestibular stereocilia tips. These observations may reflect physiological differences among myosins IIIb and IIIa as well as structural differences between vestibular and cochlear stereocilia tips. Additionally, the developmental relationship between myosin IIIb expression and stereocilia maturation is presumably different from myosin IIIa (Waguespack *et al.*, 2007). We argue that the myosin IIIa compensation hypothesis is supported since the overlap of their function is temporally constrained. That is, myosin IIIb temporarily compensates the loss-of-function of myosin IIIa in individuals with *MYO3A* mutations during the first two decades of hearing.

3.5.3 Why doesn't myosin IIIb expression endure into adulthood?

Myosin IIIa expression is steady during stereocilia maturation throughout adulthood (Schneider *et al.*, 2006). Conversely, myosin IIIb expression is detected at P0 and drops back to background levels by P8 (Fig. 3-4a). Although the difference in temporal expression pattern between myosins IIIb and IIIa is presumably attributed to their developmental roles in stereocilia lengthening, the cause of decline in myosin IIIb expression remains an open question. Possible explanations for this decline in expression include that: another molecule (e.g. myosin IIIa) may act as a competitive or noncompetitive inhibitor of myosin IIIb; the myosin IIIb gene or protein expression may be regulated; and myosin IIIb may have short half-life. Several weak PEST sequences have been detected in the myosin IIIb primary structure via the PESTfind online program (Dosé *et al.*, 2003). PEST sequences are regions rich in proline (P), glutamic acid (E), serine (S), and threonine (T). These regions are implicated in rapid intracellular proteolytic degradation (Rogers *et al.*, 1986). Multiple protein bands of myosins IIIb and IIIa from fish retinal preparations have been reported (Lin-Jones *et al*., 2009). These bands had less molecular weights than the protein standards and yielded various intensities across different fish retinal preparations which suggest that these bands are degraded protein products. Myosins IIIb and IIIa may have specific half-lives and be labile to other molecules that degrade them. Furthermore, downregulation of myosin IIIa was observed when myosin IIIb was overexpressed in vestibular stereocilia suggesting that they may influence each other's regulatory mechanism. A study on protein stability and cross-inhibition of these myosin isoforms would be an interesting avenue for future research.

3.5.4 Myosin IIIb, lacking 3THDII, depends on its espin 1 cargo for stereocilia tip localization and stereocilia elongation

We favor the model of synergistic elongation of hair cell stereocilia by myosin IIIa and espin 1, in which co-expression of these proteins produce longer stereocilia and COS-7 filopodia than the expressions of these proteins separately. The highly conserved 3THDI and 3THDII domains in the tails of myosins IIIb and IIIa have shown to influence the localization and actin elongation activities of these motor isoforms (Les Erickson *et al.*, 2003; Schneider *et al.*, 2006; Figs. 2-5, 2-9, and 3-13). Colocalization and GST pulldown assays indicate that 3THDI in the tail of both myosin isoforms mediates cargo-binding to espin 1 (Figs. 2-7 and 3-12). Myosin IIIb does not have the actin-binding 3THDII in its C-terminus, therefore, it cannot effectively localize to the filopodia tip or elongate filopodia (Fig. 3-11a) unless it is co-expressed with espin 1 (Fig. 3-13c). Espin 1 is implicated in actin polymerization through its WH2 and ABM domains, in which ABM binds to actin filaments and WH2 binds to actin monomers. ABM is found to be an essential element for tip localization of myosin IIIb. Myosin IIIb tip localization is abolished when co-expressed with V5-hEspin $1^{\Delta ABM}$ (Fig. 3-11b). These results unravel a new concept of cargo-dependent activity of a class III myosin, where the cargo, espin 1, serves as an actin-binding "crutch" necessary for myosin IIIb's processive transport along actin filaments (Fig. 3-14). Taken together, we postulate that myosin IIIb expression is transient during hearing development; directly depends on espin 1 for active co-transport toward the plus ends of actin filaments; and temporarily compensates for the function of myosin IIIa in the regulation of stereocilia length.

3.5.5 Is myosin IIIb less processive than myosin IIIa?

Although both myosins IIIb$^{\Delta K}$ and IIIa$^{\Delta K}$, when co-expressed with espin 1, synergistically elongate COS-7 filopodia, myosin IIIb$^{\Delta K}$ yielded half of the elongation length resulting from co-transfection of myosin IIIa$^{\Delta K}$ and espin 1 (Fig. 3-13g). Furthermore, myosin IIIb$^{\Delta K}$ display longer tip-to-base gradient distribution in the co-transfected filopodia than myosin IIIa$^{\Delta K}$ (e.g. compare Fig. 3-13a with d; and 3-13c with f). We use a model where the length of myosin distribution is inversely related to both the net velocity of myosin towards the tip as well as the relative fraction of immobilized myosin molecules permanently bound to the treadmilling actin core and/or diffusing away from the regions of higher concentration at the plus ends of actin filaments (Naoz *et al.*, 2008). Our preliminary quantitative analysis on myosin IIIb tip-to-base gradient distribution (data not shown) suggests that myosin IIIb has a slower net velocity than myosin IIIa. Myosin IIIb has fewer actin-binding sites than myosin IIIa and it is dependent on the binding to espin 1 to move along the actin filaments. The intrinsic walking mechanism of myosin IIIb is thought to involve domain-to-actin and domain-to-domain interactions between: the motor and F-actin (Dosé *et al.*, 2007a); the 3THDI and ARD (section 3.4.4); and the ABM and F-actin (Chen *et al.*, 1999). These binding activities enable espin 1 cargo to operate as a foot for myosin IIIb to walk (Fig. 3-14). Thus, since the complete complex of myosin IIIb/espin 1 bound to F-actin will only be formed a fraction of the time proportional to product of the on/off rates of each interacting domain (i.e. myosin IIIb head/F-actin, 3THDI/ARD, ABM/F-actin), the product of this fraction and myosin IIIa's tip-directed velocity should provide a first-approximation to the tip-directed velocity of myosin IIIb. Slower myosin IIIb that is

expressed earlier during development when stereocilia are immature perhaps suggests a different developmental role for this motor protein. A comprehensive study on the kinetics and a mathematical modeling of the myosin IIIb/espin 1 co-transport should be pursued in future research.

. Discussion

4.1 Molecular properties of myosins IIIa, IIIb, and espin 1

Our multilevel protein characterization of myosins IIIa, IIIb, and espin 1 from hair cells has revealed novel dynamic molecular complexes intimately bound around the actin cores at the tips of stereocilia. The dissection of these myosin III/espin 1 complexes was achieved by mutational analysis, in which an array of deletion and amino acid substitution mutants of myosin III and espin 1 permits a broader understanding of their domain-to-domain interactions, transport along the actin core, and elongation of actin filaments. The kinase deletion mutants, myosins III$^{\Delta K}$, are characterized as more functionally active since they localize more efficiently to actin plus ends and demonstrate a greater ability to produce longer stereocilia and filopodia when co-expressed with espin 1 (chapters 2 and 3). Further mutational experiments collectively indicate that the ARD, WH2, and ABM domains of espin 1 as well as the motor and 3THDI domains of myosin III are necessary for the myosin III:espin 1 synergistic elongation of filopodia.

The significant differences in the structure of myosins IIIa and IIIb lie in the C-terminal tail. When myosin IIIb alone is overexpressed in COS-7 cells, it does not localize to actin filaments or go to the filopodia tip. Despite the presence of the actin binding site in myosin IIIb's motor domain, the failure of filopodia tip targeting is due to the lack of a second actin-binding site, in the 3THDII, which is present in the tail of myosin IIIa. This is a strong indication that 3THDII is an important feature for an autonomous walking mechanism of myosin IIIa. In contrast to myosin IIIa, myosin IIIb

depends on espin 1 for processivity (section 3.4.5; Figs. 3-11, 3-13). The espin 1 dependency of myosin IIIb and the autonomy of myosin IIIa lead to the understanding of how the co-expression of myosin IIIa and espin 1 generates longer filopodia than the co-expression of myosin IIIb and espin 1. The autonomy of myosin IIIa also supports the hypothesis that myosin IIIa is a monomeric motor protein (Komaba *et al.,* 2003; Dosé *et al.*, 2007b). The previous studies indicate that myosin IIIa does not dimerize and this study, along with others, indicates that myosin IIIa walks without the help of espin 1. The notion is that the two *cis* actin binding sites reflect bipedalism as a walking mechanism for myosin IIIa (Kambara *et al*., 2006). Myosin IIIa may also use the ABM of espin 1 as an additional foot, although not required, as part of its walking mechanism (Fig. 3-14).

The underlying mystery that 3THDII is essential for tip localization of myosin IIIa in HeLa filopodia (Les Erickson *et al*., 2003), but not in stereocilia (Schneider *et al.*, 2006), or in COS-7 cell filopodia co-expressing espin 1 (Fig. 3-11) has been solved. The tip localization of a myosin III, lacking the 3THDII, depends on whether espin 1 is present in each cell system.

The espin 1 dependency of myosin IIIb, as well as the myosin IIIb fluorescence distributions, suggest that myosin IIIb has slower mobility than myosin IIIa due to the extra binding requirement involved with espin 1. The duration of myosin IIIb binding to both espin 1 and actin presumably depends on the on/off rates of each binding interface. Such binding requirements may render myosin IIIb with: a slower processive movement —i.e. less ability of the motor to make steps without detaching from the actin track (Reggiani and Bottinelli, 2007); and/or a lower duty ratio—i.e. the motor spends less of

its ATPase cycle time attached to its actin track (Howard, 2001). The caveat to this presumption is that biophysical properties of this unusual myosin IIIb walking mechanism have not been explored.

3THDI and 3THDII in the myosin III tail are highly conserved across vertebrate species (Dosé *et al.*, 2003). 3THDII has been characterized, in which a point mutation in the consensus amino acid motif, DFRXXL (Smith *et al.*, 1999), inside the 3THDII was found to be essential for the binding to actin filaments (Les Erickson *et al.*, 2003). Conversely, little is known about the function of the ~63 amino-acid long 3THDI (Dosé *et al.*, 2003). In this study, we characterized the 3THDI in both myosin III isoforms. The human myosins IIIa^{3THDI} and IIIb^{3THDI} share an amino acid identity of 45%. Sequence alignment of these 3THDI domains is illustrated in Figure 4-1.

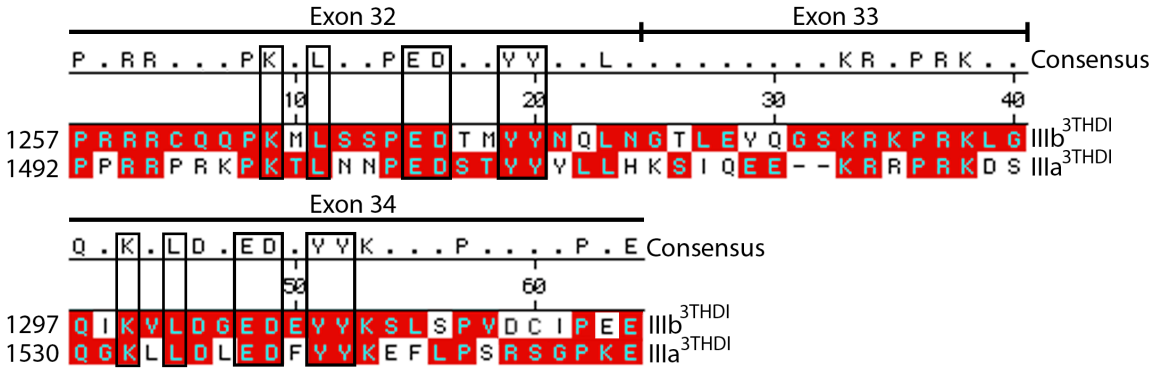

Figure 4-1 A boxshade output of a ClustalW alignment (Thompson *et al.*, 1994) of human myosin IIIb^{3THDI} (NCBI accession number NM_138995) and myosin IIIa^{3THDI} (AY101367). Exon map is indicated on top of each row. Exons 32, 33, 34 encode the 3THDI of both myosins IIIb and IIIa (Fig. 1-1). Consensus amino acid residues are indicated above the alignment (Consensus) where the residues in the alignment match, otherwise '.' is indicated. Red boxes indicate amino acid identity (i.e. residues match the Consensus) and clear boxes indicate amino acid residues that do not match. The amino acid position for the individual sequences is at the left, and the numbers above the sequences are for the overall alignment. The rectangular boxes highlight a repeat arrangement of residues in the exons 32 and 34. The lengths of myosins IIIb^{3THDI} and IIIa^{3THDI} are predicted to be 64 and 62 amino acids long, respectively (Dosé *et al.,* 2003). These sequences share 45.3% amino acid identity.

We found that the 3THDI contains a cargo-binding site for espin 1 (sections 2.4.4 and 3.4.4). The 3THDI is encoded by exons 32, 33, and 34 in both myosin III isoforms (Fig. 1-1). Myosin IIIa$^{\Delta K}$ colocalizes with espin 1 and elongates filopodia even when the exons 33 and 34 are deleted from the 3THDI (Fig. 2-9). The GST pulldown assay confirms that the exon 32 fragment alone of the 3THDI (3THDI$^{\Delta 33}$) is sufficient for binding to espin 1 (Fig. 2-11). We suspect that the cargo binding site for espin 1 is in exon 32 of 3THDI since a COS-7 overexpression experiment showed that this exon 32 fragment colocalizes with espin 1 more than the C-terminal fragment of 3THDI encoded by exons 33 and 34 (3THDI$^{\Delta 32}$; data not shown). An effort using site-directed mutagenesis was put forth to try to narrow down the binding site in the exon 32 of myosin IIIa 3THDI to fewer amino acid residues. Those amino acid residues in the 3THDI that are electrostatic and conserved across vertebrate species (Fig. 4-2) were considered as a potential requirement for the binding to the ARD of espin 1.

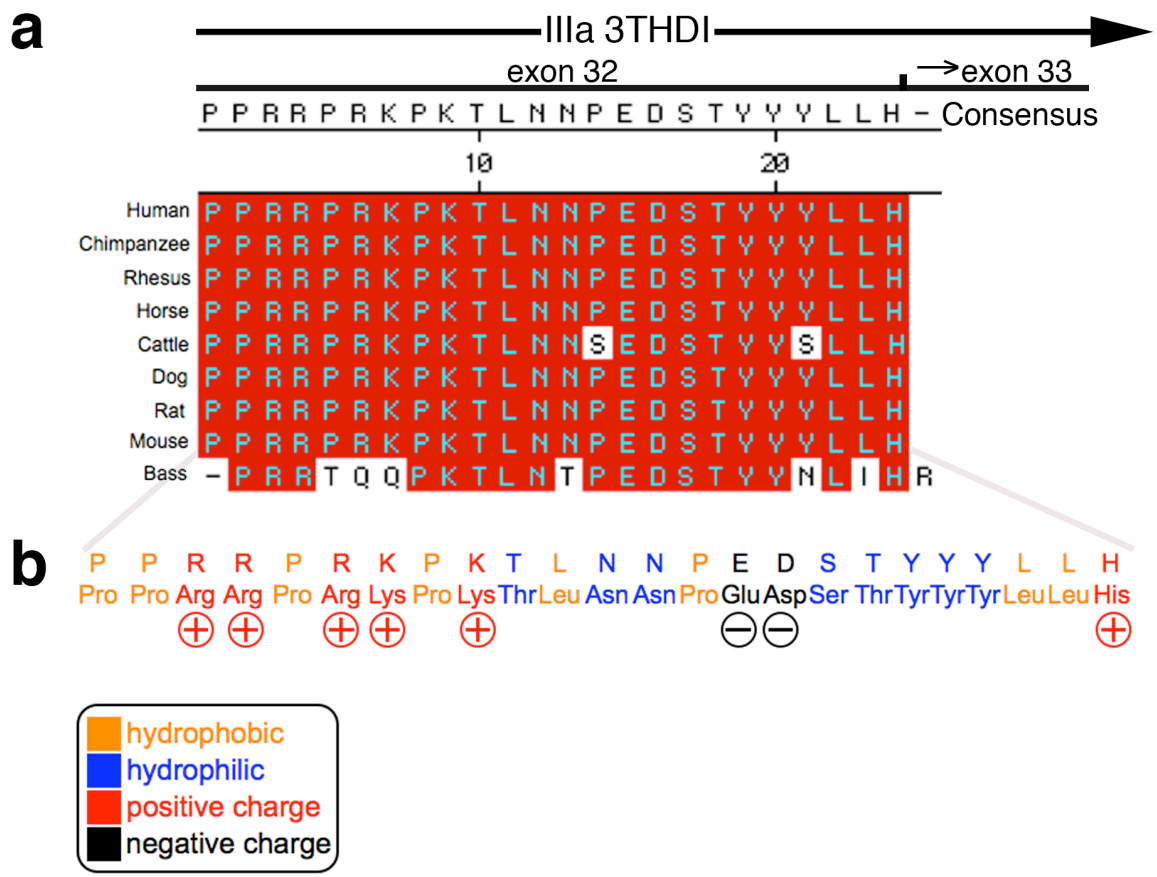

Figure 4-2 Analysis of 24 conserved amino acid N-terminal 3THDI polypeptide of myosin IIIa. (**a**) Multiple sequence alignment of N-terminal myosin IIIa 3THDI polypeptides predicted from nine vertebrate species (illustrated in left column). The N-terminal region of myosin IIIa^{3THDI} is focused since this region is sufficient for the binding to espin 1. The arrows on the top show the N-terminal orientation of 3THDI and the exon 32/exon 33 junction. The Consensus sequence above the alignment and below the exon map illustrates amino acid residues that match with the majority of residues aligned to each amino acid position. Red boxes indicate amino acid identity and clear boxes indicate amino acid residues that do not match. (**b**) The Consensus sequence is illuminated in one- and three-letter amino acid code. Biochemical property of each amino acid is codified by color (box legend). The "+" and "-" signs illuminate positive and negative charge residues as candidates for the electrostatic binding to espin 1 ARD.

The site-directed mutagenesis project in conjunction with a colocalization assay intended to identify specific amino acid(s) of myosin IIIa 3THDI responsible for the binding to espin 1 was carried out but never was completed. A total of six 3THDI (i.e. myosin IIIa cDNA encoding only the exons 32, 33, and 34 of the 3THDI) mutant probes were used to co-transfect COS-7 cells with espin 1. Each 3THDI mutant probe is conferred with one or two charge residue substitution(s) in the N-terminal region of 3THDI. No change in the colocalization was observed among the mutant probes.

Although, it is interesting to see that none of these amino acid substitutions of positive or negative charge residues in the N-terminal 3THDI abolished the colocalization with espin 1 (Fig. 4-3).

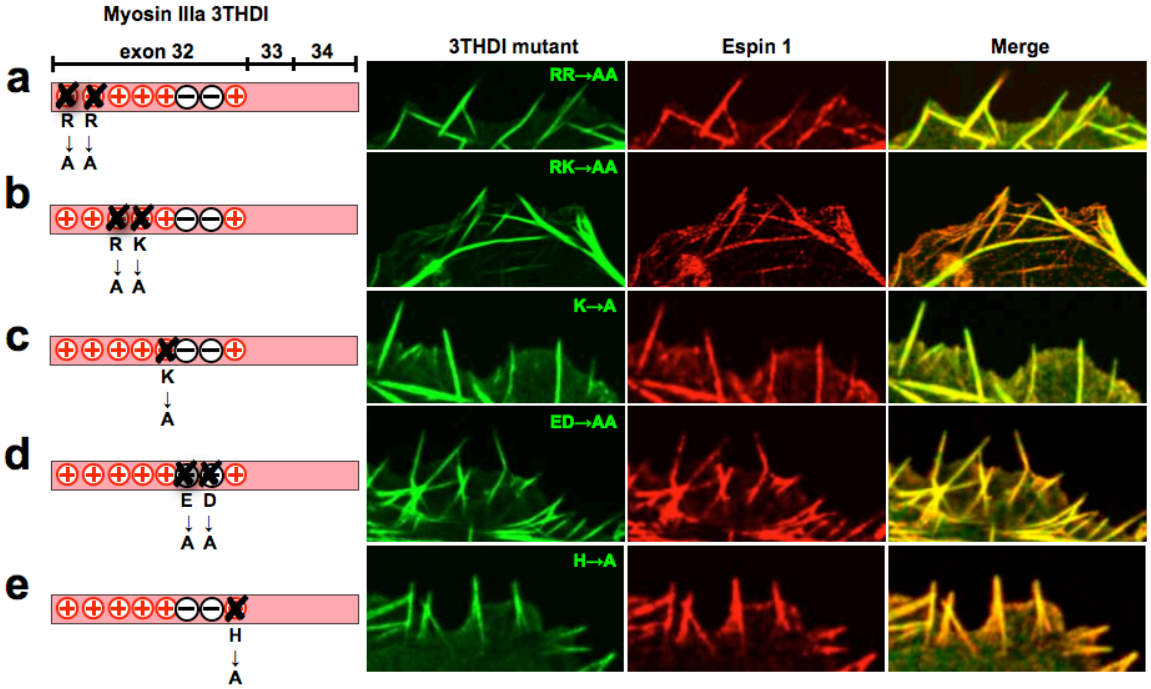

Figure 4-3 Colocalization of myosin IIIa 3THDI substitution mutants with espin 1. The leftmost column illustrates an exon map of myosin IIIa 3THDI in each row with specific charge residue substitution(s) ('X' denotes an amino acid substitution to alanine). The exon map is not to scale. (**a**) The positive charge arginine residues (aa positions 1494-1495) in the GFP-fused myosin IIIa 3THDI (GFP-hMyoIIIa^{3THDI}) are substituted with alanines (RR→AA). This GFP-hMyoIIIa^{3THDI} mutant colocalizes with espin 1. (**b**) The positive charge arginine-lysine residues (aa positions 1497-1498) in the GFP-hMyoIIIa^{3THDI} are substituted with alanines (RK→AA). This GFP-hMyoIIIa^{3THDI} mutant colocalizes with espin 1. (**c**) The positive lysine residue (aa position 1500) in the GFP-hMyoIIIa^{3THDI} is substituted with an alanine (K→A). This GFP-hMyoIIIa^{3THDI} mutant colocalizes with espin 1. (**d**) The negative charge glutamic acid-aspartic acid residues (aa positions 1506-1507) in the GFP-hMyoIIIa^{3THDI} are substituted with alanines (ED→AA). The ED residues are a part of the conserved PED motif (Dosé *et al.*, 2003). This GFP-hMyoIIIa^{3THDI} mutant colocalizes with espin 1. (**e**) The positive histidine residue (aa position 1514) in GFP-hMyoIIIa^{3THDI} is substituted with an alanine (H→A). This GFP-hMyoIIIa^{3THDI} mutant colocalizes with espin 1 too. The co-transfected COS-7 cells were stained with α-espin 1 antibody. These preliminary results suggest that none of these charge residues are completely required for the binding to espin 1.

A total of eleven amino acid substitutions (8 substitutions are shown in Figure 4-3) out of the 24 amino acids in the exon 32 fragment of myosin IIIa 3THDI did not abolish the colocalization with espin 1. Possible explanations for this observation include that the binding site is within the remaining thirteen amino acids yet to be mutated and that there

may be more than one cargo-binding site in the 3THDI domain. The 3THDI has an amino acid repeat arrangement of **K**x**L**xx**ED**xx**YY** and **K**x**L**x**ED**x**YY** in the exons 32 and 34, respectively (Fig. 4-1, rectangles). One of the two ED negative clusters are part of the conserved PED motif reported by Dosé *et al.* (2003). These repetitive negative clusters are sandwiched by leucine and tyrosine residues and the spacing in between differs by a distance of one amino acid. These preliminary observations lead to a conjecture that there may be more than one cargo-binding site, and that each site has a slightly different geometrical configuration. Perhaps there is more than one type of cargo binding to this 3THDI domain. The occurrence of a single domain in the tail of a myosin motor binding to multiple cargoes has been previously reported (Pashkova *et al.*, 2005). A future study on identifying specific binding site(s) in the 3THDI would be an interesting project since it should help elucidate the stoichiometry of the myosin III/espin 1 interaction and may offer an insight into other possible cargo-binding activities.

Studies strongly indicate that espin splice isoforms are more than just F-actin cross-linkers and favor a model where these proteins are multifunctional actin regulatory proteins (Sekerková, *et al.*, 2004; Rzadzinska *et al.*, 2005). Each espin isoform has a different combination of functional domains (reviewed by Sekerková *et al.*, 2006a) that participate in actin bundling, polymerization, binding to other proteins, and possibly other unknown functions. Myosin III specifically interacts with the espin 1 isoform, since it is the only isoform that has the N-terminal ARD. Deletion of ARD from espin 1 abolishes colocalization with myosin III while the ARD alone is sufficient for the binding to myosin III (Figs. 2-7, 2-9, and 3-12).

Because ankyrin repeats are highly conserved motifs often found to involve promiscuous interactions with heterologous proteins (reviewed by Mosavi *et al.*, 2004), we have checked the specificity of the interaction between myosin III 3THDI and espin 1 ARD. We sought to find out if ankyrin repeats from an unrelated protein can non-specifically bind to myosin III. A polypeptide of 24 ankyrin repeats was subcloned from a commercially available cDNA encoding an epithelial ankyrin (NCBI accession number BC021657) and fused to a small tag, V5. These 24 ankyrin repeats did not colocalize with the myosin IIIa tail (Fig. 4-4c).

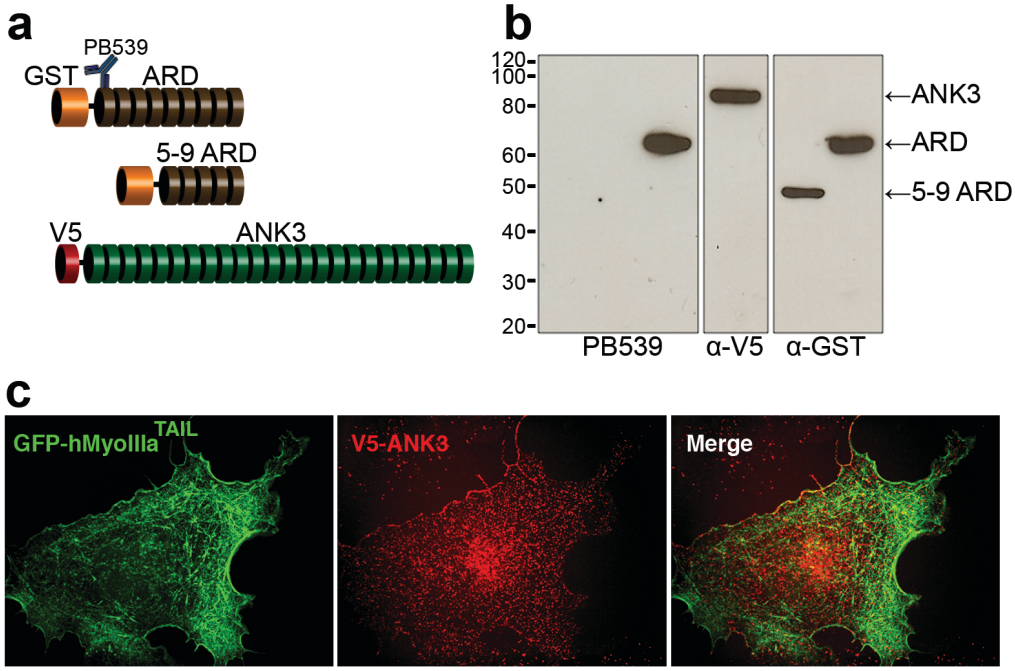

Figure 4-4 Specificity of binding of α-espin 1 (PB539) antibody and of myosin III to the first ankyrin repeat of espin 1 ARD. (**a**) Schematic representation of the constructs analyzed in this figure. GST, glutathione S-transferase tag; ARD, ankyrin repeats domain; 5-9 ARD, the last five ankyrin repeats of the ARD; V5, a 13 amino-acid tag; ANK3, 24 ankyrin repeats domain from an epithelial ankyrin (see main text for details). Position of the epitope recognized by the PB539 antibody is indicated. (**b**) Immunoblots of COS-7 cell lysates transfected with GST-ARD, GST-5-9 ARD, and V5-ANK3 show that PB539 specifically recognizes the first ankyrin repeat of espin 1 but not other ankyrin repeats. The presence of all proteins is confirmed by α-V5 and α-GST antibodies. (**c**). Co-expression of GFP-hMyosin IIIa tail (GFP-hMyoIIIa^{TAIL}) and V5-ANK3 in COS-7 cells. The specificity of myosin IIIa binding to highly homologous ankyrin repeats is tested. The GFP-hMyoIIIa^{TAIL} (green) does not colocalize with ANK3 (red), which suggests that the binding of myosin III^{3THDI} to espin 1^{ARD} is specific.

Furthermore, the specificity of our α-espin 1 antibody has been double checked because ankyrin repeats are highly homologous (Fig. 4-4b). Taken together, these findings point to espin 1 as a true interacting partner of myosins IIIa and IIIb.

4.2 Stereocilia length regulation and overtime maintenance by myosins IIIa, IIIb, and espin 1

The life of cochlear and vestibular hair cell stereocilia is divided into three phases: (1) development; (2) maturation; and (3) steady-state maintenance. During rodent development (~E18), immature stereocilia are indistinguishable from surrounding microvilli in length and width. Once into the maturational phase during ~P1, stereocilia undergo drastic morphological changes, where the stereocilia lengths elongate differentially and thicken giving rise to the staircase architecture of the hair bundle (Tilney *et al*., 1996; Kaltenbach *et al.* 1994; Zine and Romand, 1996). These morphological changes coincide with the onset and maturation of mechanosensitivity. (Waguespack *et al.*, 2007). Fully mature stereocilia, from ~P21 and onward, undergo steady-state maintenance by means of the actin treadmilling where the actin paracrystalline is constantly turned over.

The expression and localization of myosin IIIa and espin 1 coincide with the maturational and steady-state maintenance phases. According to our comprehensive developmental and functional data, we interpret that these proteins together regulate the elongation during the maturational phase and the actin treadmilling during the steady-state maintenance phase. What about myosin IIIb? The expression of myosin IIIb peaks at ~P0 and drops back to background levels by ~P8. An investigation on the myosin IIIb expression earlier in the developmental phase, before birth, is beyond the scope of our

research. However, we were able to see that the expression of myosin IIIb is at highest at the end of the developmental phase at birth and then recedes against the maturation of stereocilia. We believe that myosin IIIb plays different role than myosin IIIa, in which myosin IIIb may be more functional specifically during the developmental phase. It is possible that myosin IIIb is involved in transporting a different set of cargoes in the preparation for the maturational phase of stereocilia growth.

Overexpression of myosin IIIa or espins in the hair cells have been previously shown to influence the shape and length of stereocilia (Rzadzinska *et al.*, 2005; Schneider *et al.*, 2006). This study shows, for the first time, that these proteins, when co-expressed, co-transport with one another to the actin polymerization site and produce even longer stereocilia.

The co-transport function of espin 1 and myosin III towards the tips of stereocilia is important for bringing the WH2 domain to the site of actin polymerization. The WH2 domain has an actin-monomer binding site which is implicated in actin nucleation (Loomis *et al*., 2006), and therefore actin polymerization. The elongation of filopodia of co-expressed COS-7 is reduced when the WH2 of espin 1 is inactivated. The inactivity of WH2 does not affect the filopodia tip localization of the myosin IIIa or myosin IIIb complex. These findings reinforce the concept of espin 1 as a cargo where WH2 is brought to the actin polymerization site by myosins III.

Cargo transport by myosins XVa, X, and other unconventional myosins to the tips of actin protrusions have been implicated in the regulation of length and number of actin protrusions (Berg and Cheney, 2002; Tokuo and Ikebe, 2004; Belyantseva *et al.*, 2005;

Prosser *et al.*, 2008). However, it is the first time to directly observe a combined influence of a myosin motor and an actin-polymerizing element on the lengthening of both stereocilia and filopodia—an elongation phenotype that we coined 'synergistic elongation.' The elongation of an actin protrusion is said to be synergistic when the co-expression of two proteins results in more elongation than the sum of elongated lengths by each protein expressed individually. We proposed that myosin III and espin 1 together give rise to this previously unrecognized emergent property of synergistic elongation. A caveat to this is that our studies relies heavily on using myosin III kinase deletion mutants. This issue, however, has been addressed fully through phosphorylation and ATPase activity studies. These assays strongly suggest that the removal of kinase does not cause myosin III to behave aberrantly (section 2.4.5). The wild-type myosins III, when co-expressed with espin 1, do not produce as much actin elongation because its kinase autoregulate its motor domain. This autoregulation suggests that myosin III can fine tune its own motor activity under physiological conditions.

4.3 Proposed explanation for the myosin IIIa compensation problem

Hitherto, the underlying mechanism for the myosin IIIa late-onset deafness have been unknown. Affected *DFNB30* individuals are either myosin IIIa null or have severely truncated protein products (Walsh *et al*., 2002), yet they hear normally for the first twenty years, well after the onset of hearing function and stereocilia maturation. We revisited the working hypothesis that, in fact, there is functional redundancy among the class III myosins and that myosin IIIb, the only paralogue to myosin IIIa identified, partially compensates for myosin IIIa in affected individuals. The compensation of a myosin

isoform for another myosin isoform has been previously observed. For instance, Bao and others (2007) reported that myosin IIa, a nonmuscle myosin II isoform, compensates for a second myosin II isoform, myosin IIb. Myosin IIb knockout mice have brain and cardiac defects. They developed an additional transgenic mouse model where the myosin IIb gene is replaced with a synthetic GFP-tagged myosin IIa gene. In their results, the replacement of myosin IIb with IIa rescued the brain defects but not cardiac defects (Bao *et al.*, 2007).

Although a myosin III knockout model has been one of our top research priorities, unfortunately, no myosin IIIa or IIIb knockout models materialized by the time of writing. At any rate, we tested the myosin IIIa compensation hypothesis using different approaches with our new myosin IIIb probes on the mouse inner ear and in the COS-7 cells. Key similarities and differences between myosins IIIa and IIIb have been delineated. Myosin IIIb goes to the same compartment in the cochlear stereocilia tip as myosin IIIa and interacts with espin 1 but is expressed earlier in the developmental stage of stereocilia. The differences in distributions between myosins IIIa and IIIb are due to the presence of 3THDII in the myosin IIIa molecule since the deletion of myosin IIIa 3THDII results in identical subcellular localizations as myosin IIIb. These differences are also due to myosin IIIb's dependence upon espin 1. Co-expression of either myosin IIIa or IIIb with espin 1 results in the synergistic elongation of filopodia, but myosin IIIb produces less synergistic elongation. Collectively, these results suggest that myosin IIIb is inferior to myosin IIIa in that it: cannot function without espin 1 or other heterologous protein; crawls slower along the actin track; influences less on the stereocilia elongation;

and is transiently expressed during the development. We argue that these myosin IIIb qualities are consistent with the context of immature, short stereocilia (or microvilli) in the developmental phase, during which myosin IIIb is being expressed and myosin IIIa is not. We propose that the myosin IIIa compensation hypothesis is supported in that myosin IIIb temporarily takes the place of myosin IIIa. Our findings should be a catalyst for further research on myosin IIIb.

4.4 Myosins IIIa and IIIb may transport other cargoes

Several lines of evidence indicate that espin 1 is a cargo for myosin IIIa. Espin 1 interacts with myosin IIIa *in vivo* and *in vitro*. They co-express and colocalize to the same stereocilia tip compartment. Other unconventional myosins including myosin XVa do not have the same affinity for espin 1 or the ability to transport it in COS-7 cells (section 2.4.3). The myosin IIIb isoform is unusual in that it essentially depends on the espin 1 cargo for mobility, although it is possible that myosin IIIb has other cargoes to depend on for its mobility.

Generally, both myosins IIIa and IIIb reproducibly yield higher fluorescence intensity in the middle row of the stereocilia bundle than in the taller and shorter rows. We propose two possible explanations for the higher fluorescence intensity in the middle stereocilia row: (1) myosin III epitope masking is greater in the taller and shorter rows or (2) myosins III target to the stereocilia tips in the middle row more efficiently than other tips. Although, it seems that myosin IIIa accumulates at other tips in the taller and shorter rows slightly more than myosin IIIb, it is possible that the myosin IIIb localization to the stereocilia tips is compromised due to the dependence on the availability of espin 1

cargoes in the cytoplasmic pool. And, as a result, there is a greater impact on the attenuated myosin IIIb fluorescence intensity at the tips in the taller and shorter rows.

The myosin tail binding to multiple cargoes is a common feature seen in unconventional myosins. The tail of NINAC, a myosin III orthologue, has been implicated in interacting with INAD, a PDZ protein, and transporting phototransduction complexes to rhabdomeres in fruit fly photoreceptors (Wes *et al.*, 1999). Proteins with PDZ domains often serve as scaffolds for signaling complexes (Ranganathan and Ross, 1997). Comparably, the highly conserved ankyrin repeats and other domains in the espin 1 cargo also have been implicated as scaffolds for assembly of macromolecular complexes. There are 8 to 10 ankyrin repeats in the espin 1 ARD suggesting that extra protein-protein interactions may have not been identified in the myosin III/espin 1 complexes. Furthermore, repetitive amino acid peptides are found in the conserved 3THDI (Fig. 4-1), which putatively suggest a presence of more than one cargo binding site.

A progressive loss of myosin IIIa immunofluorescence intensity at a later stage of stereocilia maturation was observed in rat and guinea pig adults unless an antigen retrieval step is included in the immunostaining protocol. The antigen retrieval step is where samples are incubated in citrate buffer at 60 °C for 30 minutes. This retrieval step recovers the myosin IIIa antigenicity and prevents the loss of immunofluorescence intensity suggesting that the epitope is unmasked (Schneider *et al.*, 2006). This drop in intensity level in adults may indicate a time-dependent change in the crowded molecular environment around the myosin IIIa epitope, thereby obscuring the access for the

antibody to bind. When performing the antigen retrieval step, the epitope becomes accessible again. This observation putatively suggests that the molecular composition of the stereocilia tip continues to change after stereocilia development.

4.5 Closing Remarks and Perspective of Future Research

Hearing is among the least understood sensory systems in vertebrates in terms of the underlying molecular mechanisms responsible for the high capacity in sound/motion detection and discrimination. The finding of the novel myosin III/espin 1 complexes and their influence on stereocilia length is pivotal to understanding the molecular mechanism of hearing. The length and shape of stereocilia impact stereocilia bundles' response to deflection, the energy transfer into gating of the MET channels, and lead to a deeper understanding of how sound transduction is modulated. The identification of espin 1 as a cargo and the characterization of myosin IIIb as another myosin III member open doors to more research on the molecular biology of the stereocilia tips. Future research should follow on the identification of other cargoes for class III myosins, expand developmental data on myosin IIIb expression to include embryonic profiles, and development of new mathematical models for the dynamics of myosin III/espin 1 complex. Identification and characterization of molecules in the stereocilia tips involved in actin polymerization and mechanoelectrical transduction continue to serve as stepping stones toward understanding why deafness occurs.

Bibliography

1. Ahmed ZM, Morell RJ, Riazuddin S, Gropman A, Shaukat S, Ahmad MM, Mohiddin SA, Fananapazir L, Caruso RC, Husnain T, Khan SN, Riazuddin S, Griffith AJ, Friedman TB, and Wilcox ER. 2003. Mutations of *MYO6* are Associated with Recessive Deafness, DFNB37. *Amer. J. Hum. Genet*. **72**(5):1315-1322.

2. Anderson DW, Probst FJ, Belyantseva IA, Fridell RA, Beyer L, Martin DM, Wu D, Kachar B, Friedman TB, Raphael Y, and Camper SA. 2000. The Motor and Tail Regions of Myosin XV are Critical for Normal Structure and Function of Auditory and Vestibular Hair Cells. *Hum. Mol. Genet.* **9**(12):1729-1738.

3. Assad JA, Hacohen N, and Corey DP. 1989. Voltage Dependence of Adaptation and Active Bundle Movement in Bullfrog Saccular Hair Cells. *Proc. Natl. Acad. Sci. USA*. **86**(8):2918-2922.

4. Avraham KB, Hasson T, Steel KP, Kingsley DM, Russell LB, Mooseker MS, Copeland NG, and Jenkins NA. 1995. The Mouse *Snell's Waltzer* Deafness Gene Encodes an Unconventional Myosin Required for Structural Integrity of Inner Ear Hair Cells. *Nat. Genet*. **11**(4):369-375.

5. Bähler M. 2000. Are Class III and Class IX Myosins Motorized Signalling Molecules? *Biochim. Biophys. Acta.* **1496**(1):52-59.

6. Balduini C, Iolascon A, and Savoia A. 2002. Inherited Thrombocytopenias: From Genes to Therapy. *Haematologica*. **87**(8):860-880.

7. Bao J, Ma X, Liu C, and Adelstein RS. 2007. Replacement of Nonmuscle Myosin II-B with II-A Rescues Brain but Not Cardiac Defects in Mice. *J. Biol. Chem.* **282**(30):22102-22111.

8. Bartles JR. 2000. Parallel Actin Bundles and Their Multiple Actin-Bundling Proteins. *Curr. Opin. Cell Biol*. **12**(1):72-78.

9. Bartles JR, Wierda A, and Zheng L. 1996. Identification and Characterization of Espin, an Actin-Binding Protein Localized to the F-Actin-Rich Junctional Plaques of Sertoli Cell Ectoplasmic Specializations. *J. Cell Sci*. **109** (Pt 6):1229-1239.

10. Bartles JR, Zheng L, Li A, Wierda A, and Chen B. 1998. Small Espin: A Third Actin-bundling Protein and Potential Forked Protein Ortholog in Brush Border Microvilli. *J. Cell Biol*. **143**(1):107-119.

11. Battelle B-A, Andrews AW, Calman BG, Sellers JR, Greenberg RM, and Smith WC. 1998. A Myosin III from Limulus Eyes Is a Clock-Regulated Phosphoprotein. *J. Neurosci.* **18**(12):4548-4559.

12. Belyantseva IA, Boger ET, and Friedman TB. 2003. Myosin XVa Localizes to the Tips of Inner Ear Sensory Cell Stereocilia and is Essential for Staircase Formation of the Hair Bundle. *Proc. Natl. Acad. Sci. USA*. **100**(24):13958-13963.

13. Belyantseva, IA, Boger ET, Naz S, Frolenkov GI, Sellers JR, Ahmed ZM, Griffith AJ, and Friedman TB. 2005. Myosin-XVa is Required for Tip Localization of Whirlin and Differential Elongation of Hair-Cell Stereocilia. *Nat. Cell Biol*. **7**(2): 148-156.

14. Belyantseva, IA, Davies, C, Azevedo RB, Fridell, RA, Friedman TB, and Kachar B. 2002. Localization of Myosin XVA in Hair Cells. Abstract #600. The Twenty-Fifth Annual Midwinter Research Meeting. Association for Research in Otolaryngology. Saint Petersburg, FL.

15. Bennett V. 1992. Ankyrins. Adaptors Between Diverse Plasma Membrane Proteins and the Cytoplasm. *J. Biol. Chem.* **267**(13):8703-8706.

16. Bennett V and Baines AJ. 2001. Spectrin and Ankyrin-Based Pathways: Metazoan Inventions for Integrating Cells Into Tissues. *Physiol. Rev.* **81**(3):1354-1392.

17. Berg JS and Cheney RE. 2002. Myosin-X is an Unconventional Myosin that Undergoes Intrafilopodial Motility. *Nat. Cell Biol.* **4**(3):246-250.

18. Berg JS, Powell BC, and Cheney RE. 2001. A Millennial Myosin Census. *Mol. Biol. Cell*. **12**(4):780-794.

19. Beurg M, Fettiplace R, Nam J-H, and Ricci AJ. 2009. Localization of Inner Hair Cell Mechanotransducer Channels using High-Speed Calcium Imaging. *Nat. Neurosci*. **12**(5):553-558.

20. Beyer LA, Odeh H, Probst FJ, Lambert EH, Dolan DF, Camper SA, Kohrman DC, and Raphael Y. 2000. Hair Cells in the Inner Ear of the Pirouette and Shaker 2 Mutant Mice. *J. Neurocytol.* **29**(4):227-240.

21. Boëda B, El-Amraoui A, Bahloul A, Goodyear RJ, Daviet L, Blanchard S, Perfettini I, Fath KR, Shorte S, Reiners J, Houdusse A, Legrain P, Wolfrum U, Richardson GP, and Petit C. 2002. Myosin VIIa, Harmonin and Cadherin 23, Three Usher I Gene Products that Cooperate to Shape the Sensory Hair Cell Bundle. *EMBO J*. **21**(24): 6689-6699.

22. Bohil AB, Robertson BW, and Cheney RE. 2006. Myosin-X is a Molecular Motor that Functions in Filopodia Formation. *Proc. Natl. Acad. Sci. USA*. **103**(33): 12411-12416.

23. Boldogh IR and Pon LA. 2007. Mitochondria on the Move. *Trends in Cell Biol*. **17**(10):502-510.

24. Boulouiz R, Li Y, Soualhine H, Abidi O, Chafik A, Nürnberg G, Becker C, Nürnberg P, Kubisch C, Wollnik B, and Barakat A. 2008. A Novel Mutation in the *Espin* Gene Causes Autosomal Recessive Non-Syndromic Hearing Loss but No Apparent Vestibular Dysfunction in a Moroccan Family. *Amer. J. Med. Genet.* **146A**:3086-3089.

25. Boutet E, Lieberherr D, Tognolli M, Schneider M, and Bairoch A. 2007. UniProtKB/Swiss-Prot. *Methods Mol. Biol*. **406**:89-112.

26. Chen B, Wang ALD, Wang M, Zheng L, and Bartles JR. 1999. Espin Contains an Additional Actin-binding Site in Its N Terminus and Is a Major Actin-bundling Protein of the Sertoli Cell–Spermatid Ectoplasmic Specialization Junctional Plaque. *Mol. Biol. Cell.* **10**(12):4327–4339.

27. Cheney RE and Mooseker MS. 1992. Unconventional Myosins. *Curr. Opin. Cell Biol*. **4**(1):27-35.

28. Chereau D, Kerff F, Graceffa P, Grabarek Z, Langsetmo K, and Dominguez R. 2005. Actin-Bound Structures of Wiskott–Aldrich Syndrome Protein (WASP)-Homology Domain 2 and the Implications for Filament Assembly. *Proc. Natl. Acad. Sci. USA*. **102**(46):16644-16649.

29. Cheung ELM and Corey DP. 2006. Ca^{2+} Changes the Force Sensitivity of the Hair-Cell Transduction Channel. *Biophys. J*. **90**(1):124-139.

30. Collin RWJ, Kalay E, Oostrik J, Caylan R, Wollnik B, Arslan S, den Hollander AI, Birinci Y, Lichtner P, Strom TM, Toraman B, Hoefsloot LH, Cremers CWRJ, Brunner HG, Cremers FPM, Karaguzel A, and Kremer H. 2007. Involvement of *DFNB59* Mutations in Autosomal Recessive Non-Syndromic Hearing Impairment. *Hum. Mutat*. **28**(7):718-723.

31. Corey DP and Hudspeth AJ. 1983. Kinetics of the Receptor Current in Bullfrog Saccular Hair Cells. *J. Neurosci.* **3**(5):962-976.

32. Crumling MA, Tong M, Aschenbach KL, Liu LQ, Pipitone CM, and Duncan RK. 2009. P2X Antagonists Inhibit Styryl Dye Entry Into Hair Cells. *Neuroscience*. **161**(4):1144-1153.

33. Dan I, Watanabeb NM, Kobayashia T, Yamashita-Suzukia K, Fukagayaa Y, Kajikawaa E, Kimurab WK, Nakashimab TM, Matsumotobc K, Ninomiya-Tsujibc J, and Kusumiab A. 2000. Molecular Cloning of MINK, a Novel Member of Mammalian GCK Family Kinases, Which is Up-Regulated During Postnatal Mouse Cerebral Development. *FEBS Letters.* **469**(1):19-23.

34. Dan I, Watanabe NM, and Kusumi A. 2001. The Ste20 Group Kinases as Regulators of MAP Kinase Cascades. *Trends Cell Biol.* **11**(5):220-230.

35. Daudet N and Lebart M-C. 2002. Transient Expression of the T-Isoform of Plastins/ Fimbrin in the Stereocilia of Developing Auditory Hair Cells. *Cell Mot. Cytoskeleton*. **53**(4):326-336.

36. Delmaghani S, del Castillo FJ, Michel V, Leibovici M, Aghaie A, Ron U, Van Laer L, Ben-Tal N, Camp VG, Weil D, Langa F, Lathrop M, Avan P, and Petit C. 2006. Mutations in the Gene Encoding Pejvakin, a Newly Identified Protein of the Afferent Auditory Pathway, Cause DFNB59 Auditory Neuropathy. *Nat. Genet*. **38**(7):770-778.

37. DeRosier DJ and Tilney LG. 2000. F-Actin Bundles Are Derivatives of Microvilli: What Does This Tell Us about How Bundles Might Form? *J. Cell Biol*. **148**(1):1-6.

38. Denk W, Holt JR, Shepherd GMG, and Coreytt DP. 1995. Calcium Imaging of Single Stereocilia in Hair Cells: Localization of Transduction Channels at Both Ends of Tip Links. *Neuron*. **15**(6):1311-1321.

39. Donaudy F, Zheng L, Ficarella R, Ballana E, Carella M, Melchionda S, Estivill X, Bartles JR, and Gasparini P. 2006. Espin Gene (*ESPN*) Mutations Associated With Autosomal Dominant Hearing Loss Cause Defects in Microvillar Elongation or Organisation. *J. Med. Genet.* **43**(2):157-161.

40. Dosé AC, Ananthanarayanan S, Moore JE, Burnside B, and Yengo CM. 2007a. Kinetic Mechanism of Human Myosin IIIA. *J. Biol. Chem.* **282**(1):216-231.

41. Dosé AC, Ananthanarayanan S, Moore JE, Corsa AC, Burnside B, Yengo CM. 2008. The Kinase Domain Alters the Kinetic Properties of the Myosin IIIA Motor. *Biochemistry.* **47**(8):2485-2496.

42. Dosé AC and Burnside B. 2000. Cloning and Chromosomal Localization of a Human Class III Myosin. *Genomics*. **67**(3):333-342.

43. Dosé AC and Burnside B. 2002. A Class III Myosin Expressed in the Retina is a Potential Candidate for Bardet-Biedl Syndrome. *Genomics*. **79**(5):621-624.

44. Dosé AC, Hillman DW, Wong C, Sohlberg L, Lin-Jones J, and Burnside B. 2003. Myo3A, One of Two Class III Myosin Genes Expressed in Vertebrate Retina, Is Localized to the Calycal Processes of Rod and Cone Photoreceptors and Is Expressed in the Sacculus. *Mol. Biol. Cell.* **14**(3):1058-1073.

45. Dosé AC, Lin-Jones J, and Burnside B. 2007b. Class III Myosins. Ch. **8**, p. 265-287. Myosins: A Superfamily of Molecular Motors. Coluccio LM (ed.). Springer Science +Business, Inc. New York, NY.

46. Dumont RA, Zhao YD, Holt JR, Bähler M, and Gillespie PG. 2002. Myosin-I Isozymes in Neonatal Rodent Auditory and Vestibular Epithelia. *J. Assoc. Res. Otolaryngol*. **3**(4):375-389.

47. Eatock RA. 2000. Adaptation in Hair Cells. *Annu. Rev. Neurosci.* **23**(1):285-314.

48. Edwards SC and Battelle BA. 1987. Octopamine- and Cyclic AMP-Stimulated Phosphorylation of a Protein in Limulus Ventral and Lateral Eyes. *J. Neurosci.* **7**(9): 2811-2820.

49. Eisenstein M. 2006. A Look Back: Adventures in the Matrix. *Nat. Methods.* **3**(5): 410.

50. Ernest S, Rauch G-J, Haffter P, Geisler R, Petit C, and Nicolson T. 2000. Mariner is Defective in Myosin VIIA: a Zebrafish Model for Human Hereditary Deafness. *Hum. Mol. Genet.* **9**(14):2189-2196.

51. Evangelista M, Zigmond S, and Boone C. 2003. Formins: Signaling Effectors for Assembly and Polarization of Actin Filaments. *J. Cell Sci.* **116**(2):2603-2611.

52. Fettiplace R and Hackney CM. 2006. The Sensory and Motor Roles of Auditory Hair Cells. *Nat. Rev. Neurosci.* **7**(1):19-29.

53. Fettiplace R, Ricci AJ, and Hackney CM. 2001. Clues to the Cochlear Amplifier from the Turtle Ear. *Trends Neurosci*. **24**(3):169-175.

54. Finn RD, Tate J, Mistry J, Coggill PC, Sammut SJ, Hotz H-R, Ceric G, Forslund K, Eddy SR, Sonnhammer ELL, and Bateman A. 2008. The Pfam Protein Families Database. *Nucl. Acids Res.* **36**:D281-288.

55. Foth BJ, Goedecke MC, and Soldati D. 2006. New Insights into Myosin Evolution and Classification. *Proc. Natl. Acad. Sci. USA*. **103**(10):3681-3686.

56. Fukuda M, Kuroda TS, and Mikoshiba K. 2002. Slac2-a/melanophilin, the Missing Link between Rab27 and Myosin Va: implications of a Tripartite Protein Complex for Melanosome Transport. *J. Biol. Chem.* **277**(14):12432–12436.

57. Furness DN and Hackney CM. 1985. Cross-links Between Stereocilia in the Guinea Pig Cochlea. *Hear. Res.* **18**(2):177-188.

58. Furness DN and Hackney CM. 2006. The Structure and Composition of Vertebrate Hair Bundles. Ch. **3**, p. 5-153. Vertebrate Hair Cells. Eatock RA, Fay RR, and Popper AN (eds.). Springer Science+Business, Inc. New York, NY.

59. Furness DN, Karkanevatos A, West B, and Hackney CM. 2002. An Immunogold Investigation of the Distribution of Calmodulin in the Apex of Cochlear Hair Cells. *Hear. Res.* **173**(1-2):10-20.

60. Furness DN, Mahendrasingam S, Ohashi M, Fettiplace R, and Hackney CM. 2008. The Dimensions and Composition of Stereociliary Rootlets in Mammalian Cochlear Hair Cells: Comparison between High- and Low-Frequency Cells and Evidence for a Connection to the Lateral Membrane. *J. Neurosci.* **28**(25):6342-6353.

61. Furness DN, Zetes DE, Hackney CM, and Steele CR. 1997. Kinematic Analysis of Shear Displacement as a Means for Operating Mechanotransduction Channels in the Contact Region Between Adjacent Stereocilia of Mammalian Cochlear Hair Cells. *Proc. Biol. Sci*. **264**(1378):45-51.

62. Garcia JA, Yee AG, Gillespie PG, and Corey DP. 1998. Localization of Myosin-Iβ near Both Ends of Tip Links in Frog Saccular Hair Cells. *J. Neurosci.* **18**(21): 8637-8647.

63. Géléoc GS and Holt JR. 2003. Developmental Acquisition of Sensory Transduction in Hair Cells of the Mouse Inner Ear. *Nat. Neurosci.* **6**(10):1019–1020.

64. GeneCards [Internet]; Database [cited 2009 Sept. 19]; [about 8 p.]. Available from: http://www.genecards.org/cgi-bin/carddisp.pl?gene=MYO3B. Stelzer G, Harel A, Inger A, Olender T, Dalah I, Shmoish M, Ron S, Safran M and Lancet D. 2008. *GeneDecks: GeneCards-based paralog hunting and gene set distillation.* CSB2008.

65. Gibson F, Walsh J, Mburu P, Varela A, Brown KA, Antonio M, Beisel KW, Steel KP, and Brown SDM. 1995. A Type VII Myosin Encoded by the Mouse Deafness Gene Shaker-1. *Nature*. **374**(6517):62-64.

66. Gillespie PG and Cyr JL. 2004. Myosin-1c, the Hair Cell's Adaptation Motor. *Annu. Rev. Physiol.* **66**(1):521-545.

67. Gillespie PG and Müller U. 2009. Mechanotransduction by Hair Cells: Models, Molecules, and Mechanisms. *Cell.* **139**(1):33-44.

68. Gillespie PG, Shin J-B, and David L. 2009. Quantitation of the Hair-Bundle Protein Constellation. Vol. **32**, p. 170-171. The Thirty-Second Annual Midwinter Research Meeting. Santi PA (ed). Association for Research in Otolaryngology. Baltimore, MD.

69. Gillespie PG, Wagner MC, and Hudspeth AJ. 1993. Identification of a 120 kd Hair-Bundle Myosin Located Near Stereociliary Tips *Neuron*. **11**(4):581-594.

70. Glenney JR, Kaulfus P, Matsudaira P, and Weber K. 1981. F-Actin Binding and Bundling Properties of Fimbrin, a Major Cytoskeletal Protein of Microvillus Core Filaments. *J. Biol. Chem.* **256**(17):9283-9288.

71. Grati M, Aggarwal N, Strehler EE, and Wenthold RJ. 2006a. Molecular Determinants for Differential Membrane Trafficking of PMCA1 and PMCA2 in Mammalian Hair Cells. *J. Cell Sci*. **119**(14):2995-3007.

72. Grati M, Schneider ME, Lipkow K, Strehler EE, Wenthold RJ, and Kachar B. 2006b. Rapid Turnover of Stereocilia Membrane Proteins: Evidence from the Trafficking and Mobility of Plasma Membrane Ca^{2+}-ATPase 2. *J. Neurosci*. **26**(23): 6386-6395.

73. Grillet N, Kazmierczak P, Xiong W, Schwander M, Reynolds A, Sakaguchi H, Tokita J, Kachar B, and Müller U. 2009. The Mechanotransduction Machinery of Hair Cells. *Sci. Signal.* **2**(85):pt5.

74. Grüneberg H, Burnett JB, and Snell GD. 1941. The Origin of Jerker, a New Gene Mutation of the House Mouse, and Linkage Studies Made with It. *Proc. Natl. Acad. Sci. USA.* **27**(12):562-565.

75. Goodyear RJ, Marcotti W, Kros CJ, and Richardson GP. 2005. Development and Properties of Stereociliary Link Types in Hair Cells of the Mouse Cochlea. The J. Comp. Neurol. **485**(1):75-85.

76. Harasztosi C and Gummer AW. 2009. Locating MET Channels in Outer Hair Cells Near the Lower End of the Tip Link. Abstract 380. The Thirty-Second Annual Midwinter Research Meeting. Santi PA (ed). Association for Research in Otolaryngology. Baltimore, MD.

77. Hasson T, Heintzelman MB, Santos-Sacchi J, Corey DP, and Mooseker MS. 1995. Expression in Cochlea and Retina of Myosin VIIa, the Gene Product Defective in Usher Syndrome Type 1B. *Proc. Natl. Acad. Sci. USA*. **92**(21):9815-9819.

78. Holt JR and Corey DP. 2000. Two Mechanisms for Transducer Adaptation in Vertebrate Hair Cells. *Proc. Natl. Acad. of Sci. USA*. **97**(22):11730-11735.

79. Holt JR, Gillespie SKH, Provance JDW, Shah K, Shokat KM, Corey DP, Mercer JA, and Gillespie PG. 2002. A Chemical-Genetic Strategy Implicates Myosin-1c in Adaptation by Hair Cells. *Cell*. **108**(3):371-381.

80. Housley GD, Kanjhan R, Raybould NP, Greenwood D, Salih SG, Jarlebark L, Burton LD, Setz VCM, Cannell MB, Soeller C, Christie DL, Usami S, Matsubara A, Yoshie H, Ryan AF, and Thorne PR. 1999. Expression of the $P2X_2$ Receptor Subunit of the ATP-Gated Ion Channel in the Cochlea: Implications for Sound Transduction and Auditory Neurotransmission. *J. Neurosci.* **19**(19):8377-8388.

81. Howard J. 2001. Processive and Nonprocessive Motors. Ch. 13. Mechanics of Motor Proteins and the Cytoskeleton. Sinauer Associates, Inc. Sunderland, MA.

82. Howard J and Hudspeth AJ. 1988. Compliance of the Hair Bundle Associated With Gating of Mechanoelectrical Transduction Channels in the Bullfrog's Saccular Hair Cell. *Neuron.* **1**(3):189-199.

83. Hryniewicz-Jankowska A, Czogalla A, Bok E, Sikorsk AF. 2002. Ankyrins, Multifunctional Proteins Involved in Many Cellular Pathways. *Folia Histochem. Cytobiol.* **40**(3):239-49.

84. Hudspeth AJ. 2008. Making an Effort to Listen: Mechanical Amplification in the Ear. *Neuron*. **59**(4): 530–545.

85. Jaramillo FN and Hudspeth AJ. 1991. Localization of the Hair Cell's Transduction Channels at the Hair Bundle's Top by Iontophoretic Application of a Channel Blocker. *Neuron.***7**(3):409-420.

86. Jeon S-J, Oshima K, Heller S, and Edge ASB. 2007. Bone Marrow Mesenchymal Stem Cells are Progenitors *in vitro* for Inner Ear Hair Cells. *Mol. Cell. Neurosci*. **34**(1):59-68.

87. Jones SM, Johnson KR, Yu H, Erway LC, Alagramam KN, Pollak N, and Jones TA. 2005. A Quantitative Survey of Gravity Receptor Function in Mutant Mouse Strains. *J. Assoc. Res. Otolaryngol.* **6**(4):297-310.

88. Kachar B, Parakkal M, Kurc M, Zhao Y, and Gillespie PG. 2000. High-Resolution Structure of Hair-Cell Tip Links. *Proc. Natl. Acad. Sci. USA*. **97**(24):13336-13341.

89. Kaltenbach J, Falzarano P, and Simpson T. 1994. Postnatal Development of the Hamster Cochlea. II. Growth and Differentiation of Stereocilia Bundles. *J. Comp. Neurol.* **350**(2):187-198.

90. Kambara T, Komaba S, and Ikebe M. 2006. Human Myosin III Is a Motor Having an Extremely High Affinity for Actin. *J. Biol. Chem.* **281**(49):37291-37301.

91. Kappen C. 2000. Analysis of a Complete Homeobox Gene Repertoire: Implications for the Evolution of Diversity. *Proc. Natl. Acad. Sci. USA.* **97**(9):4481-4486.

92. Karkanevatos A. 2001. Ultrastructural Localization of Cytoskeletal Proteins in Guinea Pig Cochlear Hair Cells. Phil M (chair). Thesis. Keele University, UK.

93. Katti C, Dalal JS, Dosé AC, Burnside B, and Battelle B-A. 2009. Cloning and Distribution of Myosin 3B in the Mouse Retina: Differential Distribution in Cone Outer Segments. *Exp. Eye Res*. **89**(2):224-237.

94. Kawamoto K, Ishimoto S-I, Minoda R, Brough DE, and Raphael Y. 2003. *Math1* Gene Transfer Generates New Cochlear Hair Cells in Mature Guinea Pigs *In Vivo*. *J. Neurosci.* **23**(11):4395-4400.

95. Kazmierczak, P, Sakaguchi H, Tokita J, Wilson-Kubalek EM, Milligan RA, Müller U, and Kachar B. 2007. Cadherin 23 and Protocadherin 15 Interact to Form Tip-Link Filaments in Sensory Hair Cells. *Nature*. **449**(7158):87-91.

96. Kempler K, Toth J, Yamashita R, Mapel G, Robinson K, Cardasis H, Stevens S, Sellers JR, and Battelle B-A. 2007. Loop 2 of Limulus Myosin III Is Phosphorylated by Protein Kinase A and Autophosphorylation. *Biochemistry*. **46**(14):4280-4293.

97. Kennedy HJ, Evans MG, Crawford AC, and Fettiplace R. 2003. Fast Adaptation of Mechanoelectrical Transducer Channels in Mammalian Cochlear Hair Cells. *Nat. Neurosci*. **6**(8):832-836.

98. Kiehart DP, Franke JD, Chee MK, Montague RA, Chen T-I, Roote J, and Ashburner M. Drosophila *crinkled*, Mutations of Which Disrupt Morphogenesis and Cause Lethality, Encodes Fly Myosin VIIA. *Genetics*. **168**(3):1337-1352.

99. Komaba S, Inoue A, Maruta S, Hosoya H, and Ikebe M. 2003. Determination of Human Myosin III as a Motor Protein Having a Protein Kinase Activity. *J. Biol. Chem*. **278**(24):21352-21360.

100. Krendel M and Mooseker MS. 2005. Myosins: Tails (and Heads) of Functional Diversity. *Physiology (Bethesda)*. **20**(4):239-251.

101. Kros CJ, Marcotti W, van Netten SM, Self TJ, Libby RT, Brown SDM, Richardson GP, and Steel KP. 2002. Reduced Climbing and Increased Slipping Adaptation in Cochlear Hair Cells of Mice with Myo7a Mutations. *Nat. Neurosci*. **5**(1):41-47.

102. Lalwani AK, Atkin G, Li Y, Lee JY, Hillman DE, and Mhatre AN. 2008. Localization in Stereocilia, Plasma Membrane, and Mitochondria Suggests Diverse Roles for NMHC-IIa within Cochlear Hair Cells. *Brain Res*. **1197**:13-22.

103. Lambert S and Bennett V. 1993. Postmitotic Expression of Ankyrin$_R$, and β_R-Spectrin in Discrete Neuronal Populations of the Rat Brain. *J. Neurosci.* **13**(9):3725-3735.

104. Lane PW. 1987. Deaf Waddler (dfw). *Mouse News Lett*. **77**:129.

105. Lechene C, Hillion F, McMahon G, Benson D, Kleinfeld A, Kampf JP, Distel D, Luyten Y, Bonventre J, Hentschel D, Park K, Ito S, Schwartz M, Benichou G, and Slodzian G. High-Resolution Quantitative Imaging of Mammalian and Bacterial Cells Using Stable Isotope Mass Spectrometry. *J. Biol*. **5**(6):20.

106. Lee G, Abdi K, Jiang Y, Michaely P, Bennett V, and Marszalek PE. 2006. Nanospring Behaviour of Ankyrin Repeats. *Nature.* **440**(7081):246-9.

107. Legan PK, Lukashkina VA, Goodyear RJ, Lukashkin AN, Verhoeven K, Van Camp C, Russell IJ, and Richardson GP. 2005. A Deafness Mutation Isolates a Second Role for the Tectorial Membrane in Hearing. *Nat Neurosci*. **8**(8):1035-1042.

108. Les Erickson F, Corsa AC, Dosé AC, and Burnside B. 2003. Localization of a Class III Myosin to Filopodia Tips in Transfected HeLa Cells Requires an Actin-binding Site in its Tail Domain. *Mol. Biol. Cell.* **14**(10):4173-4180.

109. Li H, Liu H, Balt S, Mann S, Corrales CE, and Heller S. 2004. Correlation of Expression of the Actin Filament-Bundling Protein Espin with Stereociliary Bundle Formation in the Developing Inner Ear. *J. Comparative Neurol*. **468**(1):125-34.

110. Lim DJ and Anniko M. 1985. Developmental Morphology of the Mouse Inner Ear. A Scanning Electron Microscopic Observation. *Acta Otolaryngol. Suppl.* **422**:1-69.

111. Lin HW, Schneider ME, and Kachar B. 2005. When Size Matters: The Dynamic Regulation of Stereocilia Lengths. *Curr. Opin. in Cell Biol.* **17**(1):55-61.

112. Lin J-H, Makris A, McMahon C, Bear SE, Patriotis C, Prasad VR, Brent R, Golemis EA, and Tsichlis PN. 1999. The Ankyrin Repeat-containing Adaptor Protein Tvl-1 Is a Novel Substrate and Regulator of Raf-1. *J. Biol. Chem.* **274**(21):14706–14715.

113. Lin-Jones J, Parker E, Wu M, Dosé AC, and Burnside B. 2004. Myosin 3A Transgene Expression Produces Abnormal Actin Filament Bundles in Transgenic *Xenopus laevis* Rod Photoreceptors. *J. Cell Sci.* **117**(Pt 24):5825-5834.

114. Lin-Jones J, Sohlberg L, Dosé AC, Breckler J, Hillman DW, and Burnside B. 2009. Identification and Localization of Myosin Superfamily Members in Fish Retina and Retinal Pigmented Epithelium. *J. Comp. Neurol*. **513**(2):209-223.

115. Liu X, Udovichenko IP, Brown SDM, Steel KP, and Williams DS. 1999. Myosin VIIa Participates in Opsin Transport through The Photoreceptor Cilium. *J. Neurosci.* **19**(15):6267-6274.

116. Littlewood Evans A and Müller U. 2000. Stereocilia Defects in the Sensory Hair Cells of the Inner Ear in Mice Deficient in Integrin α8β1. *Nat Genet*. **24**(4):424-428.

117. Loomis PA, Kelly AE, Zheng L, Changyaleket B, Sekerková G, Mugnaini E, Ferreira A, Mullins RD, and Bartles JR. 2006. Targeted Wild-Type and Jerker Espins Reveal a Novel, WH2-Domain-Dependent Way to Make Actin Bundles in Cells. *J. Cell Sci.* **119**(8):1655-1665.

118. Loomis PA, Zheng L, Sekerková G, Changyaleket B, Mugnaini E, and Bartles JR. 2003. Espin Cross-Links Cause the Elongation of Microvillus-Type Parallel Actin Bundles in vivo. *J. Cell Biol.* **163**(5):1045-55.

119. Lumpkin EA and Hudspeth AJ. 1998. Regulation of Free Ca^{2+} Concentration in Hair-Cell Stereocilia. *J. Neurosci.* **18**(16):6300–6318.

120. Lux SE and John KM. 1990. Analysis of cDNA for Human Erythrocyte Ankyrin Indicates a Repeated Structure with Homology to... *Nature*. **344**(6261):36-42.

121. Macartney JS, Comis SD, and Pickles JO. 1980. Is Myosin in the Cochlea a Basis for Active Motility? *Nature*. **288**(5790):491-492.

122. Mallavarapu A and Mitchison T. 1999 Regulated Actin Cytoskeleton Assembly at Filopodium Tips Controls Their Extension and Retraction. *J. Cell Biol.* **146**(5): 1097-1106.

123. Manor U and Kachar B. 2008. Dynamic Length Regulation of Sensory Stereocilia. *Semin. Cell Dev. Biol.* **19**(6):502-510.

124. Matsuno K, Go MJ, Sun X, Eastman DS and Artavanis-Tsakonas S. 1997. Suppressor of Hairless-independent Events in Notch Signaling Imply Novel Pathway Elements. *Development.* **124**(21):4265-4273.

125. Mburu P, Kikkawa Y, Townsend S, Romero R, Yonekawa H, and Brown SDM. 2006. Whirlin Complexes With p55 at the Stereocilia Tip During Hair Cell Development. *Proc. Natl. Acad. Sci. USA*. **103**(29):10973-10978.

126. Mburu P, Mustapha M, Varela A, Weil D, El-Amraoui A, Holme RH, Rump A, Hardisty RE, Blanchard S, Coimbra RS, Perfettini I, Parkinson N, Mallon A-M, Glenister P, Rogers MJ, Paige AJ, Moir L, Clay J, Rosenthal A, Liu XZ, Blanco G, Steel KP, Petit C, and Brown SDM. 2003. Defects in Whirlin, a PDZ Domain Molecule Involved in Stereocilia Elongation, Cause Deafness in the Whirler Mouse and Families with DFNB31. *Nat. Genet*. **34**(4):421-428.

127. McCullough BJ and Tempel BL. 2004. Haplo-Insufficiency Revealed in Deafwaddler Mice When Tested for Hearing Loss and Ataxia. *Hear. Res*. **195**(1-2): 90–102.

128. Medeiros NA, Burnette DT, and Forscher P. 2006. Myosin II Functions in Actin-Bundle Turnover in Neuronal Growth Cones. *Nat. Cell Biol*. **8**(3):216-226.

129. Mehta A. 2001. Myosin Learns to Walk. *J. Cell Sci*. **114**(Pt 11):1981-1998.

130. Melchionda S, Ahituv N, Bisceglia L, Sobe T, Glaser F, Rabionet R, Arbones ML, Notarangelo A, Di Iorio E, Carella M, Zelante L, Estivill X, Avraham KB, and Gasparini P. 2001. *MYO6*, the Human Homologue of the Gene Responsible for Deafness in *Snell's Waltzer* Mice, Is Mutated in Autosomal Dominant Non-Syndromic Hearing Loss. **69**(3):635-640.

131. Meyers JR, MacDonald RB, Duggan A, Lenzi D, Standaert DG, Corwin JT, and Corey DP. 2003. Lighting up the Senses: FM1-43 Loading of Sensory Cells through Nonselective Ion Channels. *J. Neurosci.* **23**(10):4054-4065.

132. Mhatre AN, Kim Y, Brodie HA, and Lalwani AK. 2003. Macrothrombocytopenia and Progressive Deafness is Due to a Mutation in MYH9. *Otol. and Neurotol*. **24**(2): 205-209.

133. Montell C and Rubin GM. 1988. The Drosophila *ninaC* Locus Encodes Two Photoreceptor Cell Specific Proteins with Domains Homologous to Protein Kinases and the Myosin Heavy Chain Head. *Cell*. **52**(5):757-772.

134. Mosavi LK, Cammett TJ, Daniel C. Desrosiers, and Peng ZY. 2004. The Ankyrin Repeat as Molecular Architecture for Protein Recognition. *Protein Sci.* **13**(6): 1435-1448.

135. Mosavi LK, Minor DL Jr, and Peng ZY. 2002. Consensus-Derived Structural Determinants of the Ankyrin Repeat Motif. *Proc. Natl. Acad. Sci. USA*. **99**(25): 16029-34.

136. Naz S, Griffith AJ, Riazuddin S, Hampton L, Battey JFJ, Khan S, Riazuddin S, Wilcox E, and Friedman TB. 2004. Mutations of ESPN Cause Autosomal Recessive Deafness and Vestibular Dysfunction. *J. Med. Genet.* **41**(8):591-595.

137. Naoz M, Manor U, Sakaguchi H, Kachar B, and Gov NS. 2008. Protein Localization by Actin Treadmilling and Molecular Motors Regulates Stereocilia Shape and Treadmilling Rate. *Biophys. J.* **95**(12):5706-5718.

138. Ng KP, Kambara T, Matsuura M, Burke M, and Ikebe M. 1996. Identification of Myosin III as a Protein Kinase. *Biochemistry*. **35**(29):9392-9399.

139. Nguyen-Legros J and Hicks D. 2000. Renewal of Photoreceptor Outer Segments and Their Phagocytosis by the Retinal Pigment Epithelium. *Int. Rev. Cytol.* **196**:245-313.

140. North RA. 2002. Molecular Physiology of P2X Receptors. *Physiol. Rev.* **82**(4): 1013-1067.

141. Pashkova N, Catlett NL, Novak JL, and Weisman LS. 2005. A Point Mutation in the Cargo-Binding Domain of Myosin V Affects Its Interaction with Multiple Cargoes. *Eukaryotic Cell*. **4**(4):787-798.

142. Pataky F, Pironkova R, and Hudspeth AJ. 2004. Radixin is a Constituent of Stereocilia in Hair Cells. *Proc. Natl. Acad. Sci. USA*. **101**(8):2601-2606.

143. Pickles JO, Rouse GW, and von Perger M. 1991. Morphological Correlates of Mechanotransduction in Acousticolateral Hair Cells. *Scanning Microsc.* **5**(4): 1115-1128.

144. Phillips KR, Tong S, Goodyear R, Richardson GP, and Cyr JL. 2006. Stereociliary Myosin-1c Receptors Are Sensitive to Calcium Chelation and Absent from Cadherin 23 Mutant Mice. *J. Neurosci.* **26**(42):10777-10788.

145. Porter JA and Montell C. 1993a. Distinct Roles of the *Drosophila ninaC* Kinase and Myosin Domains Revealed by Systematic Mutagenesis. *J. Cell Biol.* **122**(3): 601-612.

146. Porter JA, Yu M, Doberstein SK, Pollard TD, and Montell C. 1993b. Dependence of Calmodulin Localization in the Retina on the NINAC Unconventional Myosin. *Science.* **262**(5136):1038-1042.

147. Primiani N, Gregory M, Dufresne J, Smith CE, Liu YL, Bartles JR, Cyr DG, and Hermo L. 2007. Microvillar Size and Espin Expression in Principal Cells of the Adult Rat Epididymis Are Regulated by Androgens. *J. Androl*. **28**(5):659-669.

148. Probst FJ, Fridell RA, Raphael Y, Saunders TL, Wang A, Liang Y, Morell RJ, Touchman JW, Lyons RH, Noben-Trauth K, Friedman TB, and Camper SA. 1998. Correction of Deafness in Shaker-2 Mice by an Unconventional Myosin in a BAC Transgene. *Science*. **280**(5368):1444-1446.

149. Prosser HM, Rzadzinska AK, Steel KP, and Bradley A. 2008. Mosaic Complementation Demonstrates a Regulatory Role for Myosin VIIa in Actin Dynamics of Stereocilia. *Mol. Cell. Biol.* **28**(5):1702-1712.

150. Quinlan ME, Heuser JE, Kerkhoff E, and Dyche Mullins R. 2005. *Drosophila* Spire is an Actin Nucleation Factor. *Nature.* **433**(7024):382-388.

151. Rayment I, Rypniewski WR, Schmidt-Bäse K, Smith R, Tomchick DR, Benning MM, Winkelmann DA, Wesenberg G, and Holden HM. 1993. Three-Dimensional Structure of Myosin Subfragment-1: A Molecular Motor. *Science*. **261**(5117):50-58.

152. Rędowicz MJ. 2002. Myosins and Pathology: Genetics and Biology. *Acta Biochim Pol*. **49**(4):789-804.

153. Rędowicz MJ. 2007. Unconventional Myosins in Muscle. *Eur. J. Cell Biol*. **86**(9): 549-558.

154. Reggiani C and Bottinelli R. 2007. Myosin II: Sarcomeric Myosins, The Motors of Contraction in Cardiac and Skeletal Muscles. Ch. **5**, p.133. Proteins and Cell Regulation. vol. 7. Myosins: A Superfamily of Molecular Motors. Coluccio LM (ed.). Springer Science+Business, Inc. New York, NY.

155. Ricci AJ, Kachar B, Gale J, and Van Netten SM. 2006. Mechano-electrical Transduction: New Insights into Old Ideas. *J. Membr. Biol.* **209**(2-3):71-18.

156. Ricci AJ, Wu Y-C, and Fettiplace R. 1998. The Endogenous Calcium Buffer and the Time Course of Transducer Adaptation in Auditory Hair Cells. *J. Neurosci.* **18**(20): 8261-8277.

157. Rogers S, Wells R, and Rechsteiner M. 1986. Amino Acid Sequences Common to Rapidly Degraded Proteins: the PEST Hypothesis. *Science*. **234**(4774): 364–368.

158. Rzadzinska A, Schneider ME, Noben-Trauth K, Bartles JR, and Kachar B. 2005. Balanced Levels of Espin are Critical for Stereociliary Growth and Length Maintenance. *Cell Mot. Cytoskeleton.* **62**(3):157-165.

159. Rzadzinska AK, Schneider ME, Davies C, Riordan GP, and Kachar B. 2004. An Actin Molecular Treadmill and Myosins Maintain Stereocilia Functional Architecture and Self-Renewal. *J. Cell Biol.* **164**(6):887-897.

160. Sakaguchi H, Tokita J, Naoz M, Bowen-Pope D, Gov NS, and Kachar B. 2008. Dynamic Compartmentalization of Protein Tyrosine Phosphatase Receptor Q at the Proximal End of Stereocilia: Implication of Myosin VI-based Transport. *Cell Mot. Cytoskeleton.***65**(7):528-538.

161. Salles FT, Merritt RC Jr, Manor U, Dougherty GW, Sousa AD, Moore JE, Yengo CM, Dosé AC, and Kachar B. 2009. Myosin IIIa Boosts Elongation of Stereocilia by Transporting Espin 1 to the Plus Ends of Actin Filaments. *Nat. Cell Bio.* **11**(4): 430-450.

162. Saraste M, Sibbald PR, and Wittinghofer A. 1990. The P-loop - a Common Motif in ATP- and GTP-Binding Proteins. *Trends Biochem. Sci.* **15**(11):430-434.

163. Schneider ME, Belyantseva IA, Azevedo RB, and Kachar B. 2002. Structural Cell Biology: Rapid Renewal of Auditory Hair Bundles. *Nature*. **418**(6900):837-838.

164. Schneider ME, Dosé AC, Salles FT, Chang W, Erickson FL, Burnside B, and Kachar B. 2006. A New Compartment at Stereocilia Tips Defined by Spatial and Temporal Patterns of Myosin IIIa Expression. *J. Neurosci.* **26**(40):10243-10252.

165. Schultz J, Milpetz F, Bork P, and Ponting CP. 1998. SMART, a Simple Modular Architecture Research Tool: Identification of Signaling Domains. *Proc. Natl. Acad. Sci.* **95**(11):5857-5864.

166. Schwander M, Sczaniecka A, Grillet N, Bailey JS, Avenarius M, Najmabadi H, Steffy BM, Federe GC, Lagler EA, Banan R, Hice R, Grabowski-Boase L, Keithley EM, Ryan AF, Housley GD, Wiltshire T, Smith RJH, Tarantino LM, and Müller U. 2007. A Forward Genetics Screen in Mice Identifies Recessive Deafness Traits and Reveals That Pejvakin Is Essential for Outer Hair Cell Function. *J. Neurosci.* **27**(9): 2163-2175.

167. Sedgwick SG and Smerdon SJ. 1999. The Ankyrin Repeat: a Diversity of Interactions on a Common Structural Framework. *Trends Biochem. Sci.* **24**(8):311-6.

168. Seiler C, Ben-David O, Sidi S, Hendrich O, Rusch A, Burnside B, Avraham KB, and Nicolson T. 2004. Myosin VI is Required for Structural Integrity of the Apical Surface of Sensory Hair Cells in Zebrafish. *Dev. Biol.* **272**(2):328-338.

169. Sekerková G, Loomis PA, Changyaleket B, Zheng L, Eytan R, Chen B, Mugnaini E, and Bartles JR. 2003. Novel Espin Actin-Bundling Proteins Are Localized to Purkinje Cell Dendritic Spines and Bind the Src Homology 3 Adapter Protein Insulin Receptor Substrate p53. *J. Neurosci.* **23**(4):1310 –1319.

170. Sekerková G, Zheng L, Loomis PA, Changyaleket B, Whitlon DS Mugnaini E, and Bartles JR. 2004. Espins Are Multifunctional Actin Cytoskeletal Regulatory Proteins in the Microvilli of Chemosensory and Mechanosensory Cells. *J. Neurosci.* **24**(23):5445–5456.

171. Sekerková G, Zheng L, Loomis P, Mugnaini E, and Bartles JR. 2006a. Espins and the Actin Cytoskeleton of Hair Cell Stereocilia and Sensory Cell Microvilli. *Cell. Mol. Life Sci.* **63**(19-20):2329-2341.

172. Sekerková G, Zheng L, Mugnaini E, and Bartles JR. 2006b. Differential Expression of Espin Isoforms During Epithelial Morphogenesis, Stereociliogenesis and Postnatal Maturation in the Developing Inner Ear. *Dev. Biol.* **291**:83-95.

173. Sellers JR. 2000. Myosins: a Diverse Superfamily. *Biochim. Biophys. Acta.* **1496**(1): 3-22.

174. Sells MA, Knaus UG, Bagrodia S, Ambrose DM, Bokoch GM, and Chernoff J. 1997a. Human p21-Activated Kinase (Pak1) Regulates Actin Organization in Mammalian Cells. *Curr. Biol.* **7**(3):202-210.

175. Show MD, Anway MD, and Zirkin BR. 2004. An Ex Vivo Analysis of Sertoli Cell Actin Dynamics Following Gonadotropic Hormone Withdrawal. *J. Androl*. **25**(6): 1013-1021.

176. Si F, Brodie H, Gillespie PG, Vazquez AE, and Yamoah EN. 2003. Developmental Assembly of Transduction Apparatus in Chick Basilar Papilla. *J. Neurosci.* **23**(34): 10815-10826.

177. Siemens J, Lillo C, Dumont RA, Reynolds A, Williams DS, Gillespie PG, and Müller U. Cadherin 23 is a Component of the Tip Link in Hair-Cell Stereocilia. *Nature*. **428**(6986):950-955.

178. Sjöström B and Anniko M. 1992a. Genetically Induced Inner Ear Degeneration. A Structural and Functional Study. *Acta Otolaryngol Suppl.* **493**:141-146.

179. Sjöström B and Anniko M. 1992b. Cochlear Structure and Function in a Recessive Type of Genetically Induced Inner Ear Degeneration. *ORL J Otorhinolaryngol Relat Spec.* **54**(4):220-228.

180. Small JV. 1995. Getting the Actin Filaments Straight: Nucleation-Release or Treadmilling? *Trends Cell Biol*. **5**(2):52-55.

181. Smith L, Su X, Lin P-j, Zhi G, and Stull JT. 1999. Identification of a Novel Actin Binding Motif in Smooth Muscle Myosin Light Chain Kinase. *J. Biol. Chem.* **274**(41):29433-29438.

182. Sotomayor M, Corey DP, and Schulten K. 2005. In Search of the Hair-Cell Gating Spring: Elastic Properties of Ankyrin and Cadherin Repeats. *Structure*. **13**:669-682.

183. Stepanyan R, Belyantseva IA, Griffith AJ, Friedman TB, and Frolenkov GI. 2006. Auditory Mechanotransduction in the Absence of Functional Myosin-XVa. *J. Physiol*. **576**(3):801-808.

184. Stepanyan R and Frolenkov GI. 2009. Fast Adaptation and Ca^{2+} Sensitivity of the Mechanotransducer Require Myosin-XVa in Inner But Not Outer Cochlear Hair Cells. *J. Neurosci.* **29**(13):4023-4034.

185. Steyger PS, Gillespie PG, and Baird RA. 1998. Myosin Iβ Is Located at Tip Link Anchors in Vestibular Hair Bundles. *J. Neurosci.* **18**(12):4603-4615.

186. Street VA, McKee-Johnson JW, Fonseca RC, Tempel BL, and Noben-Trauth K. 1998. Mutations in a Plasma Membrane Ca^{2+}-ATPase Gene Cause Deafness in Deafwaddler Mice. *Nat Genet.* **19**(4):390-394.

187. Stull JT. 1996. Myosin Minireview Series. *J. Biol. Chem.* **271**(27):15849.

188. Sweeney HL and Houdusse A. 2007. What Can Myosin VI Do in Cells? *Curr. Opin. Cell Biol*. **19**(1):57-66.

189. Takenawa T and Suetsugu S. 2007. The WASP-WAVE protein network: connecting the membrane to the cytoskeleton. *Nat. Rev. Mol. Cell Biol.* **8**(1):37-48.

190. Tamagawa Y, Kitamura K, Ishida T, Ishikawa K, Tanaka H, Tsuji S, and Nishizawa M. A Gene for a Dominant Form of Non-Syndromic Sensorineural Deafness (*DFNA11*) Maps within the Region Containing the *DFNB2* Recessive Deafness Gene. *Hum. Mol. Genet*. **5**(6):849-852.

191. Taunton J, Rowning BA, Coughlin ML, Wu M, Moon RT, Mitchison TJ, and Larabell CA. 2000. Actin-dependent Propulsion of Endosomes and Lysosomes by Recruitment of N-WASP. *J. Cell Biol.* **148**(3):519-530.

192. Thompson JD, Gibson TJ, and Higgins DG. 2003. Multiple Sequence Alignment Using ClustalW and ClustalX. Ch. 2, unit 2.3. *Curr. Protoc. Bioinformatics.*

193. Thompson RF and Langford GM. 2002. Myosin Superfamily Evolutionary History. *Anat. Rec*. **268**(3):276-289.

194. Tilney LG and DeRosier DJ. 2005. How to Make a Curved *Drosophila* Bristle Using Straight Actin Bundles. *Proc. Natl. Acad. Sci. USA.* **102**(52):18785-18792.

195. Tilney LG, Egelman EH, DeRosier DJ, and Saunder JC. 1983. Actin Filaments, Stereocilia, and Hair Cells of the Bird Cochlea. II. Packing of Actin Filaments in the Stereocilia and in the Cuticular Plate and What Happens to the Organization When the Stereocilia are Bent. *J. Cell Biol*. **96**(3):822-834.

196. Tilney L, Tilney M, and Cotanche DA. 1988. New Observations on the Stereocilia of Hair Cells of the Chick Cochlea. *Hear. Res*. **37**(1):71-82.

197. Tilney LG, Tilney, MS, Saunders JS and DeRosier DJ. 1986. Actin Filaments, Stereocilia, and Hair Cells of the Bird Cochlea. III. The Development and Differentiation of Hair Cells and Stereocilia. *Dev. Biol.* **116**(1)100–118.

198. Tilney M, Tilney L, Stephens R, Merte C, Drenckhahn D, Cotanche D, and Bretscher A. 1989. Preliminary Biochemical Characterization of the Stereocilia and Cuticular Plate of Hair Cells of the Chick Cochlea. *J. Cell Biol.* **109**(4):1711-1723.

199. Todi SV, Franke JD, Kiehart DP, and Eberl DF. 2005. Myosin VIIA Defects, which Underlie the Usher 1B Syndrome in Humans, Lead to Deafness in Drosophila. *Curr.Biol*. **15**(9):862-868.

200. Tokuo H and Ikebe M. 2004. Myosin X Transports Mena/VASP to the Tip of Filopodia. *Biochem. Biophys. Res. Commun.* **319**(1):214-220.

201. Tokuo H, Mabuchi K, and Ikebe M. 2007. The Motor Activity of Myosin-X Promotes Actin Fiber Convergence at the Cell Periphery to Initiate Filopodia Formation. *J. Cell Biol.* **179**(2):229-238.

202. Tyska MJ, Mackey AT, Huang J-D, Copeland NG, Jenkins NA, and Mooseker MS. 2005. Myosin-1a Is Critical for Normal Brush Border Structure and Composition. *Mol. Biol. Cell*. **16**(5):2443-2457.

203. Uyeda TQ, Abramson PD, and Spudich JA. 1996. The Neck Region of the Myosin Motor Domain Acts as a Lever Arm to Generate Movement. *Proc. Natl. Acad. Sci. USA*. **93**(9):4459–64.

204. Verpy E, Leibovici M, Zwaenepoel I, Liu X-Z, Gal A, Salem N, Mansour A, Blanchard SP, Kobayashi I, Keats BJB, Slim R, and Petit C. 2000. A Defect in

Harmonin, a PDZ Domain-Containing Protein Expressed in the Inner Ear Sensory Hair Cells, Underlies Usher Syndrome Type 1C. *Nat Genet*. **26**(1):51-55.

205. Vreugde S, Ferrai C, Miluzio A, Hauben E, Marchisio PC, Crippa MP, Bussi M, and Biffo S. 2006. Nuclear Myosin VI Enhances RNA Polymerase II-Dependent Transcription. **23**(5):749-755.

206. Waguespack J, Salles FT, Kachar B, and Ricci AJ. 2007. Stepwise Morphological and Functional Maturation of Mechanotransduction in Rat Outer Hair Cells. *J. Neurosci.* **27**(50):13890-13902.

207. Walker JE, Saraste M, Runswick MJ, and Gay NJ. 1982. Distantly Related Sequences in the α- and β-Subunits of ATP Synthase, Myosin, Kinases and Other ATP-Requiring Enzymes and a Common Nucleotide Binding Fold. *EMBO J.* **1**(8): 945–951.

208. Walsh T, Walsh V, Vreugde S, Hertzano R, Shahin H, Haika S, Lee MK, Kanaan M, King M-C, and Avraham KB. 2002. From Flies' Eyes to Our Ears: Mutations in a Human Class III Myosin Cause Progressive Non-Syndromic Hearing Loss DFNB30. *Proc. Natl. Acad. Sci. USA*. **99**(11):7518-7523.

209. Wang Y. 1985. Exchange of Actin Subunits at the Leading Edge of Living Fibroblasts: Possible Role of Treadmilling. *J. Cell Biol.* **101**(2):597-602.

210. Warrick HM and Spudich JA. 1987. Myosin Structure and Function in Cell Motility. *Annu. Rev. Cell Biol*. **3**:379-421.

211. Wegner A. 1976. Head to Tail Polymerization of Actin. *J. Mol. Biol.* **108**(1): 139-150.

212. Weil D, Blanchard S, Kaplan J, Guilford P, Gibson F, Walsh J, Mburu P, Varela A, Levilliers J, Weston MD, Kelley PM, Kimberling WJ, Wagenaar M, Levi-Acobas F, Larget-Piet D, Munnich A, Steel KP, Brown SDM, and Petit C. 1995. Defective Myosin VIIA Gene Responsible for Usher Syndrome Type IB. *Nature*. **374**(6517): 60-61.

213. Wells AL, Lin AW, Chen L-Q, Safer D, Cain SM, Hasson T, Carragher BO, Milligan RA, and Sweeney HL. 1999. Myosin VI is an Actin-Based Motor that Moves Backwards. *Nature*. **401**(6752):505-508.

214. Wes PD, Xu X-ZS, Li H-S, Chien F, Doberstein SK, and Montell C. 1999. Termination of Phototransduction Requires Binding of the NINAC Myosin III and the PDZ Protein INAD. *Nat. Neurosci.* **2**(5):447-453.

215. Wheelan SJ, Church DM, and Ostell JM. 2001. Spidey: A Tool for mRNA-to-Genomic Alignments. *Genome Res*. **11**(11):1952-1957.

216. Witt SH, Labeit D, Granzier H, Labeit S, and Witt CC. 2005. Dimerization of the Cardiac Ankyrin Protein CARP: Implications for MARP Titin-Based Signaling. *J. Muscle Res. Cell Motil.* **26**(6-8):401-408.

217. Wood JD, Muchinsky SJ, Filoteo AG, Penniston JT, and Tempel BL. 2004. Low Endolymph Calcium Concentrations in *deafwaddler*^{2J} Mice Suggest that PMCA2 Contributes to Endolymph Calcium Maintenance. *J. Assoc. Res. Otolaryngol.* **5**(2): 99-110

218. Zheng L, Sekerková G, Vranich K, Tilney LG, Mugnaini E, and Bartles JR. 2000. The Deaf Jerker Mouse Has a Mutation in the Gene Encoding the Espin Actin-Bundling Proteins of Hair Cell Stereocilia and Lacks Espins. *Cell.* **102**(3):377-385, 2000.

219. Zine A and Romand R. 1996. Development of the Auditory Receptors of the Rat: a SEM Study. *Brain Res*. **721**(1-2):49-58.